学位論文

Ecophysiological studies on refilling of the cavitated vessel surrounded by functional vessels under negative pressure

（陰圧下にある道管に隣接する空洞化した道管の再充填現象に関する生理生態学的研究）

平成２７年１２月博士（理学）申請

東京大学大学院理学系研究科
生物科学専攻

大條　弘貴

ABSTRUCT

Water flow in plants usually occurs under negative xylem pressure. Thus, the xylem vessels are vulnerable to cavitation and embolism. Embolism reduces the hydraulic conductivity in the xylem and is identified as a major factor that causes plant death. In contrast, many species can refill the embolized vessels even when the bulk of water in the xylem remains under negative pressure. Theoretically, the pressure in the gas phase in the refilling vessel must be positive while water in the adjacent vessels is under negative pressure. Then, the water in the refilling vessel would be forced to move into the adjacent functional vessels under negative pressure, preventing xylem refilling. Thus, there must exist the mechanism preventing the refilling vessel water from being lost to the adjacent functional vessels under negative pressure. Two hypotheses (the pit-membrane-osmosis hypothesis and the pit-valve hypothesis) have been proposed to explain the mechanism preventing the refilling vessel water from being lost to the surrounding functional vessels under negative pressure.

The purpose of the present study is to reveal the mechanism of xylem refilling under negative pressure by assessment of two hypotheses suggested for the mechanism for overcoming surrounding negative pressure during refilling embolized vessels. First, I confirmed that xylem refilling under negative pressure occurs in the shoots of *Morus australis* Poir. (Chapter 2). Second, to examine the pit-membrane-osmosis hypothesis, I estimated the semi-permeability of pit membranes for molecules of various sizes, and found that the pit membranes were not semi-permeable to polyethylene glycol of molecular mass less than 20,000 (Chapter 3).

In chapter 3, I estimated the threshold pressure at which the pit valves collapse for *M. australis* and *Laurus nobilis*. The gas in the pits can be retained by surface tension, even under substantial positive pressure. I also found out that all the pit valves did not collapse simultaneously. This indicates the possibility of re-cavitation of the refilling vessel.

For keeping pressurizing the remaining gases even when some pit valves are collapsed, the

inward water flow from parenchyma cells to the refilling vessel must be more than the outward flow from the refilling vessel to the surrounding functional vessels that are under negative pressure. The outward flow rate is proportional to the cumulative inter-vessel pit areas and the hydraulic conductivity across the pits. In contrast, the inward flow rate is proportional to the contact wall area between the vessel and parenchyma cells ($\propto$ non-inter-vessel pit area) and the hydraulic conductivity between them. Thus, these inward and outward flow rates must be estimated to understand the mechanisms of xylem refilling under negative pressure.

In chapter 4, I examined the inter-vessel and non-inter-vessel pit areas of vessels. The hydraulic conductivity through the inter-vessel pits was also estimated. In chapter 5, the hydraulic conductivity between a vessel and surrounding parenchyma cells was measured. Based on these results, the outflow rate to the surrounding vessels under negative pressure will be much larger than the inflow rate from surrounding parenchyma cells. For the xylem refilling under negative pressure to occur, mechanisms other than the two hypotheses are required. Possible mechanisms are discussed in a quantitative way.

ACKNOWLEDGEMENT

First of all, I would like to express my sincere gratitude and appreciation to my advisor Professor Ichiro Terashima for his kind and continuous guidance, invaluable support, and encouragement throughout my study. I also express my sincere thanks to Assistant Professor Haruhiko Taneda for his kind and continuous guidance, invaluable support, and patient encouragement throughout my study. It is he who fanned sparks of my interest on xylem cavitation and refilling.

I am grateful to Associate Professor Masaki Tateno, Professor Hiroo Fukuda, Associate Professor Munetaka Sugiyama, and Associate Professor Manabu Yoshida (The University of Tokyo), the committee of my Ph.D. dissertation, for their helpful comments and suggestions.

Special thanks go to Professor Yuzou Sano (Hokkaido University) for instructing us in the method for observations on inter-vessel pits. I owe a lot to the following people although I did not record the data obtained by their supports in the present study. I received generous support from Kenji Fukuda (The University of Tokyo), Dr. Mayumi Ogasa, Dr. Kenichi Yazaki (Forestry and Forest Products Research Institute), and Dr. Toshihiro Umebayashi (Hokkaido University). Professor Seiichi Oshita gave me excellent technical assistance on the pressure probe. Professor Emiko Maruta (Tokyo University of Agriculture) provided field research opportunities in Mt. Shimagare.

I am grateful to all the member of Prof. Terashima's laboratory for making me greatly enjoy my academic life.

Finally, I cannot find appropriate words enough to express my heartfelt gratitude to my family for their moral support and warm encouragements..

Hiroki OOEDA

December 2015, Tokyo, Japan

TABLE OF CONTENTS

ABBREVIATIONS

ROMAN ALPHABET

A	Vessel lumen area	m^2
A_{pit}	Cumulative areas of the inter-vessel pits	m^2
A_v	Interior surface area of the vessl	m^2
a_w	Water activity	—
c	Solute concentration	mol m^{-3}
c′	Feed water solute concentration	mol m^{-3}
c″	Permeate solute concentration	mol m^{-3}
c_s	Molarity	mol m^{-3}
D	Vessel diameter	μm
D_{gas}	Apparent diffusion coefficient	m^2 s^{-1}
D_p	Pit membrane pore diameter	m
E_b	Maximum value of $F(R)$	J
f_p	Fraction of the surface area of pit membranes in the inter-vessel contact area (pit field fraction)	—
$F(R)$	Minimum work required to create a sphere of vapor of radius R in the liquid water	J
g	Gravitational acceleration	m s^{-2}
G	The ratio of the perimeter to the cross-sectional area of the pit aperture opening	m^{-1}
h	Height above the reference plane	m
J	Water flow rate	m^3 s^{-1} or kg s^{-1}

j_{gas}	Flow rate of gas per unit interior surface area of the pressurized vessel	mol m^{-2} s^{-1}
j_{liq}	Inward flow rate per unit the interior surface area of a vessel	m^3 m^{-2} s^{-1}
J_s	Solute flux	mol m^{-2} s^{-1}
J_v	Volumetric water flux	m s^{-1}
k_b	Boltzmann constant	m^2 kg s^{-2} K^{-1}
k_{gas}	Rate at which gas exits a vessel per area and pressure	mol m^{-2} s^{-1} MPa^{-1}
K_h	Hydraulic conductance	kg s^{-1} MPa^{-1}
k_h	Hydraulic conductivity	kg m s^{-1} MPa^{-1}
$k_{h,\ embolized}$	hydraulic conductivity of embolized xylem	kg m s^{-1} MPa^{-1}
$k_{h,\ max}$	maximal hydraulic conductivity	kg m s^{-1} MPa^{-1}
L	Vessel length	m
L_{med}	Median vessel length	m
L_p	Hydraulic conductance of a membrane	kg s^{-1} MPa^{-1}
L_r	Area based hydraulic conductivity	m^3 m^{-2} s^{-1} MPa^{-1}
m	Mass of one water molecule	kg
n	The number of connection	—
N	Number density of the liquid	m^{-3}
N	The number of vessel observed	—
N_L	Fraction of silicone-filled vessels	—
OV	Open vessel	
p	Mean inter-vessel wall width	μm
$\bar{P}$	Local solute permeability coefficient	m^2 s^{-1}
PEG	Polyethylene glycol	

P_{gas}	Gas pressure	MPa
PLC	Percentage loss of hydraulic conductivity	%
P_{liq}	Liquid pressure	MPa
P_n	Pressure inside the nucleus	MPa
PPV	The other vessel that diverged from the vessel via the bordered pits (pit-passing vessel)	
P_s	Solute permeability coefficient	$m\ s^{-1}$
P_x	Xylem pressure	MPa
r	Curvature radius of the air bubble	m
R	Gas constant	$J\ K^{-1}\ mol^{-1}$
R	Radius of vapor bubble	m
R_c	Critical radius	m
R_{lumen}	Lumen resistivity	$MPa\ s\ mm^{-4}$
$\overline{R}_{lumen}$	Lumen resistivity for the xylem as a whole	$MPa\ s\ mm^{-4}$
r_m	Pore radius on the cellulose microfibril	m
r_o	Distance from the pressurized vessel to the nearest edge of the stem segment	m
r_p	Hydraulic resistivity per pit membrane area	$MPa\ s\ m^{-1}$
R_{total}	Hydraulic resistivity of a vessel	$MPa\ s\ mm^{-4}$
r_v	Vessel radius	μm
R_{wall}	End wall resistivity	$MPa\ s\ mm^{-4}$
$\overline{R}_{wall}$	End wall resistivity for the xylem as a whole	$MPa\ s\ mm^{-4}$
R_{xylem}	Stem xylem resistivity	$MPa\ s\ mm^{-4}$
SEM	Scanning electron microscope	
t	Time	s

T	Temperature	K
TCA	Trichloroacetic acid	
V	Volume	m^3
V_w	Partial molar volume of water	$m^3\ mol^{-1}$
w	Inter-vessel wall width	m
x	length coordinate	m

GREEK ALPHABET

α	Angle of bordered pit chamber walls	°
β	Contact angle between water and pit membrane surface	°
γ	Surface tension of water	$N\ m^{-1}$
Γ	Nucleation rate per unit volume and time	$m^{-3}\ s^{-1}$
Γ_o	Kinetic prefactor	—
γ_w	Activity coefficient	—
Δc_{gas}	Difference in concentration of dissolved gases in the water at the surface of the vessel and at the edge of stem	$mol\ m^{-3}$
Δl	Length between two points	m
Δx	Membrane thickness	m
ΔP	Pressure difference between two points	MPa
η	Viscosity of water	Pa s
θ	Contact angle of the water with the wall	°
μ	chemical potential of water	$J\ mol^{-1}$
μ_0	chemical potential of pure water	$J\ mol^{-1}$
ρ_w	Density of water	$kg\ m^{-1}$
σ	Reflection coefficient	—

Σ	Nucleation probability	—
x_w	Mole fraction of water	—
Ψ	water potential	MPa
Ψ_g	gravitational potential	MPa
Ψ_p	pressure potential	MPa
Ψ_π	osmotic potential	MPa

CHAPTER 1

GENERAL INRODUCTION

XYLEM STRUCTURE

Water is essential resources for life. Water plays various roles in plants. First, because of its highly polar structure, water acts as a solvent and is used for the transpiration carrier of nutrients (nitrogen, phosphorus, potassium, *etc*) from the soil. Second, water maintain the turgidity of cells, which is the basic support mechanism in non-woody tissues of plants. Moreover, water is used for photosynthesis and helps maintain the plant body temperature due to the highest latent heat of vaporization, and so on (Lambers *et al.* 2008).

Xylem conduits (tracheids and vessels) represent the most important pathways for long distance water transport from roots to leaves in vascular plants. In the xylem of most gymnosperms and some angiosperms, water transport is facilitated by tracheids, which are single cells. By contrast, in nearly all angiosperms and some pteridophytes, vessels serve to transport water although the tracheary elements at the vein-ending are tracheids. The vessels are composed of multiple dead cells, which are connected by perforations at both ends of each vessel element except for the elements at the end of the vessel (White 1961). The internal diameter of conduit (conduit diameter) ranges from 10 to 500 μm, depending on the species and the location within the plant (Tyree & Zimmermann 2002). Conduits are connected through the openings in the lignified secondary walls known as pits (Choat *et al.* 2008). A longitudinal column of conduits through overlapping end walls studded with inter-conduit pits creates an axial flow path. The pit membrane, which consists of the primary walls and intervening middle lamella of two opposing cells, lies in the center of the pit. The pit membrane of conifer tracheids generally is differentiated into a central thickened region, the torus, and peripherally, a margo with radiating strands of microfibrils. Scanning electron microscope (SEM) studies showed large pores in the margo region of conifer pit membranes (Sachs 1963; Liese 1967). On the other hand,

vessel-bearing species have homogeneous pit membranes. Tracheids in pteridophytes, cycads, and vesselless angiosperms (Winteraceae and Trochodendrales) also have homogeneous pit membranes instead of the torus-margo membranes of conifers (Doyle and Endress, 2000; Feild *et al.* 2000; Feild & Arens 2005; Pittermann *et al.*, 2005). The pore size of the homogeneous pit membrane is very small ranging generally from 5 to 20 nm (Choat *et al.* 2003).

The pit is a region which is not covered by the secondary cell wall, and the shape of the pit varies with secondary wall thickening. The primary xylem conduits show a variety of secondary wall thickenings (Esau 1977). The different forms of wall appear in a specific ontogenetic series that indicates a progressive increase in the region of the primary wall area covered with the secondary wall. In the earliest conduits, the secondary walls may occur as rings not connected with each other (annular thickening). The conduits differentiating next have helical thickening. Then, conduits with thickenings that may be characterized as helices with coils interconnected (scalariform thickening) follow. These are succeeded by conduits with net-like thickenings (reticulate thickening) and finally by bordered pit elements. In secondary xylem, xylem conduits generally have bordered pits.

Besides conduit cells, xylem also contains fibers and parenchyma. Xylem fibers provide structural support in vessel-bearing species. Xylem parenchyma cells store water, mineral nutrients and carbohydrates. These substances are transported between parenchyma cells and xylem conduits through pits.

WATER MOVEMENTS

Water moves spontaneously along a gradient of chemical potential of water by mass flow and/or diffusion. In soils, plants, and the atmosphere, the water status is commonly expressed as "water potential" Ψ, using pressure units. This can be calculated by dividing the chemical potential μ, by the partial molar volume of water, V_W, and plant physiologists define water potential of pure water at the atmospheric pressure as zero. Then, water potential Ψ is expressed as follow:

$$\Psi \equiv \frac{\mu - \mu_0}{V_W} \quad (1\text{-}1),$$

where μ_0 is the chemical potential of pure water at the same temperature and at the atmospheric pressure. The total liquid water potential can be divided into several components:

$$\Psi = \Psi_p + \Psi_\pi + \Psi_g \quad (1\text{-}2),$$

where Ψ_p is pressure potential, Ψ_π is osmotic potential, and Ψ_g is gravitational potential.

The pressure potential represents the difference in the hydrostatic pressure from the reference. In plant science, gauge pressure is commonly used (i.e. atmospheric pressure = 0 MPa). Mass flow in tube-like structures is driven by the difference in the hydraulic pressure. Assuming laminar flow, the water flow (J, kg s^{-1}) through pipes is inversely proportional to the length of the tube and directly proportional to the pressure difference (ΔP) between two points:

$$J = -K_h \Delta P \quad (1\text{-}3),$$

where K_h is hydraulic conductance (kg s^{-1} MPa^{-1}). The hydraulic conductance can be expressed using the length between the two points (Δl, m) and hydraulic conductivity (k_h, kg m s^{-1} MPa^{-1}):

$$J = -k_h \frac{\Delta P}{\Delta l} \quad (1\text{-}4).$$

The inverse of hydraulic conductance and the inverse of hydraulic conductivity are called hydraulic resistance and hydraulic resistivity, respectively.

The osmotic potential is due to dissolved solutes which lower the free energy of the water. It can be expressed as follow:

$$\Psi_\pi = \frac{R\,T}{V_w} \ln(\gamma_w x_w) \quad (1\text{-}5),$$

where R is gas constant (J K^{-1} mol^{-1}), T is temperature (K), γ_w is an activity coefficient that measures departure from ideal behavior by the solution, and x_w is the mole fraction of water. The product $\gamma_w x_w$ is also known as the activity of water, which is the water activity a_w. van't Hoff equation gives a very useful approximation of Eq. 1-5:

$$\Psi_\pi = -R\,T\,c_s \quad (1\text{-}6),$$

where c_s is the molarity. The difference of the osmotic potential between the two points has no

influence on the water flux in pipes shown as Eqs. 1-3 & 1-4. However, the difference has an impact at a membrane level, depending on the solute. When solutes permeate a membrane slowly compared to water, the water flux across the membrane is:

$$J = -L_p\,(\Delta P + \sigma \Delta \Psi_w) \quad (1\text{-}7),$$

where L_p is the hydraulic conductance of the membrane and σ is the reflection coefficient, which represents the degree of semi-permeability of the membrane to the solute. The value varies between 0 for completely permeable membrane to 1 for perfect semi-permeable membrane.

The gravitation potential results from difference in the potential energy due to a difference in height from the reference level:

$$\Psi_g = \rho_W\, g\, h \quad (1\text{-}8)$$

where ρ_W, g, and h are the density of water, gravitational acceleration, and the height above the reference plane, respectively. The gravitation potential is often neglected in plant systems. However, Ψ_g increases by 0.01 MPa m^{-1}, so it is an important factor when considering water movements in tall trees.

WATER TRANSPORT IN PLANTS

Water movement from the soil, through the plant, to the atmosphere, takes place in a soil-plant-atmosphere continuum (SPAC) that is interconnected by a continuous film of liquid water. As explained above, water bulk flow through plant occurs along a gradient, either from a high to a low water potential (if the transport occurs across a semi-permeable membrane), from a high to a low pressure potential (if no such a membrane is involved), or from a high to a low water vapor concentration (for water vapor).

A gradient in osmotic potential is the major driving force for water movement between the soil and the cells in the roots (Lambers *et al.* 2008). The loading of solutes into the root xylem lower the osmotic potential, and water is absorbed by root from the soil due to osmosis. Without transpiration to carry the solutes up the stem (at night and in early-spring), water absorption creates a

positive hydrostatic pressure, forcing movement of water through the xylem into the stem. This phenomenon is known as the root pressure.

On the other hand, a gradient in pressure potential is the major driving force for water movement through xylem conduits in daytime. Evaporation from leaves occurs predominantly from the cell walls of the substomatal chambers. The evaporation increases a curvature in the water menisci of apoplastic water in the pores between the cellulose microfibrils in the cell wall. The surface tension lowers the hydrostatic pressure of the water behind the menisci (the air-water interfaces). The decrease in the hydrostatic pressure is expressed by the capillary equation:

$$\Delta P = -\frac{2\gamma \cos\theta}{r_m} \quad (1\text{-}9),$$

where γ is the surface tension of water (0.072 N m^{-1} at 25°C), θ is the contact angle of water on the cellulose microfibril, and r_m is the pore radius. The tension is transmitted through a continuous water column from the leaves to the root and throughout all parts of the apoplast in every organ of the plant, and the gradient in hydrostatic pressure drives water transport through the plant. Thus, water in the xylem conduits is normally under tension (negative hydrostatic pressure, interpreted as pressure less than normal atmospheric pressure by plant scientists). This explanation for the ascent of xylem sap is known as the cohesion-tension theory (Dixon and Joly, 1894). The existence of negative pressure in xylem sap (xylem pressure, P_x) has been demonstrated indirectly by the pressure chamber (Scholander *et al.*, 1965) and directly by the pressure probe (Wei *et al.*, 1999). The pressure ranges typically −1 and −2 MPa, and sometimes as low as −10 MPa (Tyree and Sperry, 1989). This means that water must remain liquid at pressures below its vapor pressure. In this metastable state, nucleation of vaporization, or cavitation, must be prevented in order to maintain the continuity of the water column in the xylem conduits. Once cavitation occurs, the conduits are not available for water conduction, that is, become embolized. Embolism reduces the hydraulic conductivity in the xylem and is identified as a major factor that reduces the primary productivity of forests (Anderegg *et al.*, 2012) and causes plant death (Kursar *et al.*, 2009).

CAVITATION IN XYLEM CONDUITS

In general, the vulnerability to cavitation of a species correlates with the xylem pressures it experiences in nature (Tyree and Sperry, 1989). For instance, stems of *Populus fremontii* show complete cavitation at −1.6 MPa, whereas those of *Acer negundo* and *Juniperus monosperma* have a thresholds at −1.9, and less than −3.5 MPa, respectively (Lambers *et al*,. 2008). Vulnerability to cavitation can be defined by the relationship between the water pressure in the xylem conduits (xylem pressure) and percentage loss of hydraulic conductivity (PLC) by embolism; this is called as a "vulnerability curve". As the xylem pressure becomes progressively negative, the probability of cavitation in a conduit increases, resulting in the increase in PLC.

What is the possible mechanism of cavitation in xylem conduits? Four mechanisms for the nucleation of cavitation in plants have been proposed (Tyree, 1997): (A) bubble formation in bulk liquid (homogeneous nucleation), (B) bubble formation on an interface between water and a conduit wall (heterogeneous nucleation), (C) nucleation at hydrophobic cracks, and (D) meniscal failure at a pore. These are illustrated in Fig. 1-1, which shows the sequence of events that might occur as xylem pressure declines in the lumen of a conduit for each mechanism. Pickard (1981) reviewed those four possible mechanisms of cavitation.

For homogeneous nucleation (Fig. 1-1A), many physical studies have been done. Classical nucleation theory has been developed in several works (e.g. Blander and Katz, 1975). Let us consider a liquid at constant temperature T and a pressure P_{liq}. The minimum work $F(R)$ required to create a sphere of vapor of radius R in the liquid is

$$F(R) = \frac{4}{3}\pi R^3\left(P_{liq} - P_n\right) + 4\pi R^2\gamma \qquad (1\text{-}10),$$

where P_n is the pressure inside the nucleus and can be approximately regard as the saturated vapor pressure at the temperature T (Balibar and Caupin, 2006). The first term in Eq. 1-10 gives the energy gained when forming a volume of the stable phase, whereas the second term is the energy cost associated with the creation of an interface. When $R = 2\gamma/(P_n\text{-}P_{liq})$, $F(R)$ takes maximum value E_b:

$$E_b = \frac{16\pi\gamma^3}{3(\mathrm{P_n} - \mathrm{P_{liq}})^2} \quad (1\text{-}11).$$

Nuclei shrink if $R <$ the critical radius $R_c = 2\gamma/(\mathrm{P_n}-\mathrm{P_{liq}})$, and they grow if $R > R_c$. Thermal fluctuations of the system can trigger nucleation, and so nucleation occurs at a rate proportional to $\exp[-E_b/(k_b\mathrm{T})]$, where k_b is Boltzmann constant. Then, the nucleation rate per unit volume and time (Γ) can be described as

$$\Gamma = \Gamma_0 \exp\left(-\frac{E_b}{k_b\,\mathrm{T}}\right) \quad (1\text{-}12),$$

where Γ_0 is a kinetic prefactor. Nucleation in a volume V and a time t considered, the differential equations of the nucleation probability Σ is expressed as:

$$\frac{d\Sigma}{dt} = (1-\Sigma)\Gamma V \quad (1\text{-}13).$$

A simple integration leads to the calculation of the probability Σ that nucleation occurs in a volume V and a time t (Balibar and Caupin, 2006):

$$\Sigma = 1 - \exp\left[-\Gamma_0 V t \exp\left(-\frac{E_b}{k_b\,\mathrm{T}}\right)\right] \quad (1\text{-}14).$$

Γ_0 has not to be known accurately (Pettersen *et al.*, 1994), but, because of the exponential in the rate, changes by several orders of magnitude affect the results only marginally. Here, I take $\Gamma_0 = \mathrm{N}\sqrt{2\gamma/(\pi m)}$, where N is number density of the liquid and m is the mass of one water molecule (Blander and Katz 1975). Fig. 1-2 shows the predicted nucleation probability for water. Water is a strongly cohesive liquid, because of hydrogen bonding between water molecules. This makes surface tension γ high, and theoretically allows a high degree of metastability. This calculation indicates that homogeneous nucleation cannot occur in plants in the range of xylem pressure at which xylem cavitation occurs.

Also for heterogeneous nucleation, the nucleation probability can be estimated (Pickard, 1981). Considering the bubble described in Fig. 1-1B, the minimum work $F(R)$ required to create the bubble in the liquid water is

$$F(R) = \left(\frac{4}{3}\pi R^3(\mathrm{P_{liq}} - \mathrm{P_n}) + 4\pi R^2\gamma\right) f(\theta) \quad (1\text{-}15),$$

where

$$f(\theta) = (1 + \cos\theta)^2(2 - \cos\theta)/4 \quad (1\text{-}16).$$

θ is the contact angle of the water with the wall. In the same way as shown above, $F(R)$ takes maximum value E_b:

$$E_b = \frac{16\pi\gamma^3}{3(P_n - P_{liq})^2} f(\theta) \quad (1\text{-}17).$$

$f(\theta)$ ranges from 0 to 1, and is always monotonically decreasing within 0° to 180°. Therefore, the conduit is more vulnerable to cavitation with the increase in hydrophilicity of the wall. However, because the contact angle on a conduit wall ranges from 42° to 55° (Zwieniecki and Holbrook, 2000), $f(\theta)$ is assumed to range from 0.883 to 0.955. Thus, there are not large differences in the pressure when the nucleation probability Σ=0.5 between homogeneous nucleation and heterogeneous nucleation, and thus the heterogeneous nucleation is also invalid for cavitation in xylem conduits.

For nucleation at hydrophobic cracks, Pickard (1981) discussed expansion of an air bubble in a crevice of conical shape. Let us consider a submicroscopic air bubble which remains at the base of a hydrophobic crevice as described in Fig. 1-1C. As the xylem pressure becomes progressively negative, the air bubble in the crack grows and buds off into the bulk solution, resulting in conduit embolism. The air bubble with a curvature radius of the air bubble r will grow if

$$P_{liq} < P_n - \frac{2\gamma}{r} \quad (1\text{-}18).$$

r is positive when the meniscus is convex outward into the liquid, and is negative when the meniscus is convex inward into the liquid. According to Eq. 1-18, Pickard has calculated that cavitation will occur at −1 MPa when the radius of curvature is 0.14 μm. This pressure is realistic for xylem pressure at which cavitation may occur in plants. However, an air bubble in a crevice of conical shape is unstable. When $P_{liq}-P_n > -2\gamma/r$, the bubble will decrease its curvature radius more and more rapidly, which leads to vanishing of the bubble nucleus. Therefore, if nucleation at hydrophobic cracks was responsible for xylem cavitation, it would be necessary to think about the bubble nucleus so that $-2\gamma/r$ decreases with bubble dissolution, like one in inverse conically shaped crack. Nevertheless, given that

xylem conduits derive from living cells, the gas vesicles in conduit cells will be collapsed by turgor pressure, and it is doubtful that there are bubble nuclei in cracks of xylem conduits.

Although xylem cavitation is unlikely to be attributed to the expansion of air bubbles in cracks, the limitation of the mechanical suction pump lies with the cavitation due to such submicroscopic air bubbles in cracks. In general, the maximum height to which suction pumps lift water is regarded as 10.4 m. However, Hayward (1970) designed a water pump with a suction lift of 17 m, corresponding to a pressure of −0.17 MPa by applying a high pressure of 30 MPa to the system of suction pump and eliminating bubble nuclei in advance.

Forth hypothesis for the nucleation of cavitation in plant xylem is meniscal failure at a pore (Fig. 1-1D). Although Pickard (1981) disregarded the meniscal failure mechanism, the concept has revived as the air-seeding hypothesis by Zimmermann (1983). In this hypothesis, cavitation in a conduit is caused by gas being drawn into water-filled xylem conduits by negative pressure through the inter-conduit pits. In angiosperm species with homogeneous pit membranes, the movement of gas between conduits is limited by high surface tension of water and the small pores of pit membranes, while in gymnosperm species, a torus seals off the pit aperture and the strength of this seal depends on the strength and stiffness of the margo meshwork (Sperry and Tyree, 1990; Hacke *et al.*, 2004). When an interface between gas and water is drawn to a pit membrane, it will break into many small menisci in the membrane pores. The gas will be prevented from moving into the water-filled conduits under negative pressure unless the pressure difference between two conduits exceeds a critical threshold. The threshold pressure difference (ΔP) required to pull an air bubble through a pit membrane pore of a given size can be calculated from the capillary equation:

$$\Delta P = \frac{4\gamma \cos\beta}{D_p} \qquad (1\text{-}19),$$

where β is the contact angle between water and pit membrane surface and D_p is the pit membrane pore diameter. When the pressure difference exceeds the threshold, gas expands to fill the whole conduit and the conduit becomes embolized. The embolized conduit is initially filled with water vapor.

However, the pressure in the embolized conduit increase to atmospheric pressure as air diffuses into the embolism from surrounding cells, and the water vapor is replaced with air within 1000 s after cavitation (Tyree and Sperry, 1989). This mechanism can only occur if some conduits are filled with gas to begin with. However, this happens frequently by such events as herbivory and mechanical damage to stems and leaves (Tyree and Sperry, 1989).

There is considerable evidence that xylem cavitation occurs by the air seeding mechanism. Good evidence is that the blockage of water transport by cavitation in conduits depends on the pressure difference between the pressure in a water-filled conduit (i.e. xylem pressure) and surrounding air pressure, and not on the negative xylem pressure itself (Cochard *et al.,* 1992; Salleo *et al.*, 1996). The same amount of blockage is observed whether the xylem pressure is negative and air pressure is ambient, or the air is pressurized and the xylem pressure is ambient. Moreover, the vulnerability of xylem to cavitation increases when the permeability of pit membranes to air is increased by changing the surface tension of solution in xylem conduits (Sperry *et al.*, 1987). Therefore, vulnerability to cavitation of a conduit depends on the pit membrane pore size rather than conduit diameter.

However, attempts to relate pit membrane porosity with observed air-seeding pressures have resulted in different conclusions. Some studies showed that porosity corresponded well with air-seeding pressures (Jarbeau *et al.*, 1995), while others showed that average membrane pore size were much smaller than the diameter expected by the air-seeding pressure and Eq. 1-19 (Shane *et al.*, 2000; Choat *et al.*, 2003). In the interspecific study of Hacke *et al.* (2006), there was only a weak correlation between vulnerability to cavitation and the hydraulic resistance of pit membranes, which should reflect their average porosity. Moreover, contrary to the expectation, vulnerable species had high pit membrane resistivities, i.e. small average pit membrane porosity (Wheeler *et al.*, 2005).

To explain the disagreement between the average pit membrane pore size and the pore size expected by the air-seeding pressure, the rare pit hypothesis has been proposed. This hypothesis states that pores of air-seeding size are rare compared with the vast majority of pores with much narrower

size (Hargrave *et al.*, 1994; Choat *et al.*, 2003; Wheeler *et al.*, 2005). Thus, the vulnerability of a given conduit is heavily affected by the surface area of inter-conduit pit membranes. Good evidence for the hypothesis is the observation that there is a significant correlation between the inter-conduit pit membrane area and vulnerability to cavitation (Wheeler *et al.*, 2005).

XYLEM REFILLING

Plants can face the threat of xylem embolism by adopting three strategies: (a) cavitation avoidance, requiring a control of xylem pressure and xylem structure with higher resistance to cavitation; (b) embolism repair, requiring refilling with water of gas-filled conduits; and (c) production of new xylem, requiring carbon investment in the growth processes (Nardini *et al.*, 2001).

Water refilling of the embolized conduits requires gas dissolution into the surrounding water (Tyree and Yang, 1992). Henry's law states that the solubility of a gas in water is proportional to its partial pressure in the gas phase adjacent to the water. Thus, gas dissolution in the embolized conduits is facilitated by positive pressure.

Xylem embolism repair by the positive root pressure has long been known to occur (Slatyer 1967), although it requires both high soil water availability and suppression of transpiration for the production of positive pressures throughout the xylem. In contrast, studies with a wide range of species showed that refilling of embolized conduits also occurs when the bulk of water in the xylem remains under negative pressure (e.g., Sperry *et al.*, 1994; Tyree *et al.*, 1999; Ogasa, *et al.*, 2010). Concerning refilling of the embolized vessels under negative pressures, there goes controversies whether the embolism repair can be measured by changes in the hydraulic conductivity before and after rehydration (Wheeler *et al.*, 2013; Sperry, 2013; Trifilò *et al.*, 2014). However, several studies confirm xylem refilling under negative pressure by visualizations with the magnetic resonance imaging and high-resonance computed tomography (Scheenen *et al.*, 2007; Brodersen *et al.*, 2010; Brodersen *et al.*, 2013). Xylem refilling in angiosperms was enhanced and inhibited by application of fusicoccin (an activator of the plasma membrane H^+-ATPase) and orthovanadate (an inhibitor of the

plasma membrane H^+-ATPase), respectively, to the stem (Salleo *et al.*, 2004). Moreover, starch was hydrolyzed in the xylem parenchyma cells adjacent to the embolized vessels and the sucrose concentration in the wood increased during the xylem refilling (Salleo *et al.*, 2004; Secchi and Zwieniecki, 2011). These results indicate that water entry into the embolized vessel may be osmotically induced by the active transport of the compounds such as sucrose from the neighboring xylem parenchyma cells into the vessel. Water entry pressurizes and thereby solubilizes the gas bubble, eventually allowing refilling of the embolized vessel.

Theoretically, the pressure in the gas phase in the refilling vessel must be positive while water in the adjacent vessels is under negative pressure. If this were the case, the water in the refilling vessel would be forced to move into the adjacent functional vessels, preventing xylem refilling. Thus, there must exist the mechanism preventing the refilling vessel water from being lost to the adjacent functional vessels under negative pressure.

Two hypotheses have been proposed for the mechanism that prevents water in a refilling vessel from being drawn up by adjacent vessels under negative pressure. The pit-membrane-osmosis hypothesis proposes that xylem refilling involves the release of high molecular mass polysaccharides from xylem parenchyma cells into the refilling vessel lumen (Fig. 1-3A; Hacke and Sperry, 2003). The polysaccharides are assumed to be impermeable to the inter-vessel pit membranes and cause a negative osmotic potential in the vessel water in the refilling vessels. The negative osmotic potential in the sap not only prevents water in the refilling vessel from moving away but also draws water from the surrounding vessels and tissues. In contrast, the pit-valve hypothesis proposes that a small volume of gas is retained within each of the bordered pit chambers between the refilling vessel and the adjacent functional vessels during xylem refilling (Fig. 1-3B; Holbrook and Zwieniecki, 1999). Pits are regions in the cell wall without secondary cell walls, providing pathways for water and solutes between the neighboring vessels. If gas remains in the inter-vessel pits, water in the refilling lumen will be isolated from water in the surrounding functioning vessels at negative pressure. The inter-vessel pits typically have overarching walls that form small, bowl-shaped chambers. The angle

of the flare from the pit aperture and non-zero contact angle of the water with the pit wall cause a convex interface between the gas in the pit chamber and the water in the refilling lumen. The convex meniscus means that the force due to surface tension will oppose the hydrostatic pressure in the refilling lumen. As long as the positive pressure in the lumen does not exceed the force due to surface tension, the meniscus will be stable, even though the volume of gas in the pit chamber is extremely small. The bordered pits that trap gas inside are referred to pit valves hereafter.

For the pit-membrane-osmosis hypothesis, the size of pores through the inter-vessel pit membranes has been examined (Choat *et al.*, 2004). The median pore size in pit membranes is 10 nm, and the maximum osmotic potential that can be generated using 10 nm diameter particles is not sufficient to explain the xylem refilling under strong negative xylem pressure (Zwieniecki and Holbrook, 2009). However, from the pore size data only, it is difficult to judge whether the pit membranes show the semi-permeability. The pit membranes may show partial semi-permeability even for small molecules that can pass through the pit membranes. This is because 1) the size of pores in the pit membranes varies greatly (Choat *et al.*, 2004), and 2) the velocity of the solute movement can be lowered by the chemical interactions between the solutes and materials of the pit membranes (Van der Bruggen *et al.*, 1999). Moreover, for maintenance of a given osmotic pressure in the refilling vessel sap, it would not be necessary for the pit membranes to show perfect semi-permeability. The degree of semi-permeability of the inter-vessel pit membranes, however, has never been examined experimentally.

The pit-valve hypothesis assumes that pit valves are retained until the lumen of the embolized vessel has been completely filled with water. Because the pressure generated by surface tension opposes the hydrostatic pressure within the refilling lumen, the maximum pressure within the lumen up to which the pit valve is retained is equal to the pressure due to surface tension. The pressure due to surface tension is determined by the geometry and chemistry of the bordered pits, and has been theoretically estimated for six species (Zwieniecki and Holbrook, 2000). No studies, however, have confirmed experimentally that the pit valve works *in vivo*.

THE OBJECTIVE OF THIS STUDY

The purpose of the present study is to reveal the mechanism of xylem refilling under negative pressure by assessment of the two hypotheses for the mechanism for overcoming surrounding negative pressure during refilling embolized vessels. However, it has been questionable if xylem repairs under negative pressure of various species examined in previous studies are real phenomena (Wheeler *et al.* 2013). Then, first, I confirmed whether xylem refilling under negative pressure occurs in the shoots of *Morus australis* Poir. (Chapter 2).

Assessment of the pit-membrane-osmosis hypothesis requires the estimation of the semi-permeability of the pit membrane. On the other hand, assessment of the pit-valve hypothesis requires settling several questions. One question is whether the pit valve can work *in vivo*. Positive pressure is needed to force the gas into surrounding water whereas excessive pressure will cause the collapse of the pit valves before the completion of the vessel lumen refilling. The pit valve stability depends on the threshold pressure at which it collapse and the pressure in the refilling vessel during the vessel lumen refilling.

Another question relates to simultaneity of collapse of the pit valves. To complete refilling of an embolized vessel, all the pit valves must collapse finally. However, unless the gases in the pit chambers are simultaneously dissolved, it could be possible that remaining gases expand to re-embolize the vessel because the water in the vessel connected with that of the surrounding functional vessels is under negative pressure (Hacke and Sperry, 2003; Brodersen *et al.*, 2010). To overcome this problem, the inward water flow from parenchyma cells to the refilling vessel must be more than the outward flow from the refilling vessel to the surrounding functional vessels under negative pressure to keep pressurizing the remaining gases even when some pit valves are collapsed (Brodersen *et al.*, 2010). The outward flow rate is proportional to the inter-vessel pit area and the hydraulic conductivity across the pits. In contrast, the inward flow rate is proportional to the contact wall area between the vessel and parenchyma cells ($\propto$ non-inter-vessel pit area) and the hydraulic conductivity between them. Thus, estimations of these factors will contribute to understanding of

xylem refilling.

In the present study, I assessed these two hypotheses. The semi-permeability of the pit membrane was estimated with *M. australis*. The threshold pressure at which the pit valves collapse is estimated with *M. australis* and *Laurus nobilis* (Chapter 3). Next, for further assessment of the pit valve hypothesis, I examined the inter-vessel and non-inter-vessel pit area of a vessel, the hydraulic conductivity across inter-vessel pits (Chapter 4), the pressure in the refilling vessel during the vessel lumen refilling and the hydraulic conductivity between this vessel and surrounding parenchyma cells (Chapter 5). Current-year stems of three angiosperm species (*Acer rufinerve*, *M. australis* and *Vitis coignetiae*) were used in chapter 4, and those of *M. australis* and *L. nobilis* were used in chapter 5. Based on these results, I discussed the xylem refilling under negative pressures in chapter 6.

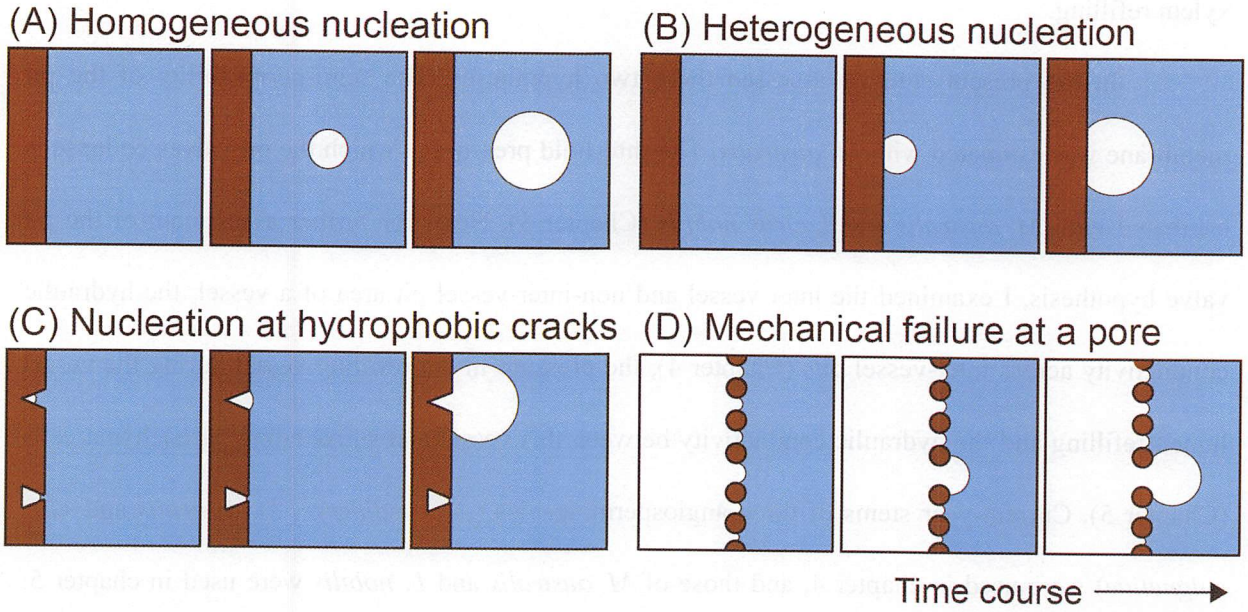

Figure 1-1. Four hypotheses for the nucleation of cavitation in the xylem conduits. (A) Homogeneous nucleation needs the spontaneous generation of a void in liquid water and a random process requiring thermal motion of the water molecules. (B) Heterogeneous nucleation is similar to homogeneous nucleation except that the generation of a void occurs on the conduit wall. (C) Air-seeding through a hydrophobic crack occurs when a stable air bubble remains at the base of a crack in the wall of a xylem conduit. When the liquid pressure (xylem pressure) decreases enough the bubble is drawn out of the crack. (D) Air-seeding through a pore occurs when the pressure difference across the meniscus is enough to allow the meniscus to overcome surface tension and pass through the pore. The air-seeding hypothesis supposes the pore to be in the inter-conduit pit membrane. See text or Tyree (1997) for detail.

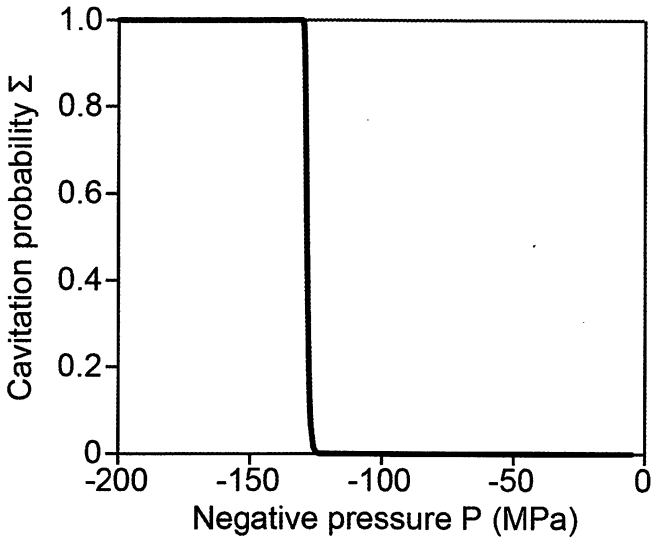

Figure 1-2. Cavitation probability as a function of pressure. The cavitation probability in a conduit with 100 μm in diameter and 1 m in length was calculated using Eq. 1-14, when t = 3 year and T = 20°C. P_n was neglected for the calculation because the vapor pressure is negligibly small compared with the negative pressure which occurs cavitation. The probability increases drastically as the pressure in the liquid water decreases.

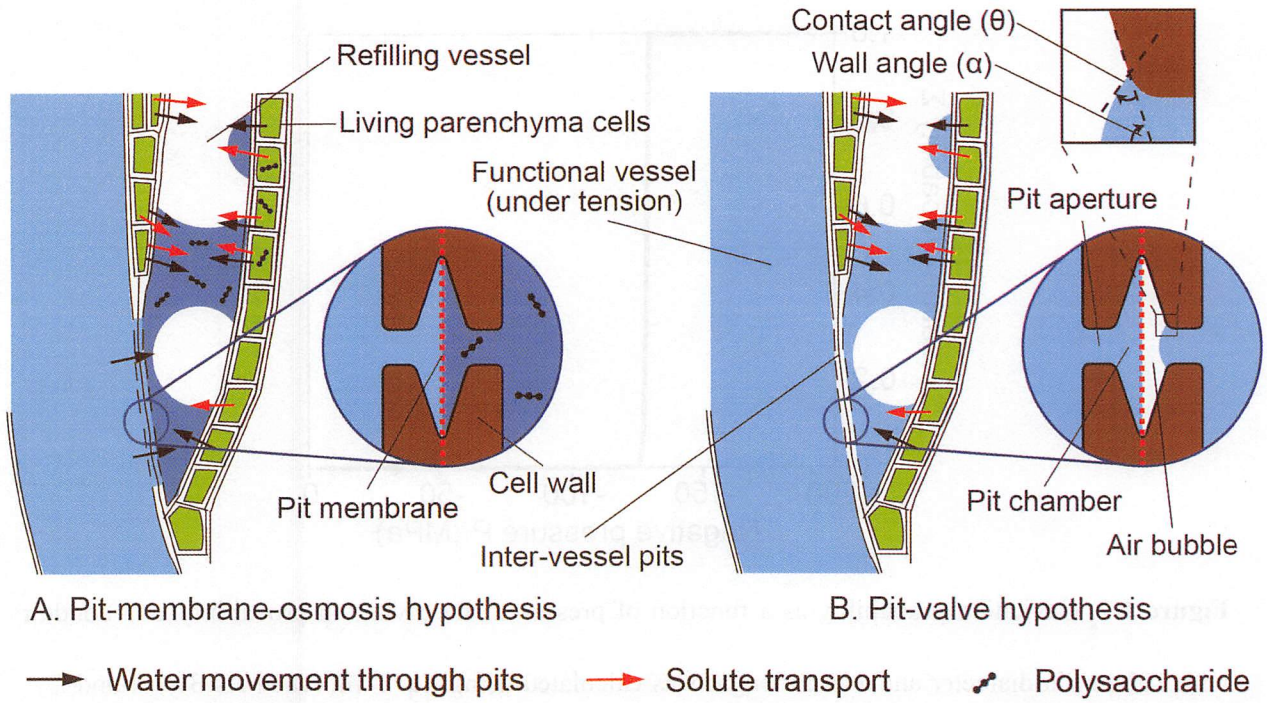

Figure 1-3. Schematic illustration of the two hypotheses for the mechanism preventing water in a refilling vessel from being drawn up by the surrounding vessels under negative pressure. A, Pit-membrane-osmosis hypothesis. This hypothesis assumes that polysaccharides with high molecular masses are released from xylem parenchyma cells into the refilling vessel lumen. The pit membrane functions as a semi-permeable membrane for the polysaccharides. If an adequate amount of the polysaccharides is transported into the refilling vessel, the water potential of refilling vessel sap decreases, and is more negative than that of the sap in the surrounding functional vessels. B, Pit-valve hypothesis. This hypothesis assumes that gas in each pit chamber can isolate water in the refilling lumen from the surrounding water. Given that the walls in the pits are moderately hydrophilic and that the pit chamber has a flared shape, a pressure difference between the gas in the pit chamber and the water in the refilling vessel due to surface tension is generated in the direction of the vessel lumen. The maximum force of this surface tension is calculated from the contact angle (θ) and the wall angle (α). As long as the positive pressure of the sap in the refilling vessels does not exceed the force due to this surface tension, the gas in the pit chamber is below the atmospheric pressure, and will be stable.

REFERENCES

Anderegg WRL, Berry JA, Smith DD, Sperry JS, Anderegg LDL, Field CB. 2012. The roles of hydraulic and carbon stress in a widespread climate-induced forest die-off. *Proceedings of the National Academy of Sciences* **109**, 233-237.

Balibar S, Caupin, F. 2006. Nucleation of crystals from their liquid phase. *Comptes Rendus Physique*, 7, 988-999.

Blander M, Katz J. 1975. Bubble nucleation in liquids. *AIChE Journal.* **21**, 833-848

Brodersen CR, Choat B, Chatelet DS, Shackel KA, Matthews MA & McElrone AJ. 2013. Xylem vessel relays contribute to radial connectivity in grapevine stems (*Vitis vinifera* and *V. arizonica*; Vitaceae). *American Journal of Botany*, **100**, 314-321

Brodersen CR, McElrone AJ, Choat B, Matthews MA, Shackel KA. 2010. The dynamics of embolism repair in xylem: *in vivo* visualizations using high-resolution computed tomography. *Plant Physiology* **154**, 1088-1095.

Choat B, Ball M, Luly J, Holtum J. 2003. Pit membrane porosity and water stress-induced cavitation in four co-existing dry rainforest tree species. *Plant Physiology* **131**, 41-48.

Choat B, Cobb AR, Jansen S. 2008 Structure and function of bordered pits: new discoveries and impacts on whole-plant hydraulic function. *New Phytologist*, **177**, 608-626.

Choat B, Jansen S, Zwieniecki MA, Smets E, Holbrook NM. 2004. Changes in pit membrane porosity due to deflection and stretching: the role of vestured pits. *Journal of Experimental Botany* **55**, 1569-1575.

Cochard H, Cruiziat P, Tyree MT. 1992. Use of positive pressures to establish vulnerability curves further support for the air-seeding hypothesis and implications for pressure-volume analysis. *Plant Physiology*, **100**, 205-209.

Dixon HH, Joly J. 1894. On the ascent of sap. Proceedings of the Royal Society of London, **57**, 3-5.

Doyle JA, Endress PK. 2000. Morphological phylogenetic analysis of basal angiosperms: comparison and combination with molecular data. *International Journal of Plant Sciences*,

161, 121-153.

Esau K. 1977. Anatomy of seed plants (2nd ed.). John Wiley and Sons, New York.

Feild TS, Arens NC. 2005. Form, function and environments of the early angiosperms: merging extant phylogeny and ecophysiology with fossils. *New Phytologist*, **166**, 383-408.

Feild TS, Zweiniecki MA, Brodribb T, Jaffré T, Donoghue MJ, Holbrook NM. 2000. Structure and function of tracheary elements in Amborella trichopoda. *International Journal of Plant Sciences*, **161**, 705-712.

Hacke UG, Sperry JS. 2003. Limits to xylem refilling under negative pressure in *Laurus nobilis* and *Acer negundo*. *Plant, Cell & Environment*, **26**, 303-311.

Hacke UG, Sperry JS, Pittermann J. 2004. Analysis of circular bordered pit function II. Gymnosperm tracheids with torus-margo pit membranes. *American Journal of Botany*, **91**, 386-400.

Hacke UG, Sperry JS, Wheeler JK, Castro L. 2006. Scaling of angiosperm xylem structure with safety and efficiency. *Tree physiology*, **26**, 689-701.

Hargrave KR, Kolb K.J, Ewers FW, Davis SD. 1994. Conduit diameter and drought-induced embolism in *Salvia mellifera* Greene (Labiatae). *New Phytologist*, **126**, 695-705.

Hayward ATJ. 1970. Mechanical pump with a suction lift of 17 metres. *Nature*, **225**, 376-377.

Holbrook NM, Zwieniecki MA. 1999. Embolism repair and xylem tension: do we need a miracle? *Plant Physiology*, **120**, 7-10.

Jarbeau JA, Ewers FW, Davis SD. 1995. The mechanism of water-stress-induced embolism in two species of chaparral shrubs. *Plant, Cell & Environment*, **18**, 189-196.

Kursar TA, Engelbrecht BMJ, Burke A, Tyree MT, Ei Omari B, Giraldo JP. 2009. Tolerance to low leaf water status of tropical tree seedlings is related to drought performance and distribution. *Functional Ecology*, **23**, 93-102.

Lambers H, Chapin FS, Pons TL. 2008. Plant Physiological Ecology. Springer New York.

Liese W, Bauch J. 1967. On the closure of bordered pits in conifers. *Wood Science and Technology*, **1**,

1-13.

Nardini A, Gullo MAL, Salleo S. 2011. Refilling embolized xylem conduits: is it a matter of phloem unloading?. *Plant Science*, **180**, 604-611.

Ogasa M, Miki N, Yoshikawa K. 2010. Changes of hydraulic conductivity during dehydration and rehydration in *Quercus serrata* Thunb. and *Betula platyphylla* var. *japonica* Hara: the effect of xylem structures. *Tree Physiology*, **30**, 608-617.

Pettersen MS, Balibar S, Maris HJ. 1994. Experimental investigation of cavitation in superfluid ^{4}He. *Physical Review B*, **49**, 12 062-12 070.

Pittermann J, Sperry JS, Hacke UG, Wheeler JK, Sikkema EH. 2005. Torus-margo pits help conifers compete with angiosperms. *Science*, **310**, 1924-1924.

Pickard WF. 1981. The ascent of sap in plants. *Progress in biophysics and molecular biology*, **37**, 181-229.

Sachs IB. 1963. Torus of bordered-pit membrane in conifers. *Nature*, **198**, 906–907.

Salleo S, Gullo M, Paoli D, & Zippo M. 1996. Xylem recovery from cavitation-induced embolism in young plants of *Laurus nobilis*: a possible mechanism. *New Phytologist*, **132**, 47-56.

Salleo S, Lo Gullo MA, Trifilò P, Nardini A. 2004. New evidence for a role of vessel-associated cells and phloem in the rapid xylem refilling of cavitated stems of *Laurus nobilis* L. *Plant, Cell & Environment*, **27**, 1065-1076.

Scholander PF, Hammel HT, Bradstreet EA, Hemmingsen EA. 1965. Sap pressure in vascular plants. *Science*, **148**, 339–346

Secchi F, Zwieniecki MA. 2011. Sensing embolism in xylem vessels: the role of sucrose as a trigger for refilling. *Plant, Cell & Environment* **34**, 514-524.

Shane MW, McCully ME, Canny MJ. 2000. Architecture of branch-root junctions in maize: structure of the connecting xylem and the porosity of pit membranes. *Annals of Botany*, **85**, 613-624.

Scheenen TW, Vergeldt FJ, Heemskerk AM, Van As H. 2007. Intact plant magnetic resonance

imaging to study dynamics in long-distance sap flow and flow-conducting surface area. *Plant Physiology* **144**, 1157-1165.

Slatyer R. 1967. Plant-water relationships. London and New York.

Sperry JS. 2013. Cutting-edge research or cutting-edge artefact? An overdue control experiment complicates the xylem refilling story. *Plant, Cell & Environment*, **36**, 1916-1918.

Sperry JS, Holbrook NM, Zimmermann MH, Tyree MT. 1987. Spring filling of xylem vessels in wild grapevine. *Plant Physiology*. **83**, 414-417

Sperry JS, Nichols KL, Sullivan JE, Eastlack SE. 1994. Xylem embolism in ring-porous, diffuse-porous, and coniferous trees of northern Utah and interior Alaska. *Ecology*, **75**, 1736-1752.

Sperry JS, Tyree MT. 1990. Water-stress-induced xylem embolism in three species of conifers. *Plant, Cell & Environment*, **13**, 427-436.

Trifilò P, Raimondo F, Lo Gullo MA, Barbera PM, Salleo S, Nardini A. 2014. Relax and refill: xylem rehydration prior to hydraulic measurements favours embolism repair in stems and generates artificially low PLC values. *Plant, Cell & Environment*, **37**, 2491–2499.

Tyree MT. 1997. The cohesion-tension theory of sap ascent: current controversies. *Journal of Experimental Botany*, **48**, 1753-1765.

Tyree MT, Salleo S, Nardini A, Assunta Lo Gullo M, Mosca R. 1999. Refilling of Embolized Vessels in Young Stems of Laurel. Do We Need a New Paradigm? *Plant Physiology*, **120**, 11-22.

Tyree MT, Sperry JS. 1989. Vulnerability of xylem to cavitation and embolism. *Annual review of plant biology*, **40**, 19-36.

Tyree MT, Yang S. 1992. Hydraulic conductivity recovery versus water pressure in xylem of *Acer saccharum*. *Plant Physiology* **100**, 669-676.

Tyree MT, Zimmermann MH. 2002. Xylem Structure and the Ascent of Sap, Springer. Berlin, Germany.

Van der Bruggen B, Schaep J, Wilms D, Vandecasteele C. 1999. Influence of molecular size, polarity and charge on the retention of organic molecules by nanofiltration. *Journal of Membrane Science* **156**, 29-41.

Wei C, Tyree MT, Steudle E. 1999. Direct measurement of xylem pressure in leaves of intact maize plants. A test of the cohesion-tension theory taking hydraulic architecture into consideration. *Plant Physiology*, **121**, 1191-1205.

Wheeler JK, Huggett BA, Tofte AN, Rockwell FE, Holbrook NM. 2013. Cutting xylem under tension or supersaturated with gas can generate PLC and the appearance of rapid recovery from embolism. *Plant, Cell & Environment* **36**, 1938-1949.

Wheeler JK, Sperry JS, Hacke UG, Hoang N. 2005. Inter-vessel pitting and cavitation in woody Rosaceae and other vesselled plants: a basis for a safety versus efficiency trade-off in xylem transport. *Plant, Cell & Environment*, **28**, 800-812.

White RA. 1961. Vessels in roots of Marsilea. *Science* **133**, 1073–1074.

Zimmermann MH. 1983. Xylem structure and the ascent of sap. New York: Springer-Verlag.

Zwieniecki MA, Holbrook NM. 2000. Bordered pit structure and vessel wall surface properties. Implications for embolism repair. *Plant Physiology*, **123**, 1015-1020.

CHAPTER 2

Xylem refilling in stem xylem of *Morus australis* Poir.

ABSTRUCT

Xylem refilling is usually detected by the hydraulic measurements. However, the cutting without a preceding relaxing treatment may cause underestimation of the hydraulic conductivity in the test segments (cutting artifact). In this chapter, I prepared the test segments which would be free from this artifact, and measured the change in the hydraulic conductivities in such the segments. The excised shoots of mulberry (*Morus australis* Poir.) and the intact shoots of the potted mulberry trees were used for the experiments. By rehydration, the hydraulic conductivity significantly recovered both in the excised shoots and potted plants. I concluded that the xylem refilling occurred in mulberry stem xylem.

INTRODUCTION

In many studies, the refilling of the cavitated vessel under negative xylem pressure has been detected as the changes in the hydraulic conductivity in the excised test segments before and after rehydration (e.g., Ogasa *et al.*, 2010; Tyree *et al.*, 1999). However, it has been reported that severing xylem vessels under significant tension may introduce embolism into the xylem even when the excisions are made under water (the cutting artifact; Wheeler *et al.*, 2013). That is, the cutting without a preceding relaxation treatment would cause the underestimation of hydraulic conductivity in the test segments. They claimed that the recovery in the hydraulic conductivity observed for many species in the previous studies would not be attributed solely to the xylem refilling but, at least partly, to the underestimations of the hydraulic conductivities of the dehydrated samples. Wheeler *et al.* (2013) have recommended that xylem tension of the shoot should be relaxed by rewatering and cut gradually to avoid this artifact when the segments for the measurement were prepared.

In this chapter, I aimed at examining whether the xylem refilling under negative pressure occurs in the stem xylem of mulberry trees (*Morus australis* Poir.). For this purpose, I first examined the recovery of the hydraulic conductivities in the dehydrated stems cut under negative pressure (native samples) and the dehydrated stems cut after sufficient relaxation (relaxed samples). I also examined whether xylem refilling under negative pressure occurs in the intact shoots of the potted mulberry trees.

MATERIALS AND METHODS

Plant materials

The experiments were conducted on current-year shoots of mulberry (*Morus australis* Poir., Moraceae) excised from trees growing on the Hongo campus, the University of Tokyo (35° 42′ 48″ N, 139° 45′ 44″ E, 20 m a.s.l.) and on intact shoots in mulberry trees growing in pots. Mulberry is a deciduous tree species and stem xylems of these current-year shoots of mulberry had wide vessels. For the field mulberry, the mean hydraulic vessel diameter defined as $\Sigma D^5/\Sigma D^4$, where D is vessel

diameter (Sperry *et al.*, 1994), was 60.5 ± 4.00 μm (mean ± 1 SD, n = 8, Fig. 2-1). The maximum vessel length obtained by the air infiltration technique (Greenidge, 1952) was 39 ± 4.0 cm (mean ± 1 SD, n = 4). The vessel length distribution in the stems of the field mulberry obtained by the silicone injection method (Christman *et al.*, 2009) is shown in Fig. 2-2. For the experiments with the excised mulberry stem, current-year shoots of the field mulberry longer than 1 m were sampled at night when their transpiration rates were low. The shoots were cut at their bases, put into plastic bags, and brought to the laboratory. These shoots were recut under water 3 cm above the cut ends and allowed hydration overnight in the plastic bags with their cut ends in the water.

For the experiments with the potted mulberry trees, I relaxed the negative pressure in the shoots and then prepared the test segments (for detail see below). Xylem refilling in excised shoots was assessed in early October 2011 for native samples and in late September 2013 for relaxed samples. Xylem refilling in potted mulberry was assessed in September 2015.

Embolism repair in the excised mulberry stem

Xylem refilling in the excised mulberry shoot was quantified by changes in the hydraulic conductivity before and after rehydration. For the excised shoots, the capillary rise can contribute to xylem refilling. Thus, considering the capillary force and gravity force, the test segments were excised from the height at which positive pressure by the capillary force hardly affected xylem refilling and the sap in the functional vessels was under negative pressure (see Results).

For the experiments in the stems cut under native pressure, eleven current-year shoots with leaves longer than 1 m were hydrated overnight as described above. Then, the cut ends of the stems were sealed with vacuum grease (Dow Corning Toray High Vacuum Grease, Dow Corning Toray Co., Ltd., Tokyo, Japan) and covered with paraffin film to prevent air entry and evaporation from the cut surface. The shoots were placed on a laboratory bench and allowed dehydration in room air for 1-1.5 h. For measurement of water potential of the stem xylem, the dehydrated shoots were placed in the plastic bags for 30 min to equilibrate water potential of the leaves with that of the stem xylem.

Subsequently, the leaves were excised and their xylem pressure was measured with a pressure chamber (Model 3000; Soilmoisture Equipment Corp., Santa Barbara, CA, USA). These shoots were desiccated to a stem xylem pressure of −1.92 ± 0.265 MPa (mean ± 1 SD, n = 11). Then, for six out of eleven dehydrated shoots, the 20 cm long stem segment was cut at more than 35 cm above the stem base without a relaxation treatment, trimmed with a fresh razor blade. Then, the leaves on the segment were eliminated. The other five shoots were recut at 3 cm from the basal cut surfaces under water and placed vertically in water (5 cm in depth). The whole shoots and the water container were covered with plastic bags for 3 h. The shoots were taken out from the water reservoir, and placed in the plastic bags. After 30 min of equilibration, their xylem pressure was assessed by measuring xylem negative pressure of their leaves. The test segments were prepared under the native pressures as described for the dehydrated shoots.

Wheeler *et al.* (2013) have recommended that when the segments for the measurement are prepared, xylem tension of the shoot should be relaxed by rewatering and cut gradually to avoid the cutting artifact. However, a recent report by Trifilò *et al.* (2014) showed that even a relatively short-term rewatering for 2 min can cause some xylem refilling. This brings about overestimation of the hydraulic conductivity (relaxation artifact).

In the experiments with the stems cut after relaxation, I excised test segments at a low tension, but without long-term relaxation, to avoid these artifacts (See also Fig. 2-3). Ten excised shoots were desiccated to a stem xylem pressure of –2.03 ± 0.146 MPa (mean ± 1 SD, n = 10). Then, for five out of ten dehydrated shoots, the hydraulic conductivity was determined (see below). The other shoots were recut at 3 cm from the basal cut surfaces under water and placed vertically in water (5 cm in depth) for 3 h, during which the whole shoots the shoots were covered with plastic bags. The rehydrated shoots were taken away from water and kept in the plastic bags. After 30 min of equilibration, their xylem pressure was assessed by measuring xylem negative pressure of their leaves. The leaves were sufficiently wetted, and the shoots were covered with the plastic bags. The shoot base of 5 cm was removed under water in two 2.5 cm cuts, with a 5 s interval between the cuts, and the

shoot was rewatered for 1 min to relax the sap tension. The stem was cut little by little, so that xylem tension at each cut position would be sufficiently relaxed. The leaf water potential measured with a pressure chamber was –0.27 ± 0.084 MPa (mean ± 1 SD, n = 5) for the dehydrated shoots and –0.066 ± 0.024 MPa for the rehydrated shoots (mean ± 1 SD, n = 5). All leaves on the shoot were then eliminated, and 30 cm of the stem base was removed under water in several 3 cm cuts, with approximately 5 s intervals between the cuts. The stem was cut at more than 60 cm above the cut end under water. Both ends of the segments were removed under water in three about 3 cm cuts (in total about 10 cm), with 5 s intervals between the cuts. The distance between the initial cut position for relaxation of the sap tension and the test segment was at least greater than one maximum vessel length. Mulberry stems produce latex and their laticifers are in barks. Then, I removed 1 cm bark segments from both cut ends of the excised 40 cm long stem segments (more than the average maximum vessel length) and trimmed the segments with a fresh razor blade.

Embolism repair in the stems of potted mulberry

For the assessment of xylem refilling in the stems of potted mulberry, the test segments were prepared at a low tension without long-term rewatering as follows. For the measurement of water potential of the stem xylem, the some attached leaves were covered with aluminum tape for 30 min to equilibrate the water potential of the leaves with that of the stem xylem. Subsequently, the leaves were excised and their xylem pressure was measured with the pressure chamber. These shoots were desiccated to a stem xylem pressure of –1.36 ± 0.0998 MPa (mean ± 1 SD, n = 10). Then, for six out of ten dehydrated plants, the test segments were excised. The rest four plants were rehydrated for 3 h, and then their xylem pressure was assessed by measuring xylem negative pressure of their leaves sealed with aluminum tape. The attached leaves in these six dehydrated and four rehydrated shoots were sufficiently wetted, and were sliced under water with a fresh razor blade little by little from periphery of the leaf blades to bases of the petioles to allow the xylem tensions to relax rapidly. Then, the apical side of the stem was cut under water, and the stem was rewatered for 1 min. The stem was cut at more

than 60 cm below the cut end under water using a funnel. Both ends of the segments were removed under water in three about 3 cm cuts (in total about 10 cm), with 5 s intervals between the cuts. Then, I removed 1 cm bark segments from both cut ends of the excised 40 cm long stem segments and trimmed the segments with a fresh razor blade.

Hydraulic conductivity measurements

The stem segment prepared was connected to silicone tubes filled with 20 mM KCl solution that had been filtered through a 0.2 μm membrane filter (Sartorius, Göttingen, Germany). Hydraulic conductivity of the stem segment ($k_{h,\ embolized}$, kg m s^{-1} MPa^{-1}) was measured by the balance method as described in Sperry *et al.* (1988). Then, the segment was flushed with 20 mM KCl solution at a positive pressure of 0.3 MPa for 15 min to remove native embolism and maximal hydraulic conductivity ($k_{h,\ max}$, kg m s^{-1} MPa^{-1}) was measured. Xylem dysfunction due to embolism was assessed as the percentage loss of conductivity (PLC):

$$PLC = (k_{h,\ max} - k_{h,\ embolized}) / k_{h,\ max} \times 100 \quad (2\text{-}1).$$

RESULTS

Xylem refilling on excised shoots

To test the cutting artifact and to confirm whether xylem refilling under negative pressure occurred in the stems of the excised shoots in mulberry, the changes in PLC before and after rehydration of the current-year stem segments cut under water at native xylem tensions (native samples) or after pressure relaxation as induced by xylem rewatering (relaxed samples) (Fig. 2-4).

When the hydrated shoots were desiccated to the stem xylem pressure of –1.92 ± 0.265 MPa (mean ± 1 SD, n = 11), PLC the in native samples was 66.7 ± 16.6% (mean ± 1 SD, n = 6). After 3 h of rehydration, stem xylem pressure recovered to –0.34 ± 0.17 MPa (mean ± 1 SD, n = 5). PLC also declined to 24.9 ± 17.7% at 3 h after the onset of rehydration.

On the other hand, when the shoots were desiccated to the stem xylem pressure of –2.03 ±

0.146 MPa (mean ± 1 SD, n = 10), PLC in the relaxed stem segments was 38.6 ± 6.62% (mean ± 1 SD, n = 5). After 3 h of rehydration, stem xylem pressure recovered to –0.27 ± 0.056 MPa (mean ± 1 SD, n = 5). PLC also declined to 6.62 ± 9.01% at 3 h after the onset of rehydration.

Because the excised shoots were used for the measurements, the capillary rise might contribute to xylem refilling. Considering the distribution of vessel diameters in the stem xylem (Fig. 2-1), hydraulic conductivity (k_h) in stems refilled only by the capillary force was estimated as a function of the height from the surface of the water reservoir by the Hagen-Poiseuille's equation. Then, recovery of k_h at a given height was expressed as relative hydraulic conductivity to the maximum value (Fig. 2-5). Assuming that the maximum hydraulic conductivity is constant along the height, the recovery of hydraulic conductivity in the segments used for the hydraulic conductance measurements due to the capillary rise can be estimated by the inverse of the average reciprocal of the recovery of k_h along the measurement stem segments. The value was calculated to be only 2.80 ± 0.879% (mean ± 1 SD, n = 8). Therefore, recovery of stem conductivity in mulberry stem should be driven by factors other than the capillary force.

Xylem refilling on potted mulberry shoots

When the mulberry shoots in the potted plants were desiccated to the stem xylem pressure of –1.37 ± 0.121 MPa (mean ± 1 SD, n = 6), PLC in the relaxed stem segments was 67.5 ± 12.9% (mean ± 1 SD, n = 6). After 3 h of rehydration, stem xylem pressure recovered to –0.39 ± 0.25 MPa (mean ± 1 SD, n = 4). PLC also declined to 41.6 ± 15.8% (mean ± 1 SD, n = 4) at 3 h after the onset of rehydration for 3 h. There was significant difference in PLC between the rehydrated and the dehydrated samples (t-test, P = 0.0214).

DISCUSSION

I found that the hydraulic conductivities of dehydrated shoots recovered even when the test segment excised after relaxation of the xylem pressure (Figs. 2-4 and 2-6). Thus, I concluded that xylem

refilling occurred in mulberry.

Xylem refilling in excised mulberry shoots

When the shoots were dehydrated to –1.94 ± 0.187 MPa (mean ± 1 SD, n = 11), the stem pressure of PLC in the native samples were significantly different from that in relaxed samples. Thus, the different preparations of the test segments certainly caused the different results. I excised relaxed segments with relaxation time of 1 min because relaxation for 2 min would cause xylem refilling, resulting in another erroneous results (relaxation artifact, Trifilò *et al.*, 2014). Nevertheless, the present relaxation treatments might cause erroneous results due to partial rehydration. Despite all these uncertainties, the hydraulic conductivity further increased by rehydration even when the present relaxation method was used (t-test, $P < 0.01$). By contrast, it might be possible that the rewatering for only 1 min could not relax the xylem pressure sufficiently, also resulting in the erroneous results as described as the cutting artifact. However, because the speed of sound in water is very high, if the sap is connected with the water reservoir, the pressure in the xylem sap will be relaxed immediately. Thus, when the initial long segments were cut under water, almost immediate relaxation would occur. At this moment, embolism due to entry of air in the stem might occur near the cut surface. However, when these segments were recut gradually under water, further entry of gases into the xylem vessels would not occur.

In the excised shoots, xylem refilling by a capillary rise can occur. However, assuming that a contact angle against a vessel wall was 42°, our estimation indicated that capillary rise results in only 2.80% recovery of total xylem conductivity. Salleo *et al.* (2004) implied that embolism repair would not occur in the short stem segments because excisions of the stem inhibit the supplies of water and sugars from phloem. They also indicated that the inhibitory effect of stem girdling on refilling process was reduced with the increase in the distance between the embolized vessels and the girdling position. However, in the present study, the segments for the conductance measurement were sufficiently distant (more than 45 cm) from the cut ends. Thus, it is highly probable that we actually observed

xylem refilling.

Xylem refilling in potted mulberry trees

In the excised shoots, because the sap in the functional vessels can be connected directly with the water reservoir, the stem xylem pressure might not be sufficiently negative compared with the xylem pressure at which the intact plants cause the xylem refilling actually. Then, I also used the potted plants to confirm the xylem refilling in the mulberry trees. Even in the potted plants, I found that xylem refilling occurred (Fig. 2-6). The percent loss of conductivity (PLC) declined from 67.5% to 41.6% by rehydration for 3 h.

Although the stem xylem pressures in the dehydrated potted plants were less negative than those in the dehydrated excised shoots, PLC in the potted plants were larger than that in the excised shoots. The potted plants might suffer from the drought-stress frequently because of the limited soil volumes in the pots. Thus, the cavitation event might also occur in the potted plants more frequently. This would cause the chronic cavitation in some vessels, resulting in raising the standard PLC.

From the present data, I confirm the xylem refilling occurred in the stem xylem of mulberry. Mulberry stem xylem has axial vasicentric parenchyma (Fig. 2-7), which should play a significant role in refilling (Salleo *et al.*, 2004).

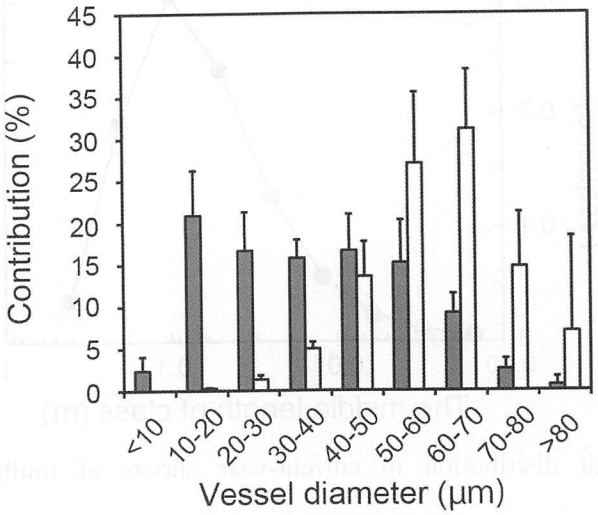

Figure 2-1. Calculated contribution to total hydraulic conductivity of each vessel diameter class. Bars show percentages relative to the sum of all vessel diameters to the fourth power (% ΣD^4). Error bars represent ± SD (n = 8).

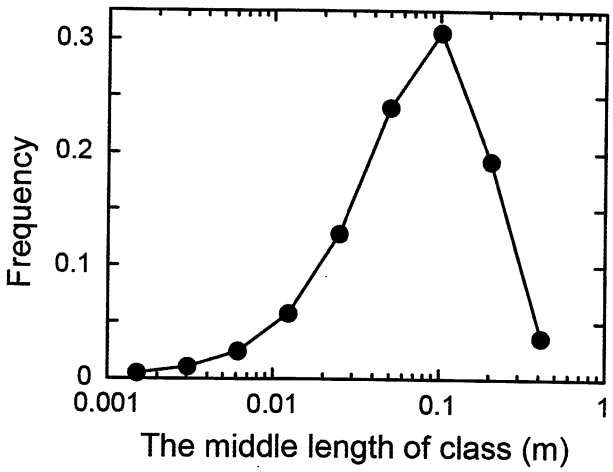

Figure 2-2. Vessel-length distribution in current-year shoots of mulberry. The vessel-length distribution was obtained using the silicone injection method (Christman *et al.*, 2009).

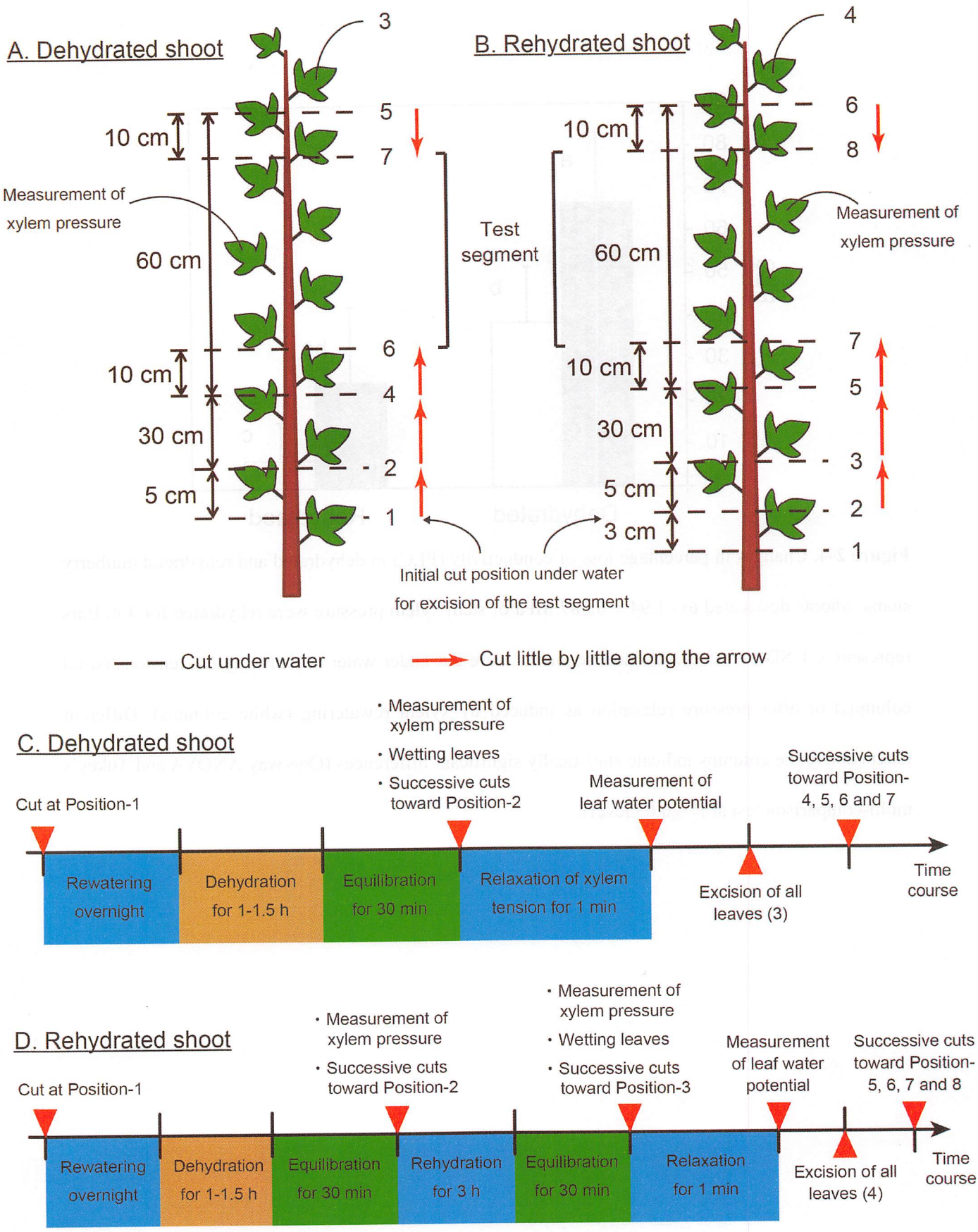

Figure 2-3. Relaxation protocol for PLC measurements in dehydrated shoots (A) and rehydrated shoots (B). The shoots were cut in serial order. C, D: The time courses of processes for preparation of test segments. See text for details.

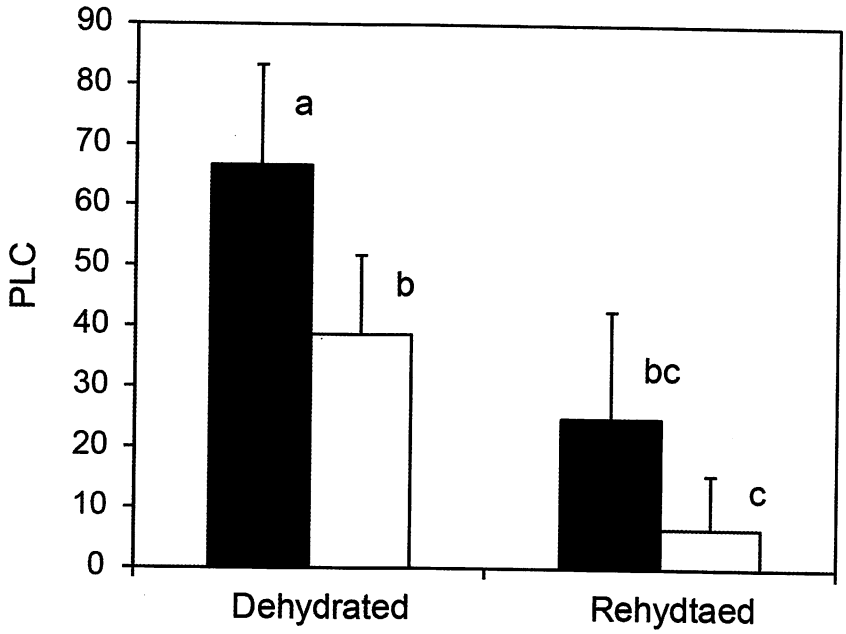

Figure 2-4. Changes in percentage loss of conductivity (PLC) in dehydrated and rehydrated mulberry stems. Shoots desiccated to –1.94 ± 0.187 MPa of stem xylem pressure were rehydrated for 3 h. Bars represent ± 1 SD (n = 5-6). The test segments were cut under water at native xylem tensions (solid columns) or after pressure relaxation as induced by xylem rewatering (white columns). Different letters above the columns indicate statistically significant differences (One-way ANOVA and Tukey's multi-comparison test at $P = 0.05$ level).

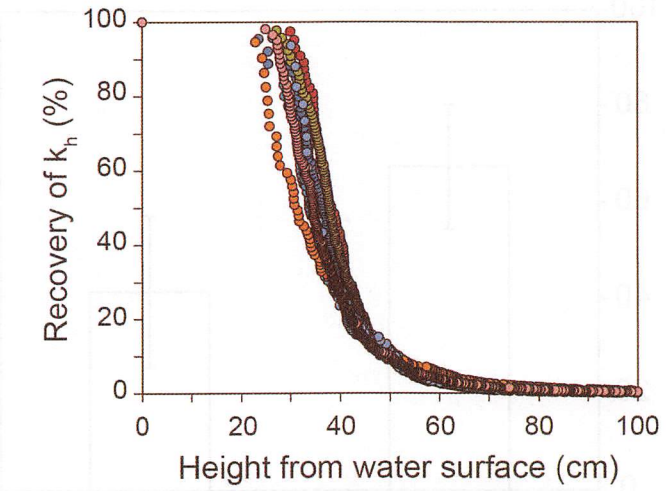

Figure 2-5. Recovery of the stem hydraulic conductivity (k_h) by capillary force. Assuming the contact angle against the vessel wall is 42°, the height of the capillary rise in each vessel can be calculated using capillary equation. Then, considering the distribution of vessel diameters in the stem xylem, relative hydraulic conductivity in stems refilled only due to the capillary force to the maximum value (Recovery of k_h) was obtained by the Hagen-Poiseuille's equation as a function of the height from the surface of the water reservoir. Each symbol represents a different stem sample.

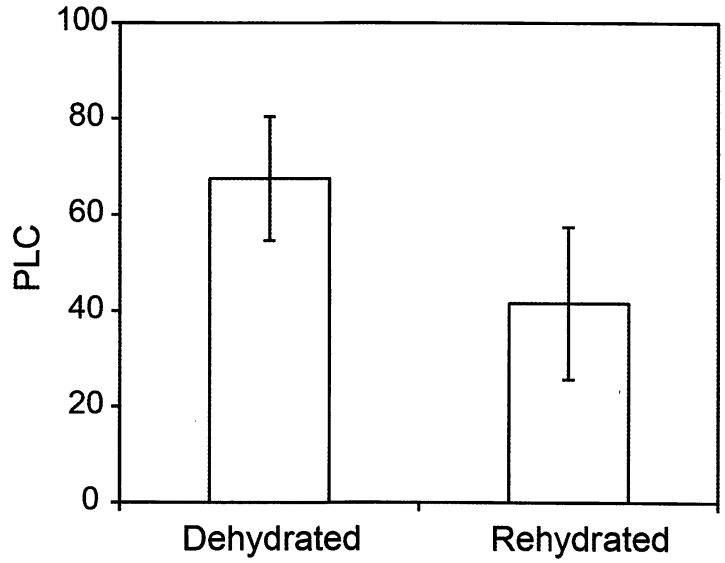

Figure 2-6. Changes in percentage loss of conductivity (PLC) in dehydrated and rehydrated stems of potted mulberry trees. Shoots desiccated to −1.36 ± 0.0998 MPa of stem xylem pressure were rehydrated for 3 h. Bars represent ± 1 SD (n = 6 or 4).

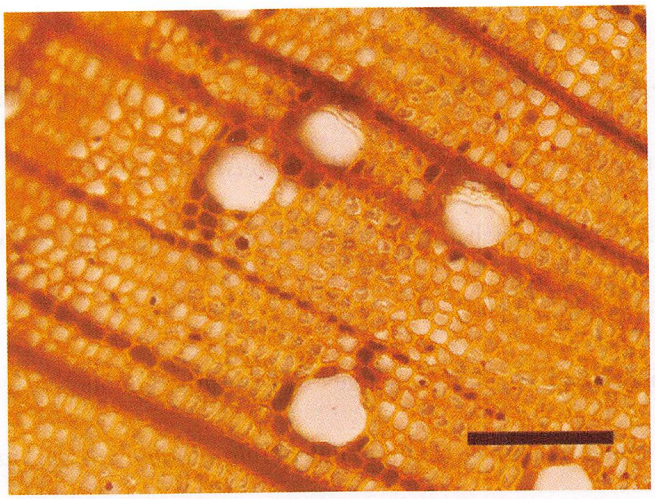

Figure 2-7. Cross-section of a current-year stem showing wood ray and vasicentric cells containing starch granules stained in dark blue with Lugol solution. Scale bar is 100 µm.

REFERENCES

Christman MA, Sperry JS, Adler FR. 2009. Testing the 'rare pit' hypothesis for xylem cavitation resistance in three species of *Acer*. *New Phytologist* **182**, 664-674.

Greenidge KNH. 1952. An approach to the study of vessel length in hardwood species. *American Journal of Botany* **39**, 570-574.

Ogasa M, Miki N, Yoshikawa K. 2010. Changes of hydraulic conductivity during dehydration and rehydration in *Quercus serrata* Thunb. and *Betula platyphylla* var. *japonica* Hara: the effect of xylem structures. *Tree Physiology*, **30**, 608-617.

Salleo S, Lo Gullo MA, Trifilò P, Nardini A. 2004. New evidence for a role of vessel-associated cells and phloem in the rapid xylem refilling of cavitated stems of *Laurus nobilis* L. *Plant, Cell & Environment* **27**, 1065-1076.

Sperry JS, Donnelly JR, Tyree MT. 1988. A method for measuring hydraulic conductivity and embolism in xylem. *Plant, Cell & Environment* **11**, 35-40.

Trifilò P, Raimondo F, Lo Gullo MA, Barbera PM, Salleo S, Nardini A. 2014. Relax and refill: xylem rehydration prior to hydraulic measurements favours embolism repair in stems and generates artificially low PLC values. *Plant, Cell & Environment*, **37**, 2491–2499.

Tyree MT, Salleo S, Nardini A, Assunta Lo Gullo M, Mosca R. 1999. Refilling of Embolized Vessels in Young Stems of Laurel. Do We Need a New Paradigm? *Plant Physiology*, **120**, 11-22.

Wheeler JK, Huggett BA, Tofte AN, Rockwell FE, Holbrook NM. 2013. Cutting xylem under tension or supersaturated with gas can generate PLC and the appearance of rapid recovery from embolism. *Plant, Cell & Environment* **36**, 1938-1949.

CHAPTER 3

Assessment of two hypotheses for the mechanism for overcoming surrounding negative pressure during refilling embolized vessels

ABSTRACT

Two hypotheses (the pit-membrane-osmosis hypothesis and the pit-valve hypothesis) have been proposed to explain the mechanism preventing the refilling vessel water from being lost to the surrounding functional vessels under negative pressure. Here, using the single-vessel method, I assessed these hypotheses in shoots of mulberry (*Morus australis* Poir.). For assessment of the pit-valve hypothesis, shoots of laurel (*Laurus nobilis* L.) was also used. To examine the pit-membrane-osmosis hypothesis, I estimated the semi-permeability of pit membranes for molecules of various sizes and found that the pit membranes were not semi-permeable to polyethylene glycol of molecular mass less than 20,000. For the pit-valve hypothesis, I formed pit-valves in the inter-vessel pits in the short shoot segments and measured the maximum liquid pressure at which gases in bordered pits could be retained *in vivo*. The threshold pressure ranged 0.025-0.10 MPa in mulberry and 0.050-0.150 MPa in laurel. These values matched the theoretical value calculated from the geometry of the pit chamber (0.0692-0.101 MPa in mulberry and 0.125-0.179 MPa in laurel). The results suggest that gas in the pits is retained by surface tension, even under substantial positive pressure, while the molecule size required for the pit-membrane-osmosis mechanism in mulberry would be unrealistically large. I also found out that all the pit valves did not collapse simultaneously, which indicates the possibility that re-cavitation of the refilling vessel occurs.

INTRODUCTION

Two hypotheses have been proposed to explain the mechanism preventing the refilling vessel water from being lost to the surrounding functional vessels under the negative pressures. The pit-membrane-osmosis hypothesis (Hacke and Sperry, 2003) proposes that the xylem parenchyma cells release polysaccharides that are impermeable to the inter-vessel pit membranes into the refilling vessel; this osmotically counter-acts the negative pressure, thereby allowing the vessel to refill (Fig. 1-3A). The pit-valve hypothesis (Holbrook and Zwieniecki, 1999) proposes that gas trapped within inter-vessel bordered pits isolates the refilling vessel water from the surrounding functional vessels (Fig. 1-3B).

In this chapter, I assessed these two hypotheses for the mechanism of refilling of the embolized xylem vessels surrounded by the vessels under negative pressure using shoots of mulberry (*Morus australis* Poir.). First, the pit-membrane-osmosis hypothesis was examined by estimating the semi-permeability of the pit membranes to the molecules with various sizes. I also examined the pit-valve hypothesis by measuring the pressure of xylem sap at which the pit valve collapsed by gas dissolution in the pit chamber. For assessments of the pit valve hypothesis, shoots of laurel (*Laurus nobilis* L.), for which xylem refilling has been reported (Salleo *et al.*, 2004), was also used.

MATERIALS AND METHODS

Plant materials

For the pit-membrane-osmosis hypothesis, the experiments were conducted with current-year shoots of mulberry (*Morus australis* Poir., Moraceae) excised from trees growing on the Hongo campus, the University of Tokyo (35° 42′ 48″ N, 139° 45′ 44″ E, 20 m a.s.l.). Besides the mulberry shoots, current-year shoots of laurel (*Laurus nobilis* L.) grown in pots were also used for assessment of the pit-valve hypothesis. Measurements of the reflection coefficient of the pit membranes were conducted between August and November 2011. Scanning electron microscope (SEM) observations of stem xylem were made in October 2011 for mulberry stems and November 2013 for laurel stems.

Measurements of pit-valve stability were made in December 2011, May 2012 and May 2013 for mulberry stems and February 2013 for laurel stems. In Tokyo, the minimum air temperature in December 2011 was 1.5°C, and plants hardly experienced the subfreezing temperature in December (Japan Meteorological Agency, http://www.jma.go.jp/jma/indexe.html). Therefore, the mulberry stems examined would not experience excessive frost damage.

Reflection coefficient of the pit membranes

The reflection coefficient is the measure of the degree of semi-permeability of the membrane and ranges from one (no passage, ideal semi-permeable membrane) to zero (passage not hindered). The reflection coefficient was measured to assess the semi-permeability of the pit membranes. Solute flux across a membrane, at a distance x (m) from the membrane surface, forced by diffusion and mass-flow, J_s (mol m^{-2} s^{-1}), is given by:

$$J_s = -\overline{P}\ dc/dx + (1 - \sigma)\ J_v\ c \qquad (3\text{-}1),$$

where $\overline{P}$ (m^2 s^{-1}) is the local solute permeability coefficient, σ is the reflection coefficient, J_v (m s^{-1}) is the solvent flux, and c (mol m^{-3}) is the solute concentration at x (Spiegler and Kedem, 1966). By integrating with respect to x and introducing the solute permeability coefficient P_s ($P_s = \overline{P}/\Delta x$, Δx is the membrane thickness (m)), I obtain:

$$c''/c' = (1 - \sigma) / (1 - \sigma F) \qquad (3\text{-}2),$$

where

$$F = \exp\{-(1 - \sigma)\ J_v / P_s\} \qquad (3\text{-}3),$$

c' is the solute concentration in the upstream side, and c'' is the solute concentration in the downstream side (i.e., $c'' = J_s / J_v$).

If the pit membranes limit solute movement, the reflection coefficient will be above zero and the solute concentration in the solution after passing through the pit membranes (downstream side) is lower than that of the upstream solution. Moreover, according to Eqs. 3-2 and 3-3, the solute concentration in the downstream solution (c'') approaches $(1 - \sigma)\ c'$ as the flow rate increases because

F approaches zero.

To calculate the reflection coefficient of the pit membranes, the flow rate of the solution through the pit membranes was gradually increased by increasing the pressure applied. The reflection coefficient was determined as the asymptotic value of $1 - c'' / c'$.

I measured the reflection coefficients of the pit membranes for sucrose and polyethylene glycol (PEG) of different molecular masses. Stem segments (about 4 cm long and about 8 mm in diameter) were cut from the shoots and trimmed with a fresh razor blade. Microcapillary tubes with the inner diameter of 0.6 mm (G-1, NARISHIGE, Tokyo, Japan) were pulled with a horizontal-type puller (PC-10, NARISHIGE). In mulberry, current-year stems have secondary xylem of diffuse-porous-like vessel distribution, while, from the second growing season, secondary xylem shows ring-porous vessel distribution (Fig. 3-1). The tip of a microcapillary (capillary-A) was inserted into an open lumen of a wide single vessel (50-80 μm in diameter) by the aid of a micromanipulator (M-152, NARISHIGE), under a stereo microscope (SMZ, Nikon, Tokyo, Japan). Subsequently, the cut end of the stem (side-A) was sealed with fast-setting acrylic glue (Loctite407, Henkel Japan, Tokyo, Japan).

The capillary-A was supported by three glass rods that were glued to the side of the stem segment (Zwieniecki *et al.*, 2001). For detection of the other vessel that diverged from the vessel via the bordered pits (pit-passing vessel, PPV), acid fuchsin dye (0.2% in deionized water) filtered through 0.2 μm filter was flushed from the capillary-A at 0.6 MPa using a N_2-cylinder for 10 s (Fig. 3-2A). At the same time, the opposite end of the segment (side-B) was kept under water to prevent the cut surface of side-B from being stained with dye that flowed out from side-B. After the pressure release, the cut surface of side-B was carefully observed using the stereo microscope, and the stained vessels were counted. When the number was greater than two, then the stem segment length was shortened until the number was reduced to two. In most cases, the segment was eventually shortened to about 2 cm. The open vessel (OV) and PPV were detected by sending air using a syringe connecting to capillary-A via a silicone tube. One of the two stained vessels on Side-B from which air

bubbles appeared at a low pressure was OV and the other vessel was PPV. The second microcapillary (capillary-B) was inserted into the lumen of PPV. Taking care not to cover OV, the capillary-B was sealed into the vessel with glue, and supported with three glass rods. The 20 mM KCl solution was supplied from the capillary-A into the vessel at 0.3 MPa to check whether the solution flowed out from OV and the capillary-B. Then, capillary-B was cut to 2-3 cm in length.

For measurement of the reflection coefficient of the pit membranes, I used solutions of sucrose, PEG 3400 (MP Biomedicals, Illkirch, France), PEG 8000 (ICN Biomedicals Inc., Aurora, Ohio), PEG 20,000, and PEG 500,000 (Wako Pure Chemical Industries, Ltd., Osaka, Japan), with average molecular masses of 3400, 8000, 15,000-25,000, and 300,000-500,000. The concentrations of sucrose, PEG 3400, 8000, 20,000 and 500,000 solutions were 20 mM, 1%, 1%, 0.7% and 0.2% (w/v), respectively. Each of these solutions was filtered through a 0.2 μm membrane filter before use except for the PEG 500,000 solution. The test solution was introduced from capillary-A at a positive pressure of 0.3, 0.6 or 0.9 MPa generated by the N_2-cylinder. To attain a steady flow at a given pressure, I waited for about 10 min. During this period, more than 10 μL of the solution flowed out through capillary-B. Then, I collected a sufficient volume of solution (> 5 μL) to measure concentration with a silicone tube connected to capillary-B (Fig. 3-2B). To avoid evaporation of the collected solution, the end of the tube was plugged with a small volume of water. The movement of the meniscus was recorded every 30 seconds, and the flow rate was calculated. Concomitantly, the solutions introduced to and the drops passed through OV were collected (Fig. 3-2B). For each of the solutions, the measurements were conducted with at least three different stem segments.

The sucrose concentration in the collected solutions was determined from the difference between the total glucose upon addition of invertase (Wako Pure Chemical Industries) and free glucose. Glucose concentration was determined with a glucose assay kit (Glucose CII-test Wako, Wako Pure Chemical Industries).

The concentrations of PEG solutions were determined by the turbidimetric method of Ty (1979), which is based on the development of a PEG-TCA-Ba complex when PEG is exposed to

trichloroacetic acid (TCA) in the presence of barium ions. Duplicate determinations were performed for all the standards and samples.

Surface tension of the gas-water interface in a pit chamber

Stability of the pit valve depends on the pressure applied to the gas in the pit chamber because the gas dissolves in the surrounding water under positive pressure (above the atmospheric pressure). Because there is a pressure difference between the gas in the pit chamber and the water in the refilling vessel (ΔP) due to the surface tension, the pressure of gas trapped in the bordered pit (P_{gas}) is given by the sum of the liquid pressure (P_{liq}) and ΔP, namely, $P_{gas} = P_{liq} + \Delta P$. When ΔP is more negative, it is easier to maintain the gas. ΔP depends on the curvature of this interface determined by the geometry of the pit and wall chemistry. When the gas-water interface reaches the flared opening of the pit chamber, ΔP will be most negative (ΔP_{min}). ΔP_{min} was calculated from the capillary equation:

$$\Delta P_{min} = \gamma G \cos(\theta + \alpha) \quad (3\text{-}4),$$

where γ is the surface tension of water (0.072 N m^{-1} at 25°C), G is the ratio of the perimeter to the cross-sectional area of the pit aperture opening (m^{-1}), θ is the contact angle of water on the pit wall and α is the wall angle (Zwieniecki and Holbrook, 2000).

To calculate ΔP_{min}, I measured the perimeter of the pit aperture, cross-sectional area of the pit aperture and angle of the bordered pit chamber walls (2α) on scanning electron microscope (SEM) images using ImageJ (http://rsb.info.nih.gov/ij/). Small pieces (5×5×5 mm) of the stem segments were fixed and dehydrated in 100% ethanol. The samples were air-dried and coated with platinum (JEOL JFC-1300 Auto Fine Coater, JEOL, Tokyo, Japan). The specimens were observed under a SEM (JEOL JSM-6510LV). θ was assumed to range from 42° to 55° (Zwieniecki and Holbrook, 2000). For θ and 2α, see Fig. 1-3B.

Measurement of the pressure at which pit valves collapse

To estimate the threshold liquid pressure at which pit valves were retained, I artificially made the pit

valves in the inter-vessel pits, and measured the maximum pressure that does not allow the flow across the pits by dissolving gases in pit valves. As for the measurements for the reflection coefficient, OV and PPV were found using the single-vessel method (Zwieniecki *et al.*, 2001). Both OV and PPV were refilled by supplying 20 mM KCl solution filtered through a 0.2 μm filter from capillary-A at a pressure of 0.3 MPa (Fig. 3-2C). To form the menisci at pores in the OV-to-PPV pit membranes, I connected capillary-B to a hydraulic suction pump (GLD-135, Ulvac/Sinkukiko, Kanagawa, Japan), and applied a negative pressure at –0.08 MPa. Simultaneously, N_2 gas was introduced through capillary-A at a positive pressure of 1.0-2.0 MPa. In this segment, theoretically, OV should be filled with gas. By contrast, PPV should be filled with water because gas entry into PPV may be blocked by capillary forces at the small pores in the pit membranes (Fig. 3-2D). The pressure applied to OV was slowly released. The 20 mM KCl solution was forced to flow into OV from capillary-A at a low pressure of *ca.* 0.015 MPa to refill OV lumen, and not to dissolve the gas in pit chambers. The samples in which liquid flow in capillary-B was detected were discarded because some of the pit valves were likely to have collapsed in these samples. After ensuring outflow of the solution from OV, the pressure applied to OV was released and the cut end of side-B was sealed with glue (Fig. 3-2E). Subsequently, the negative pressure exerted to capillary-B was released slowly. These processes were conducted carefully because even a very small pressurization would make the menisci in the pit membranes to move toward OV, resulting in disruption of the pit valves.

When the solution in OV from capillary-A side was pressurized, the flow in capillary-B would be blocked as long as pit valves were retained. A silicone tube was connected to capillary-B, and the KCl solution was forced to flow from capillary-A at a positive pressure of 0.025 MPa. Immediately after pressurization, the movement of the meniscus in the silicone tube was recorded using a digital camera (Optio W60, PENTAX, Tokyo, Japan) every 30 seconds for 5 min. The pressure applied was successively increased in steps to 1.0 MPa. No flow would be detected at low pressures due to existence of the pit valves, while a substantial flow in capillary-B should be detected after pit valves collapsed by application of higher pressure. After pressurizing to 1.0 MPa, the

pressure was successively decreased to 0.025 MPa and the flow rate through capillary-B was measured.

The velocity of the meniscus movement per unit time in capillary-B was calculated from image data using ImageJ. The hydraulic conductance was determined from a ratio of the flow rate at steady state to the pressure applied. In case the flow was not stabilized within 5 min, the hydraulic conductance was determined from a ratio of the flow rate for the last 1.5 min to the pressure applied. The changes in the flow rate through capillary-B were evaluated by the relative hydraulic conductance to maximum value of each sample.

RESULTS

Semi-permeability of pit membranes

I estimated the degree of the semi-permeability of the pit membranes. The solution of test compounds was pressurized through an open vessel (OV) in the stem segment, and the efflux from the other vessel that diverged from the vessel via the bordered pits (pit-passing vessel, PPV) was collected, using the single-vessel method (Fig. 3-2B). I calculated the reflection coefficient from the asymptotic relationship between the solute concentration and the flow rate. If the pit membranes are semi-permeable to the tested compound, the concentration of the solution through PPV will be lower than that of the solution introduced, and the reflection coefficient value will be positive. Contrary to expectation, the sucrose concentration in the solution through PPV significantly increased to 27.4 ± 1.4 mM (mean ± 1 SE, n = 19), and the concentrations of the solutions introduced to and through OV were 19.4 ± 0.8 mM (mean ± SE, n = 6) and 19.2 ± 0.9 mM (mean ± 1 SE, n = 12) (Fig. 3-3A). The sucrose concentration in the solution through PPV was not significantly related to the relative flow rate (Fig. 3-3B). Consequently, the obtained reflection coefficient for sucrose was slightly negative.

When solutions of PEG 3400, 8000, or 20,000 were tested, the concentrations of these solutions were not significantly related to the relative flow rate (correlation coefficients and significance levels were; PEG 3400, r = –0.237, P = 0.855 (n = 22); PEG 8000, r = –0.0112, P =

0.514 (n = 12); and PEG 20,000, r = 0.244, P = 0.223 (n = 12)). Moreover, there were no significant differences in PEG concentrations among the solution introduced to OV, that through OV, and that from PPV (Fig. 3-4). Hence, the reflection coefficients of the pit membranes were nearly zero for all these PEG solutions (σ = 0.012 for PEG 3400, σ = –0.036 for PEG 8000, σ = 0.016 for PEG 20,000). For the PEG 500,000 solution, interestingly, the flow rate through PPV was extremely small, probably because PEG 500,000 molecules clogged the pores of the pit membranes, and thereby suppressed flow of the solute as well as that of the solvent. In other words, the pit membranes might be semi-permeable to PEG 500,000 molecules, but the reflection coefficient for PEG 500,000 could not be estimated.

Threshold pressure for stabilization of pit valve

Stability of the pit valve during xylem refilling depends on the pressure difference (ΔP) between the gas trapped in the bordered pit and the water in the refilling vessel. ΔP is determined by the geometry of the pit chamber and the chemistry of the pit wall. For the geometry of the pit chamber, the perimeter of the pit aperture, the cross-sectional area of the pit aperture and the flaring angle of the bordered pit chamber walls (2α) were measured on SEM images (Fig. 3-5). The perimeter of the pit aperture was 6.92 ± 1.22 μm (mean ± 1 SD, n = 72) for mulberry and 4.41 ± 0.920 (mean ± 1 SD, n = T54) for laurel. In mulberry, the cross-sectional area of pit aperture was 3.15 ± 0.943 μm^2 (mean ± 1 SD, n = 72) and 2α was 146 ± 13.8° (mean ± 1 SD, n = 13). In laurel, the cross-sectional area of pit aperture was 1.18 ± 0.496 μm^2 (mean ± 1 SD, n = 54) and 2α was 148 ± 7.33° (mean ± 1 SD, n = 18). Then, the most negative pressure ΔP (ΔP_{min}) can be obtained by Eq. 3-4. The two contact angle values (42° and 55°) were used. ΔP_{min} ranged from –0.0692 to –0.101 MPa for mulberry and from –0.125 to –0.179 MPa for laurel. In other words, the maximum liquid pressure at which the pit valve is retained ranged from 0.0692 to 0.101 MPa for mulberry and from 0.125 to 0.179 MPa for laurel.

To experimentally assess the threshold pressure up to which pit valves are retained, I artificially made the pit valves in the bordered pits in the inter-vessel wall between OV and PPV using

the single-vessel method (Fig. 3-2C-E) and measured the hydraulic conductance for the flow from OV to PPV at different positive pressures. When the hydraulic conductance was zero, it was assumed that pit valves blocked the flow. On the other hand, non-zero hydraulic conductance indicated that the pit valves had collapsed. In mulberry, there was no flow through PPV at pressures lower than the threshold pressure, which ranged from 0.025 to 0.10 MPa depending on the shoot segments (0.044 ± 0.038 MPa, mean ± 1 SD, n = 4, Fig. 3-6A). Beyond the threshold pressure, substantial flows from OV to PPV were detected. The maximum hydraulic conductance was found at 0.050-0.15 MPa. When the pressure was changed from the threshold pressure to the pressure achieving the maximum hydraulic conductance, we observed gradual increases in the flow rate to the steady-state levels (Fig. 3-7). At higher pressures, the hydraulic conductance gradually decreased, and it was 30-40% of the maximum value at 1.0 MPa (Fig. 3-6). When the applied pressure was successively decreased, the hydraulic conductance recovered in three samples. Substantial hydraulic conductance was found even at 0.025-0.10 MPa, the pressures at which there had been no flows.

Similarly, in laurel, there was no flow through PPV at pressures lower than the threshold pressure, which ranged from 0.050 to 0.150 MPa depending on the shoot segments (0.092 ± 0.052 MPa, mean ± 1 SD, n = 3, Fig. 3-6B). Beyond the threshold pressure, substantial flows from OV to PPV were detected. The maximum hydraulic conductance was found at 0.15-0.25 MPa. When the pressure was changed from the threshold pressure to the pressure achieving the maximum hydraulic conductance, we observed gradual increases in the flow rate to the steady-state levels (Fig. 3-7C, D). When the applied pressure was successively decreased, the hydraulic conductance did not recover in laurel unlike in mulberry. Substantial hydraulic conductance was found even the pressures at which there had been no flows.

DISCUSSION

To examine the pit-membrane-osmosis hypothesis, I estimated the semi-permeability of pit membranes for molecules of various sizes and found that the pit membranes were not semi-permeable

to polyethylene glycol of molecular mass less than and equal to 20,000. For the pit-valve hypothesis, I formed pit-valves in the inter-vessel pits in the short shoot segments and measured the maximum liquid pressure at which gases in bordered pits could be retained *in vivo*. The threshold pressure ranged 0.025-0.10 MPa. These values matched the theoretical value calculated from the geometry of the pit chamber (0.0692-0.101 MPa). The present results suggest that gas in the pits is retained by surface tension, even under substantial positive pressure, whereas the molecule size required for the pit-membrane-osmosis mechanism in mulberry would be unrealistically large.

Testing the pit-membrane-osmosis hypothesis

The reflection coefficient of the pit membranes was zero even for PEG 20,000 (Fig. 3-4). This suggests that the velocity of the solute flow was not lowered by the hydroxyl groups in PEG molecule or by the molecular size of PEG 20,000 (Stokes' radius of 4.16 nm according to Singh *et al.*, 1998). Thus, it would be difficult for the pit membranes of mulberry stems to have semi-permeability for sugars such as sucrose that are much smaller than PEG 20,000. However, when PEG 500,000 was examined, I found a distinct decrease in the flow rate of the solution passing through the pit membranes. This was probably because the pores in the pit membranes were clogged with molecules of PEG 500,000. Because the PEG 500,000 could not pass through the pit membranes, the pit membranes could have semi-permeability for molecules with molecular size such as PEG 500,000, Stokes' radius of which is 25.0 nm (Singh *et al.*, 1998). Given that the average pore radius in the pit membranes in mulberry is similar to the values, namely 10-25 nm, reported for four woody plants by the measurement of the pressure required to force air or microparticles through the membrane (Choat *et al.*, 2003), the present results are reasonable. However, extremely large compounds are not suitable for generation of a considerable negative osmotic potential in the refilling vessel. If a solution is constituted only by molecules with 4.16 nm in radius, the minimum osmotic potential will be no less than –10 kPa (Zwieniecki and Holbrook, 2009). Hence, the pit-membrane-osmosis hypothesis can not explain the refilling under strong negative xylem pressure such as observed in mulberry shoots

(Chapter 2).

I found that the concentration of sucrose increased in the solution that passed through the bordered pits (Fig. 3-3A). This increase may be attributed to release of sucrose from the adjacent parenchyma cells into the vessel lumen (Secchi and Zwieniecki, 2012). If the rate of sucrose transport from xylem parenchyma cells were constant, the sucrose concentration of the solution through vessels would decrease with the increase in the flow rate. Conversely, the concentration of the solution through PPV tended to slightly increase with increasing flow rate (Fig. 3-3B, $r = 0.327$, $P = 0.172$, $n = 19$). Secchi and Zwieniecki (2011) reported that, in *Populus trichocarpa*, sucrose in the vessels stimulated a remarkable decrease in starch content in wood, an increase in sucrose content in wood, and increases in transcription levels of *PtBMY1, 3* and *PtSUC2*, encoding β-amylases and a sucrose transport protein, respectively. From these results, they suggested that the accumulation of sucrose in vessels induces release of sucrose from xylem parenchyma cells. In the present experiment, the pressure applied to the sucrose solution was successively increased. Thus the solution with the highest flow rate caused by the highest pressure was collected more than 30 min after the application of the sucrose solution was started. Therefore, the activation of sucrose transporters might occur during the experiment.

Testing the pit-valve hypothesis

My results indicate that the threshold pressure to retain the pit valves ranged from 0.025 to 0.10 MPa in mulberry and from 0.050 to 0.150 MPa in laurel (Fig. 3-6). These values were in the same range as the pressure estimated from the geometry of the pit chamber (0.0692-0.101 MPa in mulberry and 0.125-0.179 MPa in laurel). Notably, based on theoretical analyses of the xylem refilling, Vesala *et al.* (2003) indicated that the maximum pressure in a refilling vessel is 0.05 or 0.08 MPa for a single vessel with diameter of 100 or 15 μm. Because the vessel diameter in mulberry stem xylem is within this range, it is highly probable that the lumen of the refilling vessel can be isolated by the pit valves during the vessel refilling.

Interestingly, in mulberry, the hydraulic conductance for the flow passing through the bordered pits decreased with the increase in applied pressure, but increased again with the decrease in applied pressure in some samples (Fig. 3-6A). These hysteresial changes in the hydraulic conductance observed in mulberry can be explained by the stretching of the pit membranes (Sperry and Hacke, 2004). The pressure difference across the pit membrane will bend the pit membrane towards the side of a lower hydrostatic pressure. Under a sufficiently large pressure difference, the pit membranes will be aspirated to the roof of the pit chamber. Thus, the area of the pit membrane through which the solution can flow should decrease to that of the pit aperture, resulting in a substantial drop in the hydraulic conductance. When the pressure difference decreases, the pit membranes will be elastically relaxed, and the hydraulic conductance will recover. Sperry and Hacke (2004) calculated that a pressure difference of only 0.0928 MPa causes the pit membranes to be aspirated to the pit chamber on the basis of material mechanics. Most of the pit membranes can be bent toward the side of the functional vessel under negative pressure during refilling of the embolized vessel. Because the ratio of the area of the pit membrane to the cross-sectional area of the pit aperture was 13.6 ± 3.38 (mean ± 1 SD, n = 30, Fig. 3-5B) in mulberry, the flow through pits can substantially decrease.

In laurel, such hysteresial changes in the hydraulic conductance were not observed although the hydraulic conductance through pits decreased with the increase in applied pressure in two cases out of three. The decrease in the hydraulic conductance in laurel can be also explained by the stretching of the pit membranes as with that in mulberry. However, in one sample of laurel, the hydraulic conductance did not decrease with the increase in applied pressure. The thicker pit membrane of laurel compared with that of mulberry might lead to the higher pressure required to aspirate the pit membrane to the pit chamber, resulting in no decrease in the hydraulic conductance. Even so, the ratio of the area of the pit membrane to the cross-sectional area of the pit aperture was 14.8 ± 3.54 (mean ± 1 SD, n = 31, Fig. 3-5D) in laurel. Therefore, the flow through pits will substantially decrease when the pit membranes are aspirated. On the other hand, in laurel, the hydraulic conductance did not recover with the decrease in applied pressure. The formation of

hydrogen bonds between the pit membrane and the border might prevent the pit membrane peeling off (Thomas and Kringstad, 1971).

I also found that it took several minutes for the flow through PPV to reach a steady state at low pressures just above the threshold, but at the other pressures the steady flow rate was reached immediately after the pressure change (Fig. 3-7). The time lag for reaching the steady flow implies that the pit valves disappeared progressively. That is, gases in the pit chambers might be dissolved at different rates under a given pressure. In two out of four segments, I observed very gradual increases in the hydraulic conductance with the increase in the pressure above the threshold pressure (Fig. 3-6). This also suggests that all the pit chambers were not refilled simultaneously. The pressure difference due to surface tension at the gas-water interface in the bordered pit is dependent on the geometry of the bordered pit. The variation in the geometry of the pits (Fig. 3-5) could explain the differences in the rate for the gas dissolution. Unless the gases in the pit chambers are simultaneously dissolved, it could be possible that remaining gases expand to re-embolize the vessel because the water in the vessel connected with that of the surrounding functional vessels is under negative pressure (Hacke and Sperry, 2003; Brodersen *et al.*, 2010).

Based on my calculation of the pressure difference by capillary force ($\Delta P = \gamma G$), the gas trapped in the pit chamber should expand to fill the vessel lumen when xylem sap tension is less than –0.16 MPa in mulberry and −0.28 MPa in laurel. I propose that the drop in the hydraulic conductance in pits due to aspiration of the pit membranes may prevent such a failure in refilling of the embolized vessel. If the hydraulic conductance of the bordered pits between the refilling and the adjacent functional vessels is extremely low, the inward water flow from parenchyma cells due to osmotic pressure can be more than the outward flow from the refilling vessel. This water balance would allow the plant to maintain a positive pressure in the refilling vessel even when some pit valves are collapsed. For a model vessel (60 μm in diameter and 10 cm in length, see Figs. 2-1 and 2-2), I estimated the inflow rates to be 1×10^{-5} and 1.3×10^{-3} mm^3 s^{-1} using the refilling speeds of 6×10^{-7} mm s^{-1} reported for *Vitis vinifera* by Brodersen *et al.* (2010) and of 6.8×10^{-5} mm s^{-1} for *Cucumis*

sativus by Scheenen *et al.* (2007), respectively. The outflow rates of vessels, all pits of which are permeable, will be 4.4×10^{-2} mm^3 s^{-1}, if the hydraulic conductance across pits and pressure difference between refilling and the neighboring vessels are 0.164 mm^3 MPa^{-1} s^{-1} (the average maximum hydraulic conductance across pits obtained in the pit-valve measurements) and 0.27 MPa. Given that aspiration of the pit membranes reduces the outflow to one-tenth, the inflow from Scheenen's study was the same order as the outflow in mulberry. A similar calculation for laurel (considering that a vessel is 35 μm in diameter (Fig. 3-8) and 10 cm in length (Gasco *et al.*, 2006) and the hydraulic conductance across pits is 0.0332 mm^3 MPa^{-1} s^{-1}) expected the similar result to mulberry. The drop of outward flow due to aspiration of the pit membranes will facilitate successful connections between the refilling and the neighboring vessel.

Brodersen *et al.* (2010) studied xylem refilling processes using high-resonance computed tomography (HRCT) and suggested that pit-valve hypothesis did not appear to be possible in grapevine because the wall of the vessels was less hydrophobic and because some droplets in the refilling vessels were drained to the neighboring functional vessels before the completion of the vessel lumen refilling. I think, however, that their results with grapevine do not necessarily exclude the pit-valve hypothesis in general. When cavitation occurs, high hydrophilicity of the cell wall in the pits could prevent water in the pit chamber of the refilling vessel from moving into the neighbouring functional vessels and, thereby, pit-valve formation itself would not occur. If the meniscus between the water and gas stays in the pit channel of the refilling vessel, the water in the pits would be retained until the threshold xylem sap tension of –0.16 MPa in mulberry and −0.28 MPa in laurel ($\Delta P = \gamma G$). This value is much greater than the pressure required to induce cavitation (air-seeding pressure). Thus, when a vessel cavitates, pit chambers will be initially filled with gas under comparatively less negative pressure. Once the pit chamber is filled with gas, it will be easy to form the pit valve as the refilling proceeds. The study by Brodersen *et al.* (2010) indicated that the mean contact angle was 42° around the pit area. The contact angle allows the gas in a pit to retain until the pressure of the water in the refilling vessel reaches 0.0692 MPa for mulberry and 0.125 MPa for laurel. The pit-valve

hypothesis, however, predicts that the gases in the pits will dissolve and the refilling vessel water will connect with the functional vessel sap when the pressure in the refilling vessel exceeds the threshold pressure. Even though gases are retained in pits, the extra high positive lumen pressure can result in dissolution of gases in pits before completion of vessel lumen refilling. The high positive pressure can be generated by high inflow rate of water from xylem parenchyma or by slow air dissolution into surrounding water (Zwieniecki *et al.*, 2001). The balance would be necessary for successful refilling. If the balance is satisfied, the pits valves could function in grapevine as well. However, large inter-vessel scalariform pits in grapevine vessels could often lead to the failure in refilling of the embolized vessel as reported by Brodersen *et al.* (2010). This is because, in scalariform pits, pressure difference between the gas in the pit chamber and the water in the refilling vessel will be small, and thereby pit valves will collapse easily.

CONCLUSION

The pit-membrane-osmosis hypothesis proposes that refilling is achieved by the release of polysaccharides of high molecular masses which are impermeable to the pit membranes from xylem parenchyma into the refilling vessel lumen. However, the molecule size required for the non-zero reflection coefficient of pit membranes in mulberry would be unrealistically large. In contrast, the pit-valve hypothesis proposes that gas is trapped within each bordered pit. In the present work, I demonstrated that the gases can be retained *in vivo*. If the pressure in the refilling vessel is below the threshold pressure to retain the pit valve, this hypothesis may be relevant. I also showed that all the pit valves did not collapse simultaneously, which means the possibility that re-cavitation of the refilling vessel occurs. To resolve this problem, the balance between the inflow rate and the outflow rate of water is important for the completion of the refilling eventually when the lumen is refilled completely and gas exists only in pits. Nevertheless, the pit valves will form spontaneously when the refilling occurs. Then, pit valves will reduce the outflow of refilling vessel water and contribute to the efficient refilling of the vessel lumen.

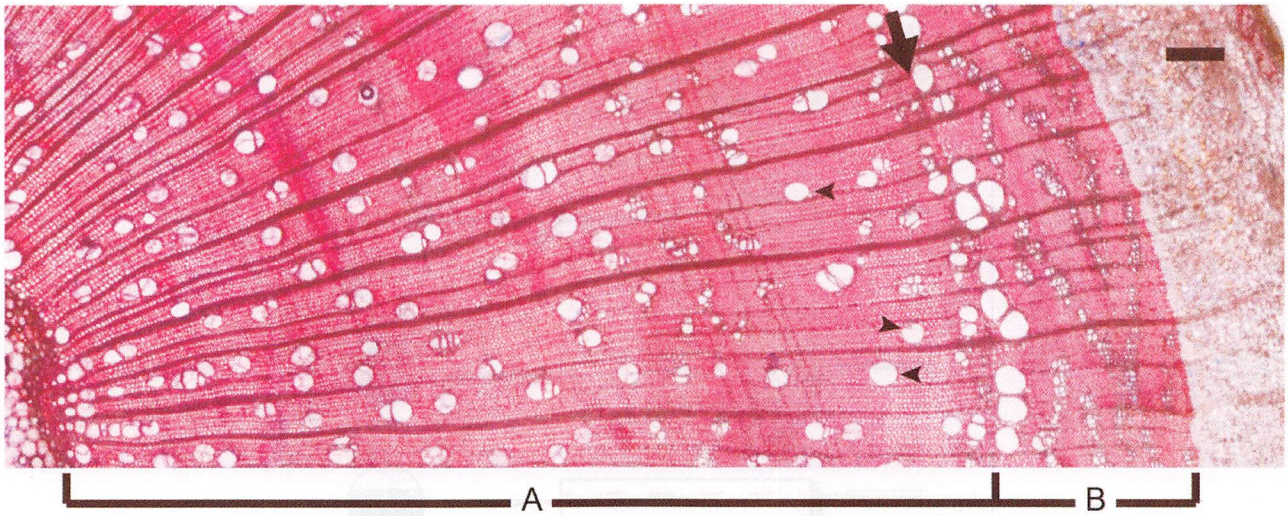

Figure 3-1. Cross-section of a one-year-old stem. In mulberry, current-year stems have secondary xylem of diffuse-porous-like vessel distribution (A), while from the second growing season, secondary xylem shows ring-porous vessel distribution (B). Solitary vessels (arrow heads) in current-year stems were used for measurements of the reflection coefficient and of pit-valve stability. Arrow shows a growth ring boundary. Scale bar is 200 µm.

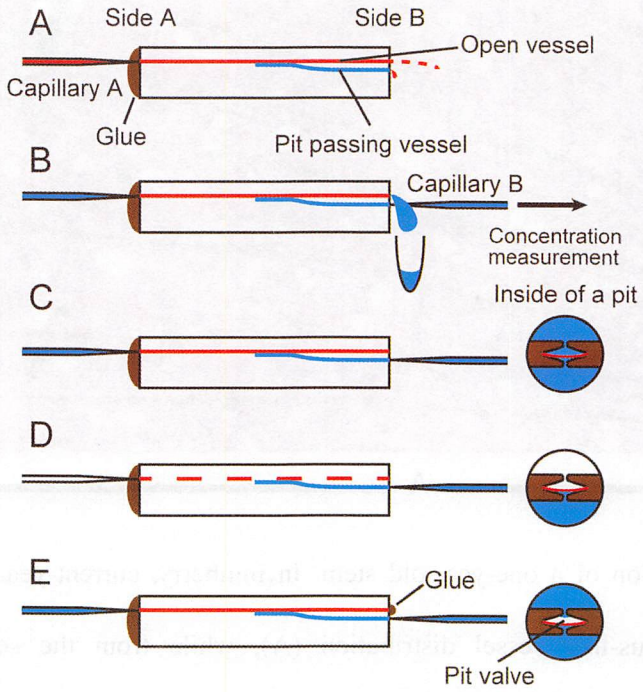

Figure 3-2. The single vessel method. A, Open vessel and the diverging vessel via pits were detected by dye perfusion from Capillary-A inserted into a single vessel lumen. B, Solution was introduced into the open vessel (OV) at a positive pressure and solutions passing through the OV and the diverging vessel (pit-passing vessel, PPV) were collected. Because the flow rate of the solution through the diverging vessel was slow, the solution was collected with capillary-B inserted into the lumen of PPV. C-E, Pit valve was artificially made on the pits of the inter-vessel between OV and PPV. C, Both OV and PPV were refilled by pushing 20 mM KCl solution from capillary-A.; D, The solutions in OV were removed by injecting N_2 gas from capillary-A while pulling the solution in PPV from capillary-B.; E, Then, the lumen of the OV was refilled with KCl solution by pushing the solution from capillary-A at a low pressure. Solid and broken lines are vessels filled with liquid and gas, respectively. See text for details.

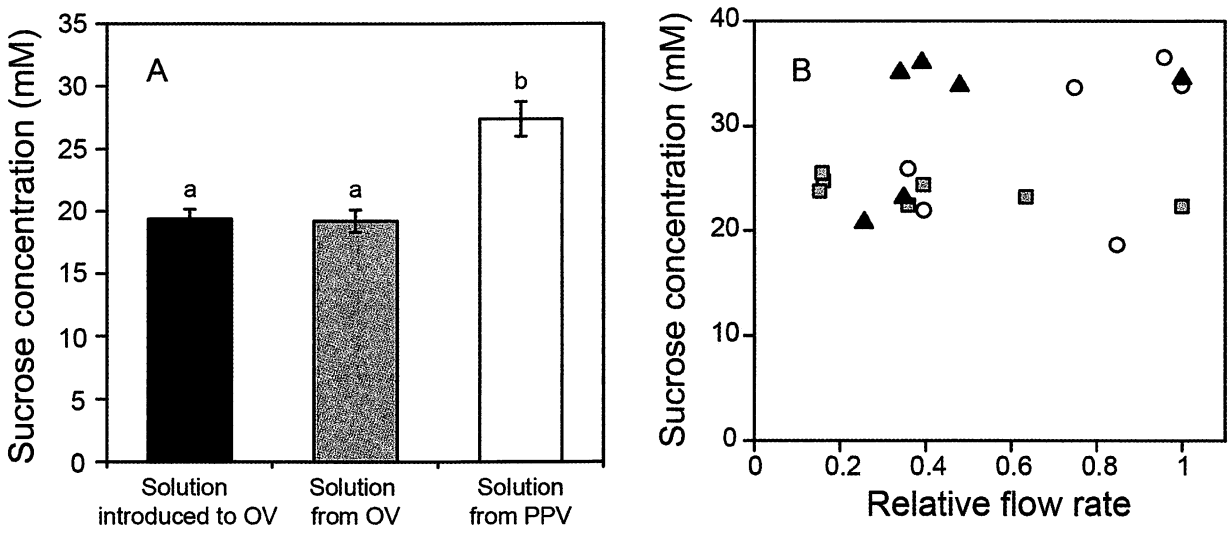

Figure 3-3. Changes in concentrations of sucrose solutions before and after passing through pit membranes. A, The concentrations of sucrose among the solutions introduced and through an open vessel (OV), and a diverging vessel via pits (pit-passing vessel, PPV) are compared. Bars represent ± 1 SE (n = 6 for solution introduced to OV, n = 12 for solution through OV, n = 19 for solution through PPV). Different letters above the columns indicate statistically significant differences (One-way ANOVA and Tukey's multi-comparison test at P = 0.05 level, F = 13.1). B, The relationship between sucrose concentrations in the solutions passing through PPV and the relative flow rate (relative to the maximum flow rate in each sample). Each symbol represents a different sample. The sucrose concentration was not significantly related to relative flow rate (test for significance of the regression, r = 0.327, P = 0.172, n = 19).

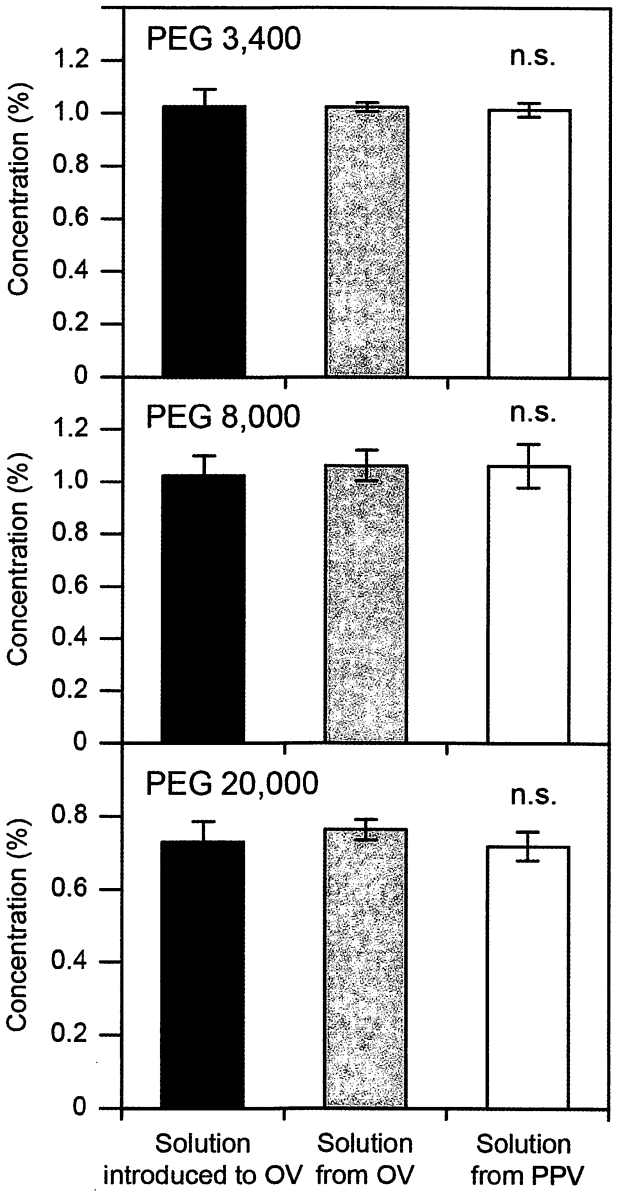

Figure 3-4. The concentration of polyethylene glycol (PEG) in solutions before and after passing the pit membrane. PEG concentrations in the solutions introduced to and through an open vessel (OV), and in the solution through a diverging one via pits (pit-passing vessel, PPV) are compared. Bars represent ± 1 SE. For each PEG molecule, no significant differences were detected among the concentrations of the solution introduced to OV, solution through OV, and solution through PPV (One-way ANOVA. PEG 3,400: $P = 0.956$, $n \geq 8$; PEG 8,000: $P = 0.924$, $n \geq 9$; PEG 20,000: $P = 0.706$, $n \geq 9$).

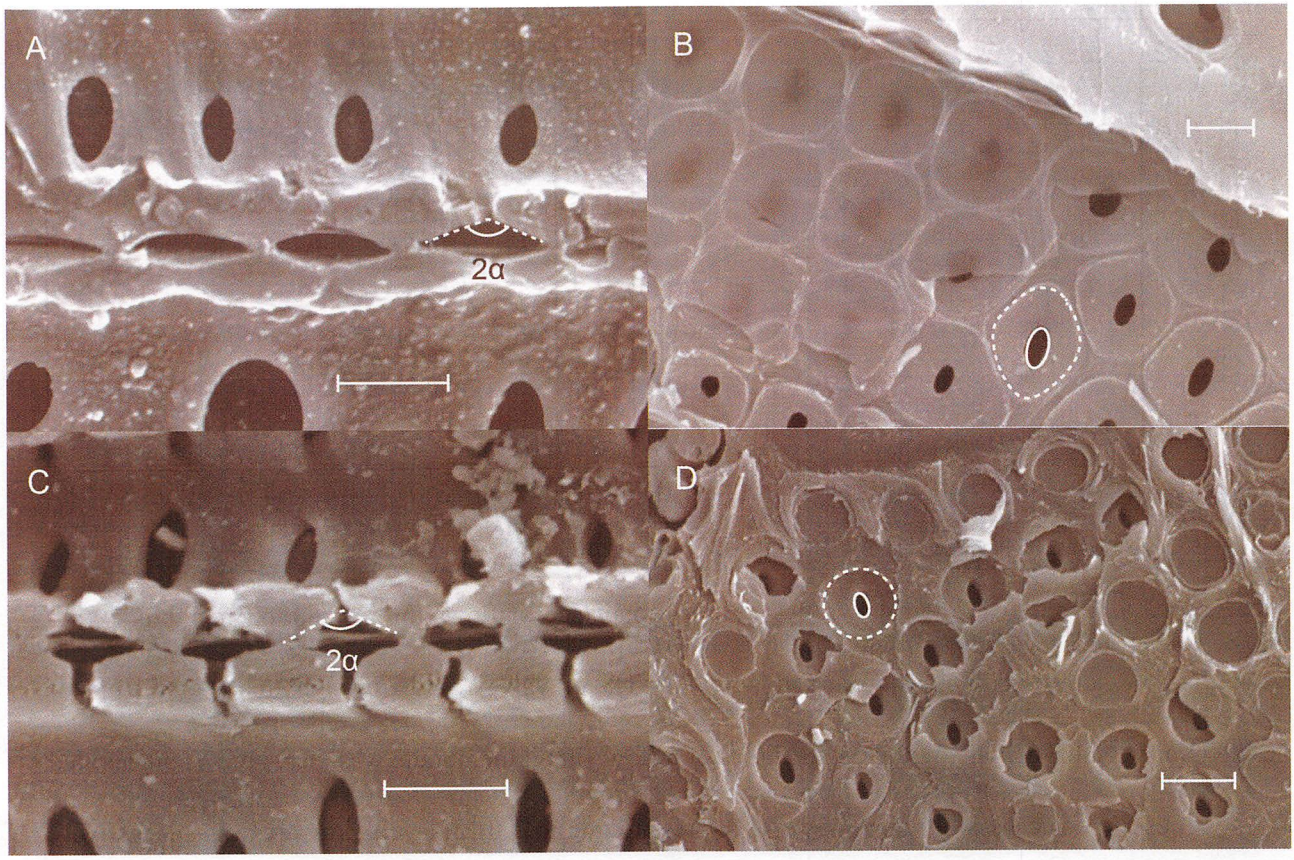

Figure 3-5. SEM images of inter-vessel pits of mulberry stem xylem (A, B) and of laurel stem xylem (C, D). A, Cross-sections of the bordered pits in mulberry. 2α is a flaring angle of bordered pits. B, Inter-vessel pits of mulberry. The pit aperture and border are surrounded by solid and broken lines, respectively. C, Cross-sections of the bordered pits in laurel. D, Inter-vessel pits of laurel. The pit aperture and border are surrounded by solid and broken lines, respectively. Scale bars are 5 μm.

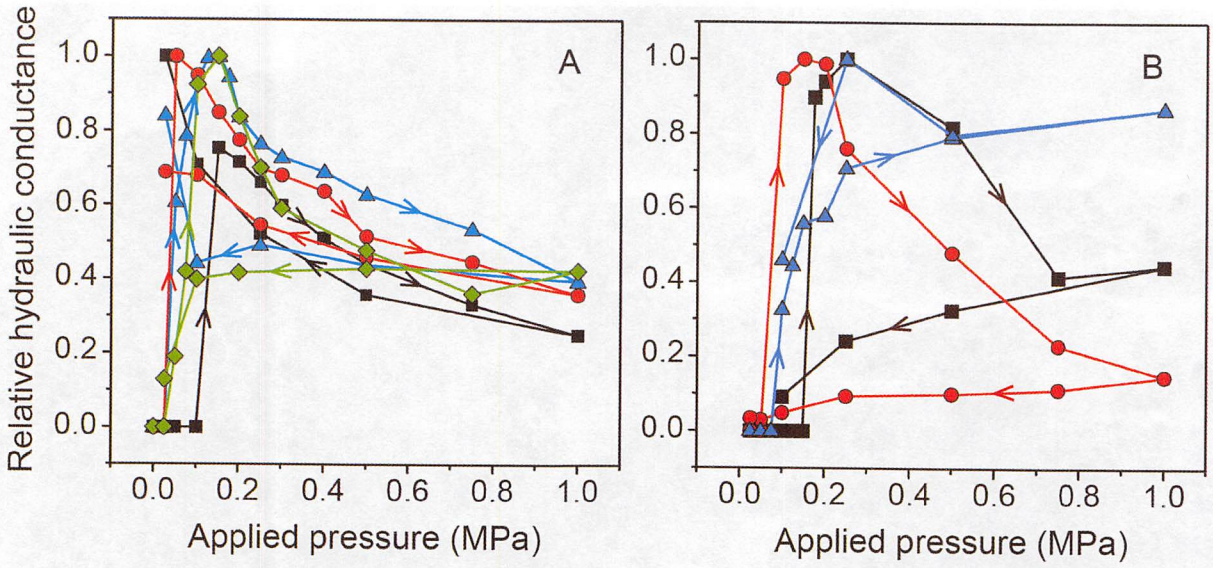

Figure 3-6. Changes in the relative hydraulic conductance of flows through the pit membrane with applied pressures in mulberry (A) and in laurel (B). The pit valves were artificially made on the pits of the inter-vessel. Then, hydraulic conductance of a flow via pit membrane was measured as the applied pressures were successively increased. After pressurizing to 1.0 MPa, the pressure was successively decreased to 0.025 MPa. Each curve represents a different stem sample.

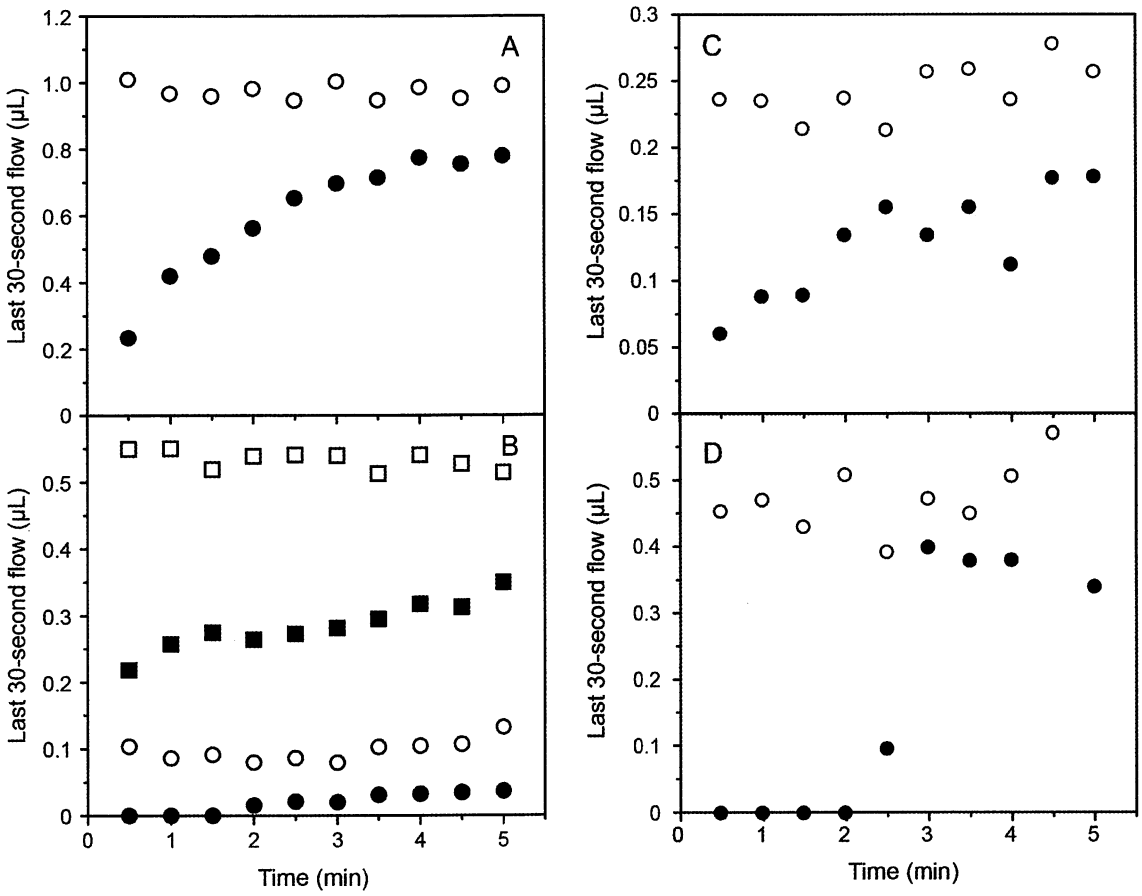

Figure 3-7. Changes in the flow rate of the solution passing through pits with time after the applied pressure changed. The pit valves were artificially made in the pits of the inter-vessel. Then, the flow rate of the solution passing through the pits was measured as the applied pressure was successively increased. A and B represent two different stem samples in mulberry, and C and D represent two different stem samples in laurel. A, Solid circles represent the time-dependent changes in the flow rates at a pressure of 0.15 MPa, and open circles show the constant flow rate at a pressure of 0.20 MPa following the measurement at 0.15 MPa. B, Solid circles, open circles, solid squares and open squares represent the changes in the flow rates at pressures of 0.050, 0.075, 0.10 and 0.15 MPa, respectively. C, Solid circles represent the time-dependent changes in the flow rates at a pressure of 0.175 MPa, and open circles show the constant flow rate at a pressure of 0.20 MPa following the measurement at 0.175 MPa. D, Solid circles represent the time-dependent changes in the flow rates at a pressure of 0.10 MPa, and open circles show the constant flow rate at a pressure of 0.125 MPa following the measurement at 0.10 MPa.

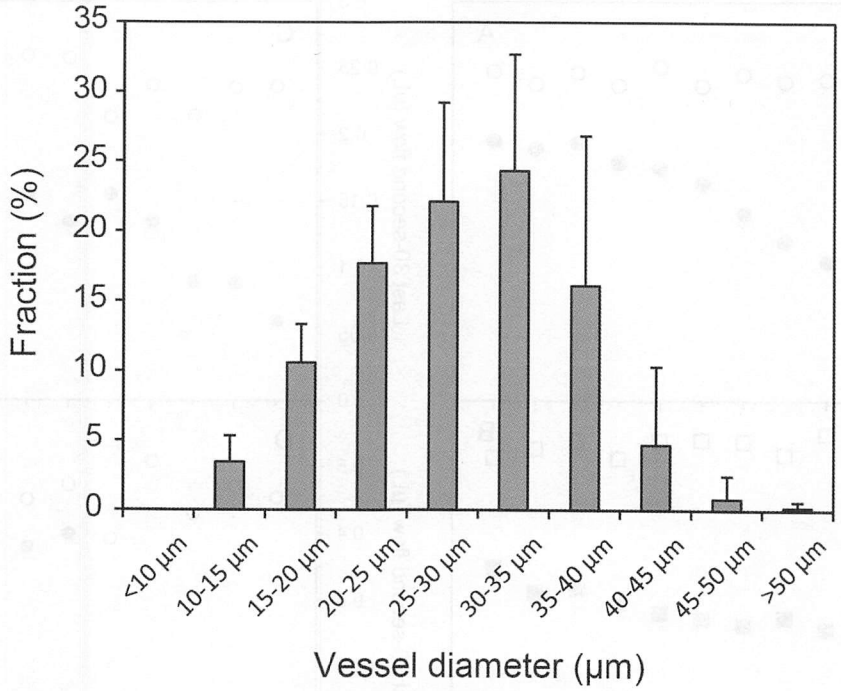

Figure 3-8. Distribution of vessel diameter classes in laurel stems. Error bars represent ± SD (n = 4).

REFERENCES

Brodersen CR, McElrone AJ, Choat B, Matthews MA, Shackel KA. 2010. The dynamics of embolism repair in xylem: in vivo visualizations using high-resolution computed tomography. *Plant Physiology* **154**, 1088-1095.

Choat B, Ball M, Luly J, Holtum J. 2003. Pit membrane porosity and water stress-induced cavitation in four co-existing dry rainforest tree species. *Plant Physiology* **131**, 41-48.

Gasco A, Nardini A, Gortan E, Salleo S. 2006. Ion-mediated increase in the hydraulic conductivity of Laurel stems: role of pits and consequences for the impact of cavitation on water transport. *Plant, Cell & Environment*, 29, 1946-1955.

Hacke UG, Sperry JS. 2003. Limits to xylem refilling under negative pressure in *Laurus nobilis* and *Acer negundo*. *Plant, Cell & Environment* **26**, 303-311.

Holbrook NM, Zwieniecki MA. 1999. Embolism repair and xylem tension: do we need a miracle? *Plant Physiology*, **120**, 7-10.

Salleo S, Lo Gullo MA, Trifilò P, Nardini A. 2004. New evidence for a role of vessel-associated cells and phloem in the rapid xylem refilling of cavitated stems of *Laurus nobilis* L. *Plant, Cell & Environment* **27**, 1065-1076.

Scheenen TW, Vergeldt FJ, Heemskerk AM, Van As H. 2007. Intact plant magnetic resonance imaging to study dynamics in long-distance sap flow and flow-conducting surface area. *Plant Physiology* **144**, 1157-1165.

Secchi F, Zwieniecki MA. 2011. Sensing embolism in xylem vessels: the role of sucrose as a trigger for refilling. *Plant, Cell & Environment* **34**, 514-524.

Secchi F, Zwieniecki MA. 2012. Analysis of Xylem Sap from Functional (Nonembolized) and Nonfunctional (Embolized) Vessels of *Populus nigra*: Chemistry of Refilling. *Plant Physiology* **160**, 955-964.

Singh S, Khulbe K, Matsuura T, Ramamurthy P. 1998. Membrane characterization by solute transport and atomic force microscopy. *Journal of Membrane Science* **142**, 111-127.

Sperry JS, Hacke UG. 2004. Analysis of circular bordered pit function I. Angiosperm vessels with homogenous pit membranes. *American Journal of Botany* **91**, 369-385.

Spiegler KS, Kedem O. 1966. Thermodynamics of hyperfiltration (reverse osmosis): criteria for efficient membranes. *Desalination*, **1**, 311-326.

Thomas RJ, Kringstad KP. 1971. The role of hydrogen bonding in pit aspiration. *Holzforschung-International Journal of the Biology, Chemistry, Physics and Technology of Wood*, **25**, 143-149.

Ty A. 1979. PEG determinations in urine, plasma, and various protein solutions. *Microchemical Journal* **24**, 287-290.

Vesala T, Hölttä T, Perämäki M, Nikinmaa E. 2003. Refilling of a hydraulically isolated embolized xylem vessel: model calculations. *Annals of Botany* **91**, 419-428.

Zwieniecki MA, Holbrook NM. 2000. Bordered pit structure and vessel wall surface properties. Implications for embolism repair. *Plant Physiology* **123**, 1015-1020.

Zwieniecki MA, Holbrook NM. 2009. Confronting Maxwell's demon: biophysics of xylem embolism repair. *Trends in Plant Science* **14**, 530-534.

Zwieniecki MA, Melcher PJ, Holbrook NM. 2001. Hydraulic properties of individual xylem vessels of *Fraxinus americana*. *Journal of Experimental Botany* **52**, 257-264.

CHAPTER 4

Dependence of the ratio between lumen resistivity and end wall resistivity on vessel diameter within stems of three angiosperm species

ABSTRACT

A rate of water transport in xylem is constrained by frictions in passing through the vessel lumen and pits of the vessel end walls. In comparisons among woody species with different vessel diameters, the hydraulic resistivity (= pressure gradient / volumetric flow rate) of the stem xylem is co-limited by the frictions through the vessel lumen and the end wall because the wide vessel is associated with the long vessel lumen length and the large inter-vessel pit area at end walls. I tested whether this interspecific relationship was applicable to intraspecific variations in vessel diameter within a given stem. Several vessel traits were measured in vessels with different diameter classes using current-year stem of three angiosperm species (*Acer rufinerve*, *Morus australis* and *Vitis coignetiae*). For all species, the vessel length was related positively to the vessel diameter. The inter-vessel pit area per unit length was correlated negatively with the vessel diameter in vessels of *A. rufinerve* and *M. australis*, while there was no difference in the inter-vessel pit area per unit length in *V. coignetiae*. From these data, in *M. australis* and *V. coignetiae*, it is suspected that the lumen resistivity relatively largely limits the water flow for wider vessels, and the end wall resistivity relatively largely limits it through narrower vessels. On the other hand, in *A. rufinerve*, it is suspected that the end wall resistivity relatively largely limits the water flow for wider vessels, and lumen resistivity relatively largely limits it for narrower vessels.

INTRODUCTION

In the experiment in chapter 3, I have shown that the pit valves did not collapse simultaneously. This might cause the failure in xylem refilling. To complete xylem refilling, the net flow into the refilling vessel must be positive to maintain the positive pressure in gases even when some pits are collapsed. Studies of the vessel structural traits contribute to the estimation of the inward flow to the refilling vessel and the outward flow to the surrounding vessels under negative pressures, because they are proportional to cumulative non-inter- and inter- vessel pit areas, respectively. The primary objective of this chapter is to investigate the vessel structural traits to estimate these pit areas.

My question also relates to the balance between the hydraulic resistance caused by the vessel lumen and that caused by the pits. Xylem vessels represent the most important pathways for long distance water transport from roots to leaves in angiosperm species. The vessels are long tubes of vessel elements connected by perforation and are connected one another through opening in the lignified secondary walls known as pits (Choat *et al.*, 2008). Water must move laterally through pits at vessel end walls, and thus the vessel end walls are a limiting factor for the water flow. Assuming the vessel geometry as the lumen and wall components in sereis, the hydraulic resistivity of a vessel (R_{total}, MPa s mm^{-4}) can be expressed as the sum of two terms of hydraulic resistivity (Sperry *et al.*, 2005). One is the lumen resistivity (R_{lumen}, MPa s mm^{-4}), and it can be quantified by the Hagen-Poiseuille equation. Thus, R_{lumen} is inversely proportional to the fourth of the vessel diameter: $R_{lumen} \propto 1/D^4$, where D is the vessel diameter. The other is the end wall resistivity (R_{wall}, MPa s mm^{-4}), and is assumed to be inversely proportional to the cumulative area of the inter-vessel pits (Wheeler *et al.*, 2005). The transport pathway composed of shorter vessels has more end walls than that of longer vessels when water flow for a given distance is considered. In other words, the end wall resistivity is inversely proportional to the vessel length. Thus, $R_{wall} \propto 1/(L\,A_{pit})$, where L is the vessel length and A_{pit} is the cumulative areas of the inter-vessel pits.

Although there are large differences in the vessel diameter among species, the lumen resistivity and the end wall resistivity are nearly co-limiting the water flow in the xylem as a whole

(Zimmermann, 1983; Tyree and Ewers, 1991; Hargrave *et al.*, 1994; Sperry *et al.*, 2005). For angiosperm vessels, pits account for 58% of total xylem hydraulic resistance (Choat *et al.* 2008), and the lumen resistivity approximately equals to the end wall resistivity for the xylem as a whole. Namely, $\overline{R}_{lumen}/\overline{R}_{wall} \approx 1$, where $\overline{R}_{lumen}$ and $\overline{R}_{wall}$ are the lumen and the end wall resistivities, respectively. From this tendency and the relationship between the vessel diameter and the vessel length, Sperry *et al.* (2005) concluded that the species with wider vessels have longer vessels and larger regions of the inter-vessel pit areas. While such the species have lower hydraulic resistivity, the probability of cavitation in vessels increases because of the greater total area of the inter-vessels pits (Christman *et al.*, 2009). Thus, there would be a trade-off between the stem hydraulic efficiency and safety against cavitation among species. These previous works, however, showed only the average vessel trait for xylem of each species.

Even in a single stem, there is a large variation in the vessel diameter, especially in ring-porous species. Therefore, even for a single stem, it is not certain whether the lumen resistivity approximately equals to the end wall resistivity for all vessels (Fig. 4-1). The ratio of R_{lumen} and R_{wall} might be constant for all vessels within the xylem for an unknown reason (Fig. 4-1A). Otherwise, if a species imparts roles as routes with larger hydraulic conductivity even to narrower vessels, the narrower vessels may also have large inter-vessel pit areas to lower the end wall resistivity (Fig. 4-1B). Conversely, if the narrower vessels function as bypasses in case of cavitation in wider vessels, narrower vessels may have small inter-vessel pit areas. By having higher R_{wall}/R_{total} ratios, they may have high resistance to cavitation (Fig. 4-1C). Therefore, it is important for understanding the roles of individual vessels with different diameters in the same stem to evaluate the individual vessel traits.

The purpose of this study is to examine whether the lumen resistivity and the end wall resistivity are co-limiting water flow in the vessels with different diameters within a given stem. For this purpose, I first determined the mean values of fractions of $\overline{R}_{lumen}$ and $\overline{R}_{wall}$ for the stem. Secondly, I evaluated relationships between the diameter versus length and between the diameter versus inter-vessel pit area for vessels of various diameter classes. According to Sperry *et al.* (2005), who

compared the vessel traits across species, the data of the vessel length and the inter-vessel pit area were fitted with a power function of the vessel diameter. Subsequently, from the data obtained, I estimated the fraction of R_{lumen} and R_{wall} for vessels with different diameter classes.

MATERIALS AND METHODS

Plant materials

Experiments were conducted on stem segments from current-year shoots of three deciduous woody species, *Acer rufinerve* Siebold et Zucc., *Morus australis* Poir. and *Vitis coignetiae* Pulliat ex Planch.. *M. australis* trees were growing on the Hongo campus, the University of Tokyo (35° 42′ 48″ N, 139° 45′ 44″ E, 20 m a.s.l.). For *A. rufinerve* and *V. coignetiae*, 4- to 5-year-old saplings grown in pots were used. Although the current-year stems of *M. australis* had diffuse-porous like wood, *M. australis* and *V. coignetiae* are ring-porous species, and *A. rufinerve* is a diffuse-porous species (Fig. 4-2). These species have vessels with simple perforations. Measurements of the hydraulic resistivity and estimations of the lumen resistivity ($\overline{R}_{lumen}$, MPa s mm^{-4}) and the end wall resistivity ($\overline{R}_{wall}$, MPa s mm^{-4}) for stem xylem were conducted between June and August 2014. Measurements of the vessel length and vessel diameter distributions were made between June and October 2013. Scanning electron microscope observations of the stem xylem were made in July 2012, April 2013 and November 2015. The maximum vessel length obtained by the air infiltration technique (Greenidge 1952) was 13 ± 1.3 cm (mean ± 1 SD, $n = 8$) in *A. rufinerve*, 39 ± 4.0 cm (mean ± 1 SD, $n = 4$) in *M. australis* and 62 ± 10 cm (mean ± 1 SD, $n = 3$) in *V. coignetiae*. In anatomical analyses of vessel traits, primary xylem vessels and the vessels connected with the protoxylem vessels were excluded because primary xylem vessels may have traits different from those of secondary xylem vessels.

Lumen resistivity and end wall resistivity at the stem-xylem scale

For water transport in the vessel-bearing xylem, water moves through vessel lumina and inter-vessel pits. Thus, stem xylem resistivity (R_{xylem}, MPa s mm^{-4}) can be expressed by a sum of the lumen

resistivity ($\overline{R}_{lumen}$) and the end wall resistivity ($\overline{R}_{wall}$). First, the stem-mean wall fractions ($\overline{R}_{wall}/R_{xylem}$) of three woody species were evaluated. R_{xylem} was measured with the balance method (Chapter 2; Sperry *et al.*, 1988). $\overline{R}_{lumen}$ was obtained according to the Hagen-Poiseuille equation. $\overline{R}_{wall}$ was calculated as difference between R_{xylem} and $\overline{R}_{lumen}$.

For determination of the xylem hydraulic resistivity, R_{xylem}, in stems, the stem segments longer than the maximum vessel length were excised under water for *A. rufinerve* and *M. australis*. In current-year stems of *V. coignetiae*, when the stem segments longer than the maximum vessel length were used, maximum vessel diameter and hydraulic vessel diameter $(\Sigma D^4/n)^{1/4}$ at the apical end were considerably smaller than those at the basal end (Figs. 4-3 & 4-4). Thus, I used the test segments of 25-40 cm in length for *V. coignetiae*. Because of the lengths of the test segments and the existence of open vessels, the wall fraction might be underestimated. Based on the vessel length distribution (See Results), the fraction of open vessels in the 25 cm test segment can be estimated. The value was calculated to be only 7.0% even for wide vessels with >70 μm in diameter. Then, most vessels in the test segments had vessel ends. Sperry *et al.* (2005) calculated the wall fraction from the changes in the hydraulic resistivity with the proportion of open vessels in stem segments. I also calculated the wall fraction from the changes in the hydraulic resistivity with segment length instead of with the proportion of open vessels in stem segments. Then, a similar wall fraction (0.56 ± 0.14, mean ± 1 SD, n = 4) was obtained with the stem shorting experiment by (Fig. 4-5). Thus, open vessels in test segments will not markedly affect the calculation of the wall fraction.

The stem segments were flushed with 20 mM KCl solution at 150 kPa for 20 min to remove reversible embolism. Then, the stem hydraulic resistivity (R_{xylem}) was determined by a positive pressure of about 5 kPa induced by gravitational force.

$\overline{R}_{lumen}$ was obtained using the Hagen-Poiseuille equation (Zwieniecki *et al.*, 2001). Resistivity of a vessel lumen (R_{lumen}) is expressed as follow:

$$R_{lumen} = 128\eta/(\pi D^4) \quad (4\text{-}1),$$

where η is viscosity of water at 25°C (0.00089 Pa s), and D is vessel diameter. To measure $\overline{R}_{lumen}$, I prepared the cross-sections at the middle and both ends of the stem segments used for R_{xylem} using a sliding microtome. The cross-sections were photographed with a digital camera (DP71, Olympus, Tokyo, Japan) mounted on a light microscope (BX50, Olympus). From the images, xylem area and vessel lumen area (A) were measured using Image J (http://rsb.info.nih.gov/ij/). The vessel lumen area were measured and converted to equivalent diameters ($D = \sqrt{4A/\pi}$). For *M. australis* and *A. rufinerve* stems, vessel lumen areas were measured in the xylem parts surrounded by rays. The measured regions included at least 105 vessels. Area-based lumen resistivity (MPa s mm^{-2}) was the reciprocal of a ratio of $\Sigma(1/R_{lumen})$ to the area of the measured region. The lumen resistivity ($\overline{R}_{lumen}$, MPa s mm^{-4}) was calculated as the quotient of the area-based lumen resistivity and the xylem area. Secondary xylem of *V. coignetiae* consists of three regions with different vessel diameter distributions (Brodersen *et al.* 2011). Thus, for *V. coignetiae*, all vessels in the cross-section were analyzed.

When long segments were used for measurements, the cross-sectional xylem area changed depending on the position in the segment, and thereby $\overline{R}_{lumen}$ also changed (Fig. 4-6). Considering this effect, I calculated representative $\overline{R}_{lumen}$ for each sample segment as follows. The cross-sections were prepared at three different positions of each segment, and a regression line for the relationship between xylem area and $\overline{R}_{lumen}$ at the cross-sections was obtained for each segment. The regression line for the relationship between distance from the distal end of the segment and xylem area was obtained, and the average xylem area was calculated using this regression line. $\overline{R}_{lumen}$ for the stem segment was determined by substituting the average xylem area into the regression line of the relationship between xylem area and $\overline{R}_{lumen}$. $\overline{R}_{wall}$ was determined as the difference between R_{xylem} and $\overline{R}_{lumen}$, and the fraction of $\overline{R}_{wall}$ (i.e. $\overline{R}_{wall}/R_{xylem}$) was calculated.

Vessel length distributions

The vessel length was determined by the silicone injection method (Christman *et al.* 2009). Three or four stems larger than the maximum vessel length were flushed with 20 mM KCl solution at 150 kPa

for 20 min to remove reversible embolism. A 10:1 silicone/harder mix (RTV-141, Rhodia, Cranbury, NJ, USA) was prepared and 1% (w/v) fluorescent optimal brightener (Ciba Uvitex OB, Ciba Specialty Chemicals, Tarrytown, NY, USA) in chloroform were added to the silicone (one drop g^{-1}). The silicone mixture was injected into the stem segments at 100 kPa of a positive pressure overnight. After allowing the silicone to harden, the stems were sectioned at eight or nine different distances from the injected surface. The distances were 0.001, 0.005, 0.01, 0.015, 0.02, 0.025, 0.03 and 0.05 m for *A. rufinerve*, 0.001, 0.01, 0.05, 0.1, 0.15, 0.2, 0.25 and 0.3 m for *M. australis* and 0.001, 0.01, 0.02, 0.05, 0.1, 0.15, 0.2, 0.25 and 0.3 m for *V. coignetiae*. The cross-sections were photographed with a digital camera mounted on a fluorescence microscopy (BX50, Olympus) to detect the silicone-filled vessels. The fraction of silicone-filled vessels (N_L) at each distance L was counted separately for different diameter classes and the data were fitted with a Weibull function:

$$N_L = e^{-(kL)^c} \quad (4\text{-}2),$$

where k and c are curve-fitting parameters. The best fit was then used to estimate the vessel length distribution. The second derivative of the Weibull multiplied by L provides the probability density of vessels of length L:

$$F_L = ck^c L^{(c-1)}\, e^{-(kL)^c}\, [c(kL)^c - c + 1] \quad (4\text{-}3).$$

When $c > 1$, F_L becomes negative below a minimum length $L_{\min} = (1/k)\ [(c - 1)/c]\ (1/c)$. The $L_{\min}$ represented the minimum vessel length. Otherwise (i.e. $c \leq 1$), the minimum vessel length was regarded as 0.0001 m. I set a maximum vessel length $L_{\max} = L$ at $N_L = 0.0001$ and adjusted F_L accordingly by dividing it by the integral of Eq. 4-3 from $L_{\min}$ to $L_{\max}$. The integral was calculated using maxima (http://maxima.sourceforge.net/). For each species, I also used nine length classes according to Christman *et al.* (2009). The upper limit of each length class (L_i) was given as:

$$L_i = L_{min} \left(\frac{L_{max}}{L_{min}}\right)^{(i/9)} \quad (4\text{-}4).$$

Equation 4-4 was integrated between length class limits to obtain the fraction of vessels in each class [$F_L(i)$]. We also set L_i to the mid-length of the class instead of the upper limit. Moreover, the median

vessel length (L_{med}) which satisfies the following equation was calculated for each vessel diameter class:

$$\int_{L_{min}}^{L_{med}} F_L \, dL \Big/ \int_{L_{min}}^{L_{max}} F_L \, dL = 0.5 \quad (4\text{-}5).$$

The data of the median vessel length for each vessel diameter class were fitted with a power function, $p = a\,D^b$, where a and b are curve-fitting parameters.

Calculation of the inter-vessel pit area

For estimation of the inter-vessel pit area for each vessel-diameter class, the mean inter-vessel wall width, p (μm) for each vessel diameter class was measured as $\Sigma w/N$ where w is inter-vessel wall width and N is the number of vessels observed. For solitary vessels, the inter-vessel wall width was regarded as zero. The data were fitted with a power function to determine the relationship between the mean inter-vessel wall width and the vessel diameter of each class, and the exponent was determined for each species. Subsequently, the inter-vessel pit area per vessel, A_{pit} (mm^2) was estimated for each vessel diameter class as follows:

$$A_{pit} = p\,f_p\,L_{med} \quad (4\text{-}6),$$

where f_p is the fraction of the surface area of pit membranes in the inter-vessel contact area (pit field fraction), and L_{med} is the median vessel length determined from vessel length distributions. f_p was measured on scanning electron microscope (JEOL JSM-6510LV, JEOL, Tokyo, Japan) images. Small pieces (5 × 5 × 5 mm) of the stem segments were fixed and dehydrated in 100% ethanol. The samples were air-dried and coated with platinum (JEOL JFC-1300 Auto Fine Coater, JEOL, Tokyo, Japan). The specimens were observed under a scanning electron microscope (JEOL JSM-6510LV, JEOL) with a 10 kV electron beam. According to Eq. 4-6, the exponent in the scaling relationship between A_{pit} and the vessel diameter was calculated as a sum of the exponent in p calculated above and the exponent in L_{med}. The relationship between the vessel diameter and the inter-vessel pit area was determined.

Calculation of the wall fraction for different vessel diameter classes

To explore the change in wall fraction (= R_{wall}/R_{total}) with the vessel diameter, the wall fractions should be expressed by a function of vessel diameter. The hydraulic resistivity of a vessel (R_{total}) is given as:

$$R_{total} = 128\eta/(\pi D^4) + 2r_p/(L A_{pit}) \quad (4\text{-}7),$$

where r_p is the hydraulic resistivity per pit membrane area (MPa s m^{-1}). I substituted the median vessel length L_{med} for L and the regression functions of D for L and A_{pit} obtained above. Then, using the data in "Lumen resistivity and end wall resistivity at the stem-xylem scale" section, r_p was determined for each test segment so that the mean value of wall fractions ($\Sigma(1/R_{tatal})/\Sigma(1/R_{lumen})$) of three cross sections equals the wall fraction of the test segment. The fraction of the end wall resistivity, R_{wall}, of a vessel was obtained as a function of D from the average r_p for each species.

Statistics

Fitting parameters and the 95% confidence intervals were calculated using Origin software (Microcal Software, Northampton, MA, USA).

RESULTS

Fractions of lumen resistivity and end wall resistivity for stem xylem

For three vessel-bearing angiosperm species, the hydraulic resistivity (R_{xylem}, MPa s mm^{-4}) was measured with the balance method (Sperry *et al.* 1988). Then, for these stem segments, the lumen resistivity ($\overline{R}_{lumen}$) was calculated by the Hagen-Poiseuille equation, and the relationship between $\overline{R}_{lumen}$ and $\overline{R}_{wall}$ (= $R_{xylem} - \overline{R}_{lumen}$) was determined (Fig. 4-7). Wall fractions ($\overline{R}_{wall}/R_{xylem}$) were 0.49 ± 0.16 (mean ± 1 SD, n = 4), 0.63 ± 0.035 (mean ± 1 SD, n = 4) and 0.58 ± 0.15 (mean ± 1 SD, n = 4) for *A. rufinerve*, *M. australis* and *V. coignetiae*, respectively. The wall fractions were not significantly different from 0.5 for *A. rufinerve* (t-test, P=0.958) or *V. coignetiae* (t-test, P=0.402). However, in *M. australis*, the wall fractions were significantly higher than 0.5 (t-test, P=0.00817).

Scaling of xylem vessels within stem xylem

The vessel length distributions for vessel-diameter classes were calculated by the silicone injection method (Fig. 4-8). Then, the relationship between vessel diameter and the median vessel lengths for different vessel-diameter classes were determined, and fitted to a power function (Fig. 4-9). When regression curves were applied to the data, the vessel length L_{med} is proportional to $D^{1.47}$ ($r^2 = 0.704$), $D^{3.18}$ ($r^2 = 0.973$) and $D^{2.86}$ ($r^2 = 0.963$) in *A. rufinerve*, *M. australis* and *V. coignetiae*, respectively. The 95% confidence intervals for the exponent are 1.05 to 1.90, 2.97 to 3.39 and 2.47 to 3.26 in *A. rufinerve*, *M. australis* and *V. coignetiae*, respectively.

Next, the relationship between the vessel diameter and the mean the inter-vessel wall width (p) was examined (Fig. 4-10). In *A.refinerve* and *M. australis*, p was related negatively to vessel diameter except for the vessels with 10-20 μm in diameter of *M. australis*. It is expected that vessels with 10-20 μm in diameter has negligible impact on the hydraulic conductivity of stems by the Hagen-Poiseuille equation. Thus, in this study, I obtained the regression function for vessels with diameters of >20 μm for *M. australis*. In contrast, p was not significantly related to the vessel diameter in *V. coignetiae*. When these relationships were regressed by power functions, p was proportional to $D^{-1.23}$ ($r^2 = 0.489$), $D^{-1.07}$ ($r^2 = 0.558$) or $D^{-0.184}$ ($r^2 = 0.0558$) in *A. rufinerve*, *M. australis* or *V. coignetiae*, respectively. The 95% confidence intervals for the exponent are −1.79 to −0.674, −1.54 to −0.596 and −0.619 to 0.250 in *A. rufinerve*, *M. australis* and *V. coignetiae*, respectively. The fraction of the pit membrane in the inter-vessel pit field (f_p) was 0.730 ± 0.0701 (mean ± 1 SD, $n = 5$) in *A. rufinerve*, 0.723 ± 0.0468 (mean ± 1 SD, $n = 5$) in *M. australis*, and 0.734 ± 0.122 (mean ± 1 SD, $n = 7$) in *V. coignetiae*. By substitution of the relationships between D and L_{med}, between D and p, and between D and f_p to Eq. 4-6, the inter-vessel pit area, A_{pit}, was expressed as proportional to $D^{0.242}$, $D^{2.11}$ or $D^{2.68}$ in *A. rufinerve*, *M. australis* or *V. coignetiae*, respectively.

Because $R_{wall} \propto 1/(L A_{pit})$, R_{wall} is proportional to $D^{-1.72}$, $D^{-5.30}$ or $D^{-5.54}$ in *A. rufinerve*, *M. australis* or *V. coignetiae*, respectively. The interval for the exponent calculated from the 95%

confidence intervals of correlation between D and L_{med} and between D and p was −3.12~−0.314, −6.19~−4.40 or −6.77~−4.31 in *A. rufinerve*, *M. australis* or *V. coignetiae*, respectively. By Hagen-Poiseuille equation, the lumen resistivity R_{lumen} is proportional to D^{-4}, where D is the vessel diameter. From the above data, the ratio of R_{lumen} to R_{wall}, R_{lumen}/R_{wall}, became proportional to $D^{-2.28}$, $D^{1.30}$ or $D^{1.54}$ in *A. rufinerve*, *M. australis* or *V. coignetiae*, respectively. Therefore, R_{lumen}/R_{wall} and wall fraction differed for vessel diameter classes within xylem.

Fractions of lumen resistivity and end wall resistivity for individual vessels

For evaluating quantitatively the wall fractions of different vessel diameter classes, the hydraulic resistivity per pit membrane area was calculated from the above data. Then, the resistance of the inter-vessel pits per pit area (r_p in Eq. 4-7) was calculated. r_p values were 48.6 ± 26.9 (mean ± 1 SD, n = 4), 279 ± 49.3 (mean ± 1 SD, n = 4) and 256 ± 164 (mean ± 1 SD, n = 4) MPa s m^{-1} in *A. rufinerve*, *M. australis* and *V. coignetiae*, respectively. From these results, the relationship between the vessel diameter and the wall fractions for different vessel diameter classes of each species were calculated (Fig. 4-11). In *M. australis* and *V. coignetiae*, it was expected that R_{lumen} was larger than R_{wall} in wider vessels and R_{wall} was larger than R_{lumen} in narrower vessels. On the other hand, in *A. rufinerve*, it was expected that R_{wall} was larger than R_{lumen} in wider vessels and R_{lumen} was larger than R_{wall} in narrower vessels.

DISCUSSION

Lumen and end wall were co-limiting the water flow for stem xylem of three species. However, I found that the wall fractions were different for vessel diameter classes in three woody species (Fig. 4-11), indicating that the interspecific relationship between R_{lumen} and R_{wall} is inapplicable to the vessels within stem xylem.

Concerning the present objective, the inter-vessel pit area per unit length decreased or did not change with the increase in the vessel diameter (Fig. 4-10). This means that the outflow per unit

vessel length is smaller in wider vessels. In contrast, assuming the columnar-shaped vessels, non-inter-vessel pit area unit vessel length is larger in wider vessel, and so the inflow per unit vessel length is larger in wider vessels. Thus it will be easier to refill the wider vessels than narrower vessels. It is consistent with the fact that the wider vessels are more vulnerable to cavitation. Cavitation and thus refilling events will occur more frequently in wider vessels.

The stem-mean wall fractions ($\overline{R}_{wall}$ /R_{xylem}) were 0.49, 0.63 and 0.58 in *A. rufinerve*, *M. australis* and *V. coignetiae*, respectively. Therefore, $\overline{R}_{lumen}$ and $\overline{R}_{wall}$ were nearly co-limiting the water flow in the stem xylem. These results agree with Sperry *et al.* (2005). The wall fraction of *M. australis*, however, was significantly higher than 0.5. In *M. australis*, the changes in the hydraulic diameter, the maximum vessel diameter and the lumen resistivity with stem xylem area were smaller than in the other species (Figs. 4-3, 4-4 and 4-6), resulting in the small fluctuation of the wall fraction and the significant difference. Originally, the wall fraction may be different from 0.5.

However, the interspecific relationship between R_{lumen} and R_{wall} is inapplicable to the vessels of different diameters. In *M. australis* and *V. coignetiae*, the end wall would limit water flow in narrower vessels and would not markedly limit it in wider vessels (Fig. 4-11). Fast-growing species may have vessels with such the traits. The lower end wall resistivity of wider vessels can lead to increase in the hydraulic efficiency of wider vessels, which give higher maximum hydraulic capacity to the plants. In contrast, the higher end wall resistivity of narrower vessels can lead to the increase in the resistance to cavitation of narrower vessels. The narrower vessels with higher resistance to cavitation wound function as bypasses in case of embolism of the wider vessels although the narrower vessels may form vessel relays and contribute only to radial connectivity (Brodersen *et al.* 2013). On the other hand, in *A. rufinerve*, the lumen would limit water flow for narrower vessels and would not so limit it for wider vessels (Fig. 4-11). In *A. rufinerve*, even narrower vessels will play roles as routes with larger hydraulic conductivity. As calculated by the Hagen-Poiseuille equation, it is believed that wider vessels play a major role in the hydraulic conductivity in xylem. In *A. rufinerve*, however, the contribution to hydraulic conductivity of narrower vessels will be more than expected by the

Hagen-Poiseuille equation. Moreover, in *A. rufinerve*, the end wall would limit water flow for wider vessels. Thus, wider vessels will have comparatively higher resistance to cavitation although they will have lower hydraulic conductivity. This pattern appears to be a deliberate strategy. On one vessel basis, the ring-porous woods tend to have higher hydraulic efficiency and lower cavitation resistance, while diffuse-porous woods tend to have lower hydraulic efficiency and higher cavitation resistance (Hacke *et al.* 2006). The difference in the relationship between vessel diameter and end wall fraction may be attributed to the difference in strategy between ring-porous and diffuse-porous woods.

The major factor which affects the dependence of R_{wall} and thus wall fraction on vessel diameter is the vessel length because R_{wall} is inversely proportional to the square of the vessel length (Eqs. 4-6 and 4-7). For all species analyzed, wider vessels tended to be longer and had larger median vessel length L_{med} (Figs. 4-8 & 4-9). In *A. rufinerve*, the difference in distribution of the vessel length is small compared with the other species examined. L_{med} was proportional to $D^{1.47}$, $D^{3.18}$ and $D^{2.86}$ in *A. rufinerve*, *M. australis* and *V. coignetiae*, respectively. Sperry *et al.* (2005) showed that mean vessel length L is proportional to D^2 among species. For three species analyzed in the present study, these 95% confidence intervals for the exponents did not overlap the value obtained by the interspecific comparison. Thus, inter- and intra-specific vessel traits of vessel length differed. The exponent in *A. rufinerve* was smaller than the other species, and narrower vessels of *A. rufinerve* were longer than those of the other species. Cai *et al.* (2010) examined the relationship between vessel diameter and mean vessel length in *Populus*. They showed a lower exponent when a regression with the power function was performed (the average exponent '*b*' for three species was 0.43). To compare with the study of Cai *et al.*, I also calculated the relationship between vessel diameter and mean vessel length. Then, the best fit exponent was 0.513 in *A. rufinerve*, while the values were 2.99 and 2.25 in *M. australis* and *V. coignetiae*, respectively. The lower exponents observed for *Populus* by Cai *et al.* (2010) and for *A. rufinerve* in this study may be common for diffuse-porous species.

Another major factor that affects the dependence of the wall fraction on vessel diameter is the mean inter-vessel wall width (Eqs. 4-6 and 4-7). The mean inter-vessel wall width p (i.e. the

inter-vessel wall area per unit length) varied markedly among the species (Fig. 4-10). In *A. rufinerve* and *M. australis*, p tended to decrease with the increase in vessel diameter except for vessels with 10-20 μm in diameter of *M. australis*. On the other hand, in *V. coignetiae*, p did not change with vessel diameter, although the value varied widely. Because $p = \Sigma w/N$, where w is the inter-vessel wall width and N is the number of vessels observed, p can be also regarded as the product of inter-vessel wall width, $\Sigma w/n$, where n is the number of connections, and the contact probability, n/N. For all species, the contact probability tended to decrease with the increase in the vessel diameter except for the vessels with 10-20 μm in diameter of *M. australis*, while the inter-vessel wall width tended to increase with the increase in the vessel diameter (Figs. 4-12 & 4-13). In *V. coignetiae*, wider vessels had larger contact probability compared with those of the other two species, resulting in the diameter-independent p.

The minor factor which affects the dependence of the wall fraction on vessel diameter is end wall resistivity. End wall resistivity per inter-vessel pit membrane area (r_p) found in the present study was in the same order of that obtained by Wheeler *et al.* (2005). In three species analyzed, *A. rufinerve* had the lowest end wall resistivity per inter-vessel pit membrane area. The lower pit membrane resistivity in *A. rufinerve* may be attributed to higher average porosity and/or the smaller thickness of pit membranes (Choat *et al.*, 2006).

CONCLUSION

The lumen and the end wall were not co-limiting the water flow equally in all vessels with different diameters, while they were nearly co-limiting the water flow on average. The difference in dependence of the wall fraction on vessel diameter may relate to the difference in strategies about the hydraulic capacity and resistance to cavitation.

In this study, I assumed the vessel geometry with lumen and wall components in series. However, vessels connect each other even at non-vessel end walls (Zimmermann & Brown, 1971). When the non-vessel end connection is considered, the end wall resistivity should not be proportional

to the inter-vessel pit area (Loepfe *et al.*, 2007). Thus, there may be error in the present calculation of r_p and wall fraction. Thus, observation of three dimensional structure and connections of xylem vessels should be important for detailed understanding of roles of the vessels of different diameters.

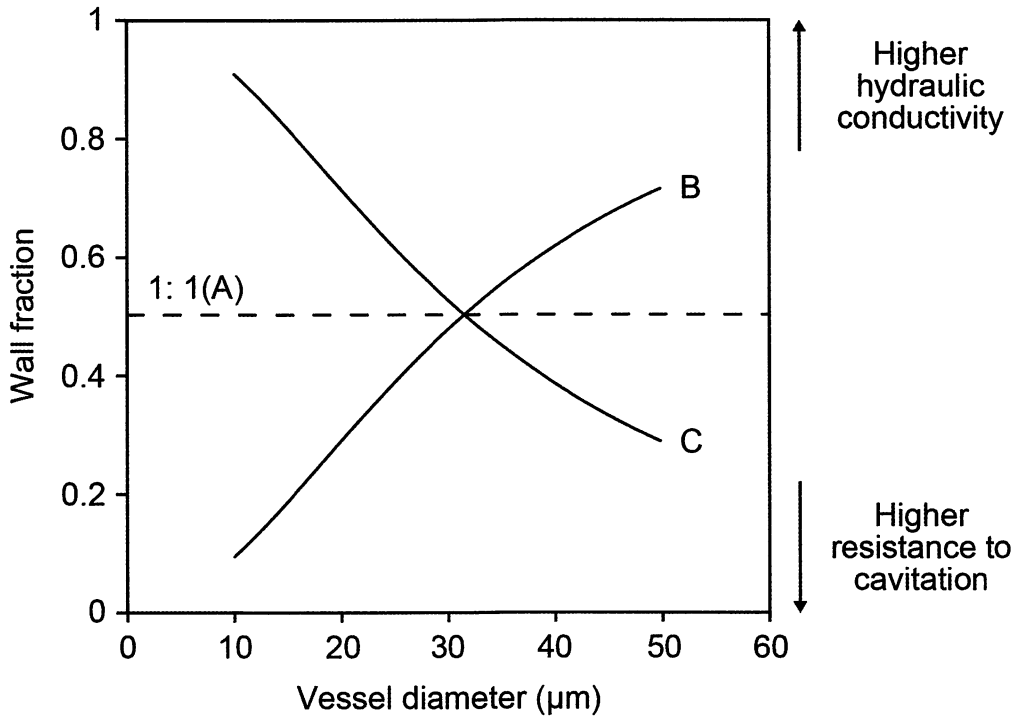

Figure 4-1. Relationship of vessel diameter to wall fraction (R_{wall}/R_{total}). It is not certain whether R_{lumen} and R_{wall} are co-limiting water flow for individual vessels with different diameters although the wall fraction is almost constant for the xylem as a whole from various species (Sperry *et al.*, 2005). If the average trait is applicable to individual vessels, R_{lumen}/R_{wall} equals one for all vessels (A, 1: 1 line). Otherwise, the wall fraction will vary for individual vessels. I assume two different vessel traits, B and C. In B-type species, wider vessels have larger wall fractions, while narrower vessels have smaller wall fractions. In this species, wider vessels are resistant to cavitation, and narrower vessels have high hydraulic conductivity. Conversely, in C-type species, wider vessels have smaller wall fractions, and narrower vessels have larger wall fractions. In this species, wider vessels have comparatively high hydraulic conductivity, and narrower vessels have comparatively high resistance to cavitation.

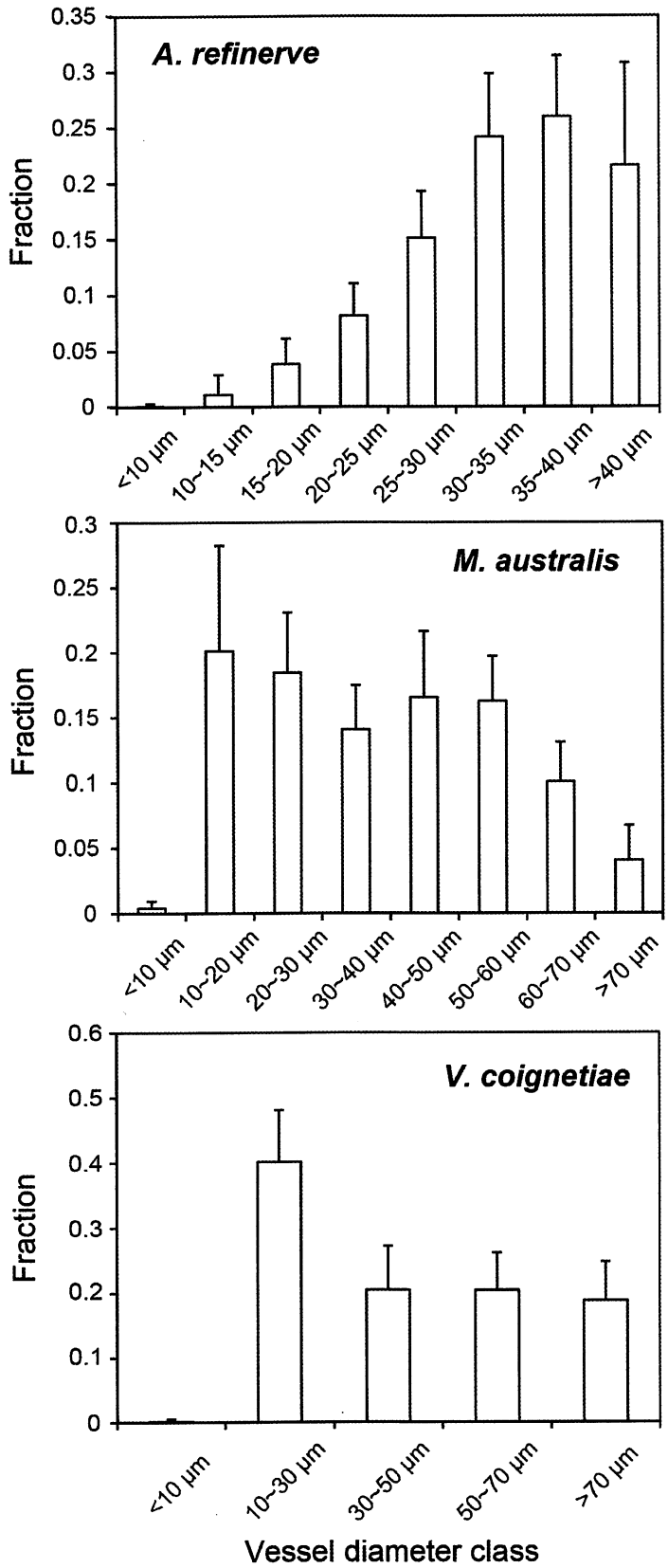

Figure 4-2. Distribution of vessel diameter classes. Error bars represent ± SD (n = 4 in each species).

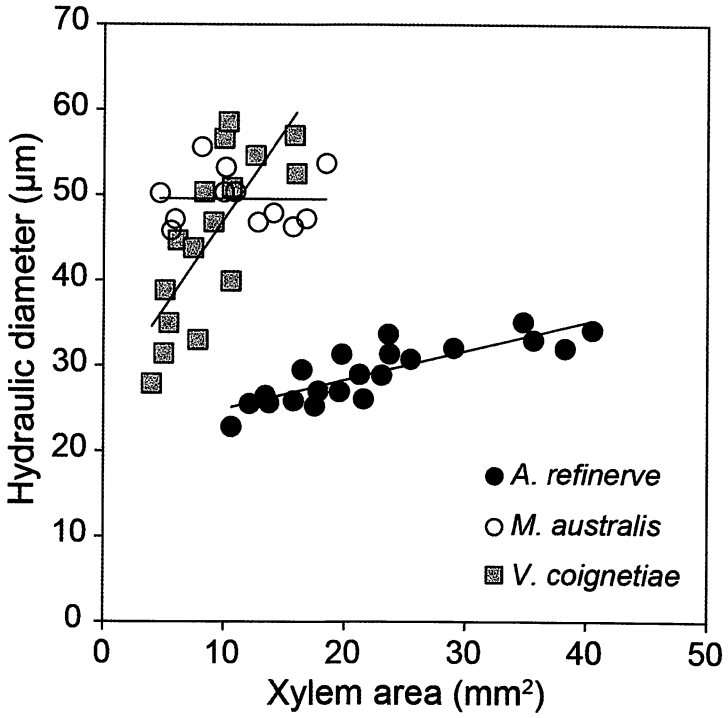

Figure 4-3. Relationship of the hydraulic vessel diameter to the xylem area in current-year shoots of *A. rufinerve*, *M. australis* and *V. coignetiae*.

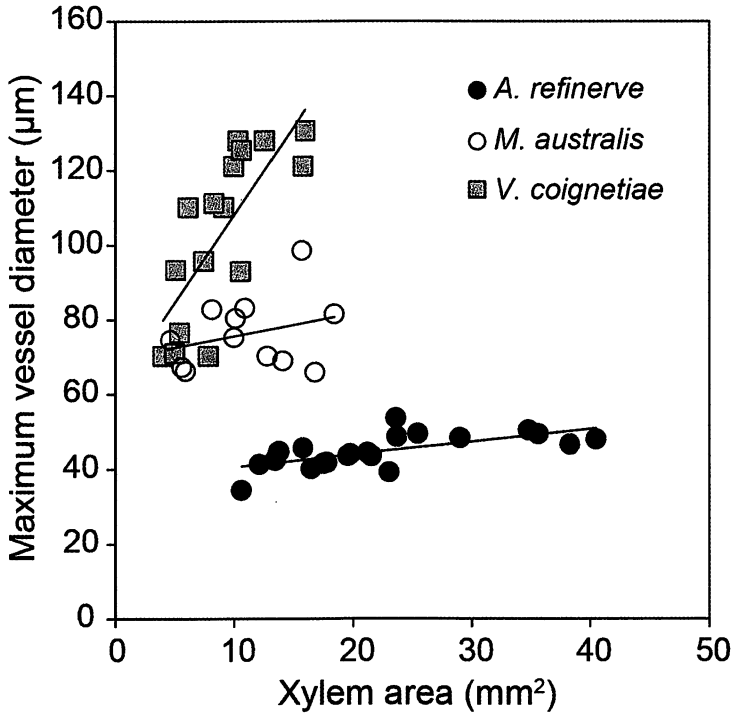

Figure 4-4. Relationship of the maximum vessel diameter to the xylem area in current-year shoots of *A. rufinerve*, *M. australis* and *V. coignetiae*.

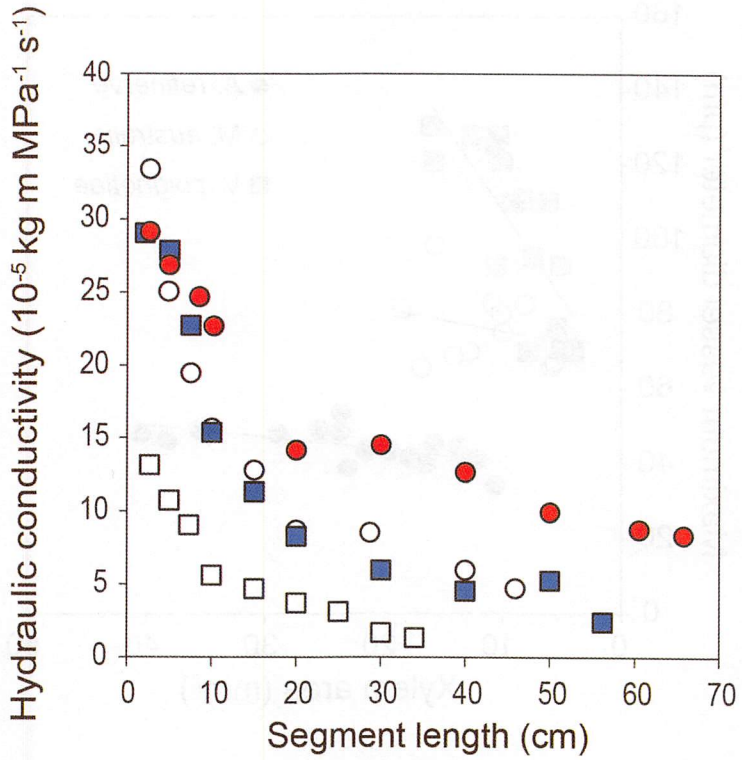

Figure 4-5. Stem segment length versus stem hydraulic conductivity in current-year stems of *V. coignetiae*. According to Sperry *et al.* (2005), I measured the hydraulic conductivity of the stem segments at different stem segment lengths. Different symbols represent different stem samples. The hydraulic conductivity increased gradually with increase of average xylem area of the segments at lengths longer than the threshold length, which depending on the stem segments (10~20 cm). Regression was extended to 0 cm segment length to give the estimated stem xylem resistivity (R_{xylem}). Beyond the threshold length, the considerable changes of the hydraulic conductivity of the stem segments were detected. This change is believed to be due to the proportion of open vessels in stem segments. Regression was extended to 0 cm segment length (when the fraction of open vessels is 100%) to give the estimated lumen resistivity ($\overline{R}_{lumen}$). Then, the wall fraction for whole stem xylem ($\overline{R}_{wall}/R_{xylem}$) in current-year stem xylem of *V. coignetiae* was calculated. The wall fraction was 0.56 ± 0.14 (mean ± 1 SD, n = 4), and this result corresponded well with the wall fraction obtained by the Hagen–Poiseuille lumen resistivity.

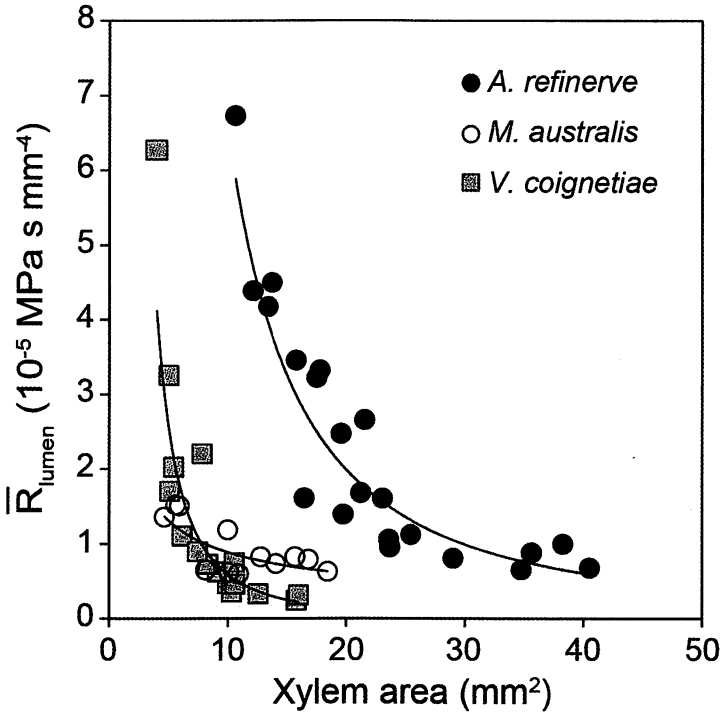

Figure 4-6. Relationship of the lumen resistivity ($\overline{R}_{lumen}$) to the xylem area in current-year shoots of *A. rufinerve*, *M. australis* and *V. coignetiae*.

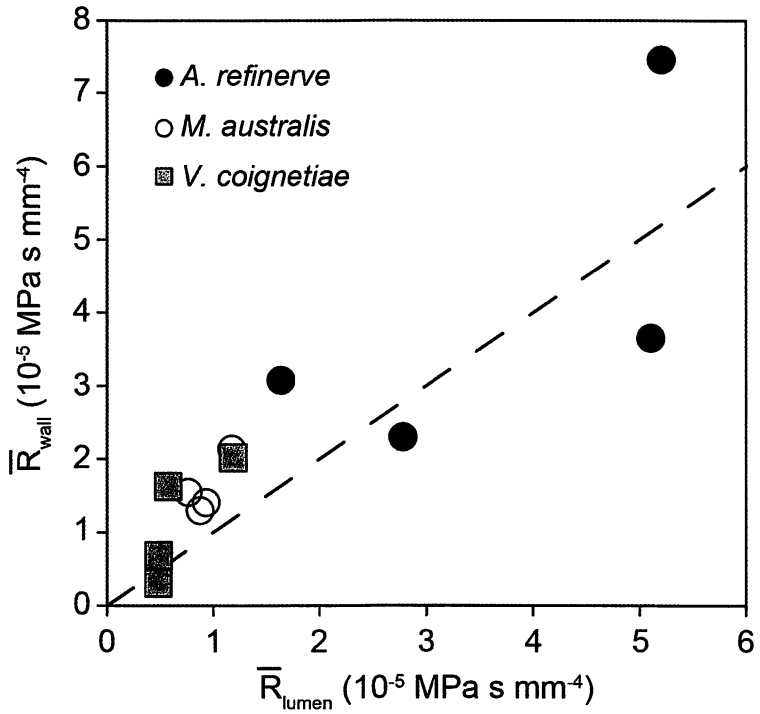

Figure 4-7. Lumen resistivity ($\overline{R}_{lumen}$) versus end wall resistivity ($\overline{R}_{wall}$) for the whole stem xylem in current-year shoots of *M. australis*, *A. rufinerve* and *V. coignetiae*. Stem xylem resistivity (R_{xylem}) was measured with the balance method (Sperry *et al.*, 1988). Then, $\overline{R}_{lumen}$ was obtained according to Hagen-Poiseuille equation, and $\overline{R}_{wall}$ was calculated as difference between R_{xylem} and $\overline{R}_{lumen}$. The data were close to the 1: 1 line.

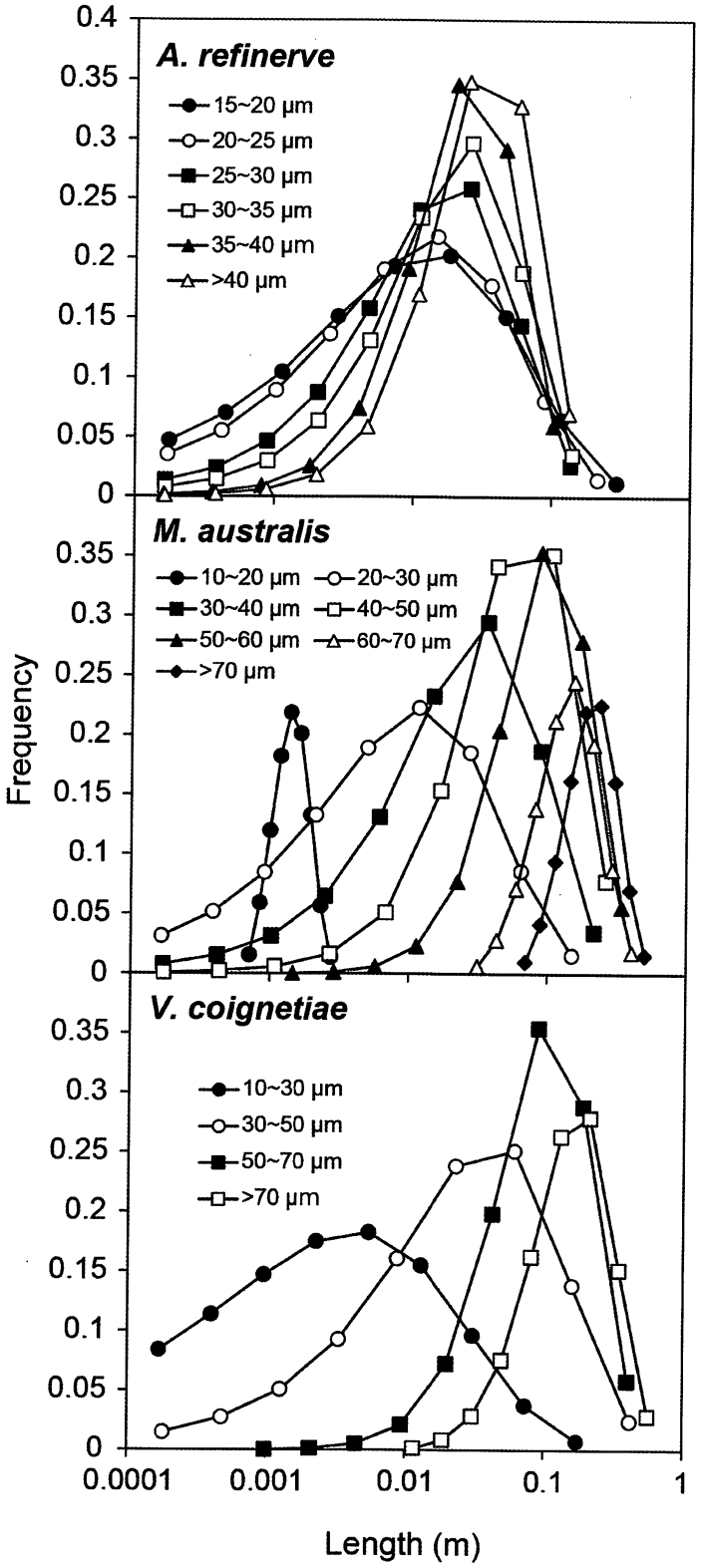

Figure 4-8. Vessel-length distribution for different diameter classes in current-year shoots of *A. rufinerve*, *M. australis* and *V. coignetiae*.. The vessel-length distribution was obtained using the silicone injection method (Christman *et al.*, 2009).

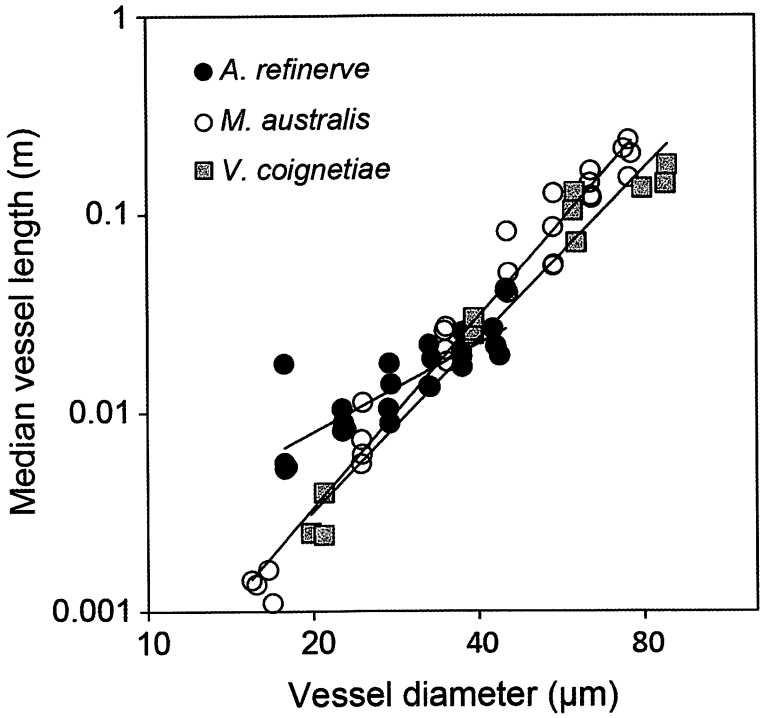

Figure 4-9. Relationship of the median vessel length to the mean vessel diameter for different diameter classes in current-year shoots of *A. rufinerve*, *M. australis* and *V. coignetiae*. The median vessel lengths were obtained using the silicone injection method (Christman *et al.*, 2009).

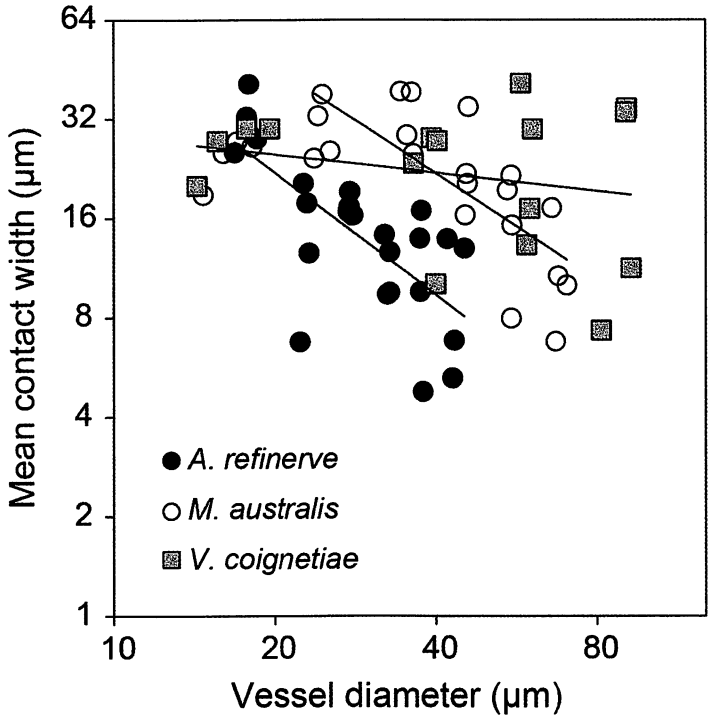

Figure 4-10. Relationship of the mean inter-vessel contact wall width to the mean vessel diameter for different diameter classes. Average inter-vessel contact width with other vessels was measured for different diameter classes in current-year shoots of *A. rufinerve*, *M. australis* and *V. coignetiae*.

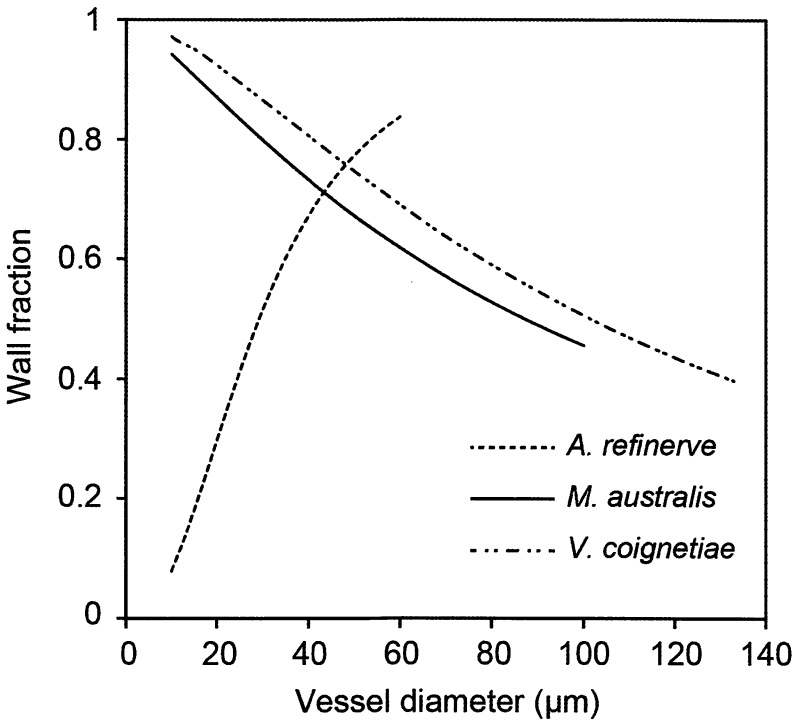

Figure 4-11. Relationship of estimated wall fractions to vessel diameter in current-year shoots of *A. rufinerve*, *M. australis* and *V. coignetiae*. The hydraulic resistivity per pit membrane area r_p which satisfies $1/R_{xylem} = \Sigma(1/R_{total})$ is calculated for each sample. Then, the fraction of the end wall resistivity was estimated for a vessel with a certain diameter.

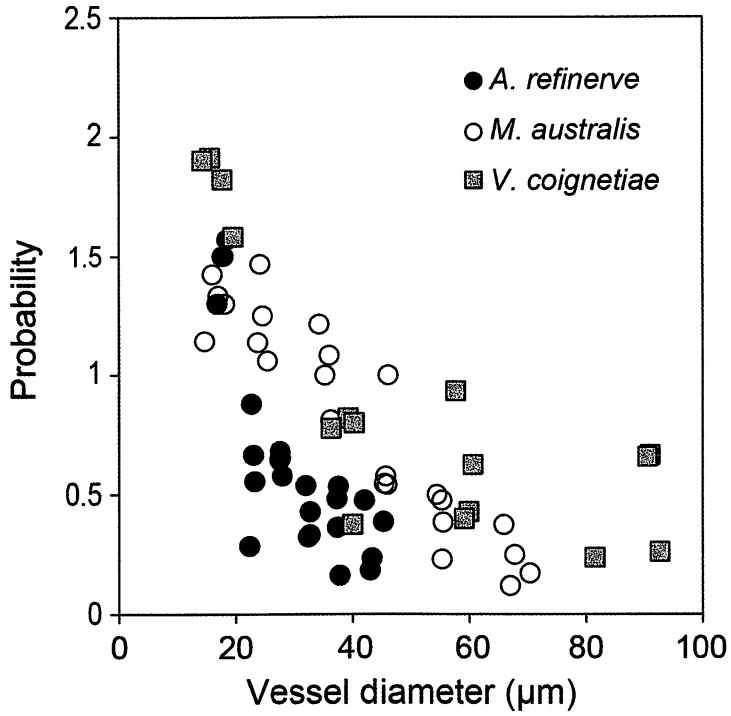

Figure 4-12. The contact probability for different vessel diameter classes. The mean connectivities of vessels in a cross-section were obtained. A vessel with a connectivity value greater than one means that the vessel connects with more than two vessels in a cross-section.

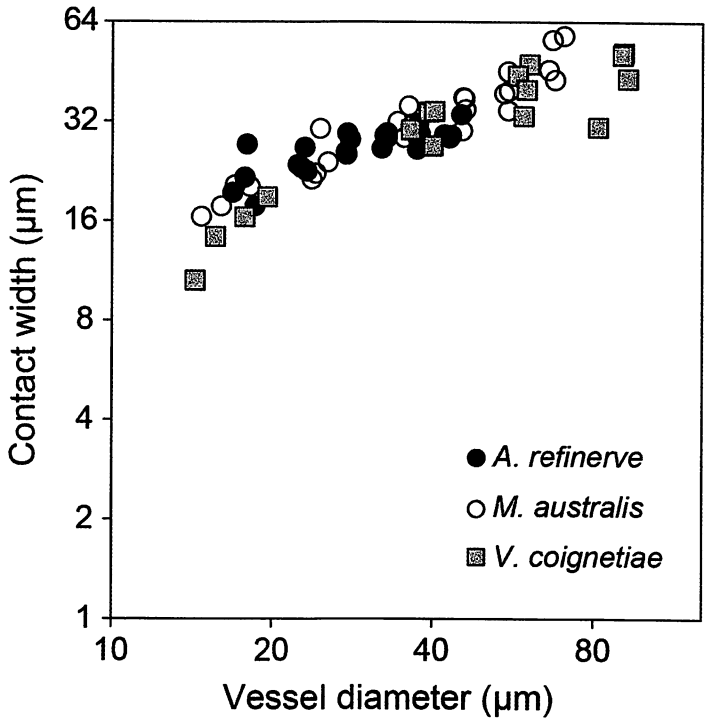

Figure 4-13. The inter-vessel wall width for different vessel diameter classes. The relationships between the vessel diameter and the inter-vessel wall width ($\Sigma w/n$, where w is inter-vessel wall width and n is the number of connections) are showed.

REFERENCES

Brodersen CR, Choat B, Chatelet DS, Shackel KA, Matthews MA, McElrone AJ. 2013. Xylem vessel relays contribute to radial connectivity in grapevine stems (*Vitis vinifera* and *V. arizonica*; Vitaceae). *American Journal of Botany*, **100**, 314-321

Brodersen CR, Lee EF, Choat B, Jansen S, Phillips RJ, Shackel KA, McElrone AJ, Matthews MA. 2011. Automated analysis of three-dimensional xylem networks using high-resolution computed tomography. *New Phytologist*, **191**, 1168-1179.

Cai J, Zhang S, Tyree MT. 2010. A computational algorithm addressing how vessel length might depend on vessel diameter. *Plant, Cell & Environment*, **33**, 1234-1238.

Choat B, Brodie TW, Cobb AR, Zwieniecki MA, Holbrook NM. 2006. Direct measurements of intervessel pit membrane hydraulic resistance in two angiosperm tree species. *American Journal of Botany*, **93**, 993–1000.

Choat B, Cobb AR, Jansen S. 2008. Structure and function of bordered pits: new discoveries and impacts on whole-plant hydraulic function. *New Phytologist*, **177**, 608-626.

Christman MA, Sperry JS, Adler FR. 2009. Testing the 'rare pit' hypothesis for xylem cavitation resistance in three species of *Acer*. *New Phytologist*, **182**, 664-674.

Hacke UG, Sperry JS, Wheeler JK, Castro L. 2006. Scaling of angiosperm xylem structure with safety and efficiency. *Tree Physiology*, **26**, 689-701.

Hargrave KR, Kolb KJ, Ewers FW, Davis SD. 1994. Conduit diameter and drought-induced embolism in *Salvia mellifera* Greene (Labiatae). *New Phytologist*, **126**, 695–705.

Loepfe L, Martinez-Vilalta J, Piñol J, Mencuccini M. 2007. The relevance of xylem network structure for plant hydraulic efficiency and safety. *Journal of Theoretical Biology*, **247**, 788-803.

Sperry JS, Donnelly JR, Tyree MT. 1988. A method for measuring hydraulic conductivity and embolism in xylem. *Plant, Cell & Environment* **11**, 35-40.

Sperry JS, Hacke UG, Wheeler JK. 2005. Comparative analysis of end wall resistivity in xylem

conduits. *Plant, Cell & Environment*, **28**, 456-465.

Tyree MT, Ewers FW. 1991. Tansley review, 34: The hydraulic architecture of trees and other woody plants. *New Phytologist*, **119**, 345–360.

Wheeler JK, Sperry JS, Hacke UG, Hoang N. 2005. Inter-vessel pitting and cavitation in woody Rosaceae and other vesselled plants: a basis for a safety versus efficiency trade-off in xylem transport. *Plant, Cell & Environment*, **28**, 800-812.

Zimmermann MH. 1983. *Xylem Structure and the Ascent of Sap*. Springer-Verlag, Berlin, Germany.

Zwieniecki MA, Melcher PJ, Holbrook NM. 2001. Hydraulic properties of individual xylem vessels of *Fraxinus americana*. *Journal of Experimental Botany*, **52**, 257-264.

CHAPTER 5

Gas diffusion in stem xylem and hydraulic conductivity between a vessel and surrounding parenchyma cells

ABSTRACT

Two values concerning the stability of the pit valves, the area based hydraulic conductivity between a vessel and surrounding parenchyma cells, and the removal rate of the gas in the vessel, were determined using the single-vessel method (Zwieniecki *et al.*, 2001) in *Morus australis* (mulberry) and in *Laurus nobilis* (laurel). There was a significant difference in the hydraulic conductivity between these species when KCl solution was forced into the individual vessels. The hydraulic conductivity per unit vessel surface area was $9.12 \pm 6.16 \times 10^{-8}$ m MPa^{-1} s^{-1} for mulberry and $3.55 \pm 2.15 \times 10^{-7}$ m MPa^{-1} s^{-1} for laurel. The rate at which gas was forced out from the pressurized vessels was also measured. The values were $1.26 \pm 0.24 \times 10^{-5}$ mol m^{-2} s^{-1} MPa^{-1} for mulberry and $1.55 \pm 0.26 \times 10^{-5}$ mol m^{-2} s^{-1} MPa^{-1} for laurel. Then, the relationship between the gas pressure in the refilling vessel lumen and the inflow rate into the vessel was estimated. The pressures requred refilling of the vessel within the time reported in the previous study (Salleo *et al.*, 2004) or observed in the present study were substantially below the threshold pressure up to which the pit valves can be retained. Therefore, the pit valves will work during the vessel lumen refilling and contribute to the efficient refilling of the vessel.

INTRODUCTION

According to the pit-valve hypothesis (Holbrook and Zwieniecki, 1999), the gas trapped within the inter-vessel bordered pits (pit valve) prevents the refilling vessel water from being lost to the surrounding functional vessels under negative pressure. To complete refilling of an embolized vessel, however, all the pit valves must collapse. All the pit valves did not collapse simultaneously (Chapter 3), and thus the inward water flow from parenchyma cells should be more than the outward flow from the refilling vessel even after some pit valves collapse. The outward flow rate is proportional to the cumulative area of the collapsed inter-vessel pits and the hydraulic conductivity across the pits (in Chapter 4). On the other hand, the inward flow rate is proportional to the contact wall area between the vessel and surrounding parenchyma cells (Chapter 4) and the hydraulic conductivity between them. Thus, the measurement of the hydraulic conductivity between the vessel and parenchyma cells is indispensable to estimation of the inward flow rate.

Although the pit valves must collapse eventually, the pit valves contribute to the efficient refilling of the vessel by reducing the outflow of refilling vessel water during refilling of the embolized vessel. The pit valve stability depends on the threshold liquid pressure at which it collapse (Chapter 3) and the liquid pressure in the refilling vessel during the vessel lumen refilling. Pressurization of the refilling vessel is prevented by rapid gas dissolution into surrounding water, and is accelerated by the large inward water flow from parenchyma cells to the vessel. Thus, the liquid pressure in the refilling vessel depends on the gas removal from the vessel and the inward flow rate from surrounding parenchyma cells.

Here, I aimed at estimating the hydraulic conductivity between a vessel and surrounding parenchyma cells and the pressure in the refilling vessel. For this purpose, the rates at which water and gas can exit radially from an individual vessel were quantified using the single-vessel method (Zwieniecki *et al.*, 2001). The vessels of mulberry (*Morus australis* Poir.) and of laurel (*Laurus nobilis* L.) were used.

MATERIALS AND METHODS

Plant materials

All measurements were conducted on current-year shoots of *Morus australis* Poir. (mulberry) excised from trees growing on the Hongo campus, the University of Tokyo (35° 42′ 48″ N, 139° 45′ 44″ E, 20 m a.s.l.) or those of *Laurus nobilis* L. (laurel) grown in pots. The hydraulic conductivity measurements were made in June 2013 for mulberry stems and in February 2013 for laurel stems. Measurements of the gas removal rate were conducted between August and October 2011 in mulberry and between November and December 2013 in laurel.

Hydraulic conductivity

For estimation of the hydraulic conductivity between a vessel and surrounding parenchyma cells, a solution was pushed into a vessel which did not connect with other vessels in the segment unlike the experiments in chapter 3. Stem segments, about 3 cm long, and about 8 mm in diameter for mulberry and about 6 mm in diameter for laurel, were cut from the shoots and trimmed with a fresh razor blade. Microcapillary tubes with an inner diameter of 0.6 mm (G-1, NARISHIGE, Tokyo, Japan) were pulled on a horizontal pipette puller (PC-10, NARISHIGE) and the glass tips subsequently broken such that the opening was about 80 μm for mulberry and about 40 μm for laurel in diameter. The tip was then inserted into an open lumen of a single vessel by the aid of a micromanipulator (M-152, NARISHIGE) under a stereo microscope (SMZ, Nikon, Tokyo, Japan). The capillary was fixed to the segment using a low viscosity, fast setting acrylic glue (Loctite407, Henkel Japan, Tokyo, Japan). The glue was applied carefully not to block the other vessels on the cut surface of the segment. The capillary was supported by three glass rods that were glued to the side of the stem segment (side-A, see Fig. 5-1). I confirmed that the vessel attached with the microcapillary was open by sending air using a syringe connecting to capillary-A via a silicone tube.

For detection of the other vessel that diverged from the vessel via the bordered pits (pit-passing vessel, PPV), acid fuchsin dye (0.2% in deionized water) filtered through 0.2 μm filter

was flushed from the capillary-A at 0.6 MPa using a N_2-cylinder (Fig. 5-1A). The opposite end of the segment (side-B) was kept under water to prevent the cut surface of side-B from being stained with the dye that flowed out from side-B. The samples in which the cut surfaces of side-A were stained were discarded. After the pressure release, the cut surface of side-B was carefully observed using the stereo microscope, and the stained vessels were counted. When the number was greater than one, then the stem segment length was shortened until the number was reduced to one. In most cases, the segments were eventually shortened to about 2 cm for mulberry and about 3 cm for laurel. The 20 mM KCl solution filtered through 0.2 μm filter was forced to flow into the vessel from the microcapillary using a syringe. Then, the distal end of the vessel was carefully sealed under a stereo microscope with the glue such that the adjacent vessel openings remained unblocked. The vessel into which the microcapillary had been inserted was detected by observation of the movement of the meniscus in the vessel when pressurizing by the syringe. The KCl solution in the microcapillary-vessel system was then pressurized to 1.0 MPa for 30 or 60 min, and the volume flow rate into the vessel was determined by measuring the time required for the meniscus to move a specified distance along the microcapillary tube (Fig. 5-1B). The movement of the meniscus was recorded every 5 or 10 min using a digital camera (Optio W60, PENTAX, Tokyo, Japan), and the volume flow rate of water movement into the vessel J ($m^3 s^{-1}$) was calculated. During the experiment, the both cut surfaces of the test segment were kept wet with deionized water so that the water potential of surrounding tissues came close to zero. In laurel, the flow rates were also measured for 0.2% acid fuchsin solution and 20 mM sucrose solution in addition to for the KCl solution.

After the pressure release, the cut surface of side-B was trimmed with a fresh razor blade and the glue on the cut surface was removed. Then, safranin dye was pushed into the vessel lumen using a syringe connecting to the microcapillary to stain the vessel walls. The three cross-sections of the segment were photographed with a digital camera (DP71, Olympus, Tokyo, Japan) mounted on a light microscope (BX50, Olympus). From the images, the average circumference of the stained vessel was measured using Image J (http://rsb.info.nih.gov/ij/).

According to Zwieniecki *et al.* (2001), the hydraulic conductivity per unit vessel surface area, L_r, was calculated as the rate at which water exits the vessel normalized by the area and the applied pressure ($m^3\ m^{-2}\ s^{-1}\ MPa^{-1}$):

$$L_r = J/(\Delta P\ A_V) \quad (5\text{-}1),$$

where ΔP (MPa) is the difference between the pressure applied to the vessel and the outside ambient pressure, and A_v (m^2) is the interior surface area of the vessel. A_v was calculated as the product of the vessel circumference and the segment length.

Gas movement from a pressurized vessel

Gas removal from a vessel was determined according to Zwieniecki and Holbrook (2001). For the measurement, a microcapillary tube was attached to a solitary vessel within the test segment as described above. The acid fuchsin dye was pushed out of the vessel lumen and the vessel lumen was then filled with air using N_2-cylinder. Subsequently, the both cut surfaces were sealed with the glue (Fig. 5-1C). A small volume of dye was inserted into the end of the microcapillary to provide an indicator whose movement was used to determine the flow rate of gas from the vessel. The microcapillary-vessel system was pressurized to 0.1, 0.2 or 0.4 MPa generated by the N_2-cylinder, and the movement of gas from the vessel lumen was determined by recording the movement of the dye within the microcapillary every 5 or 10 min. The digital camera was used to record the dye movement. Then, the rate at which gas exits the vessel per vessel surface area per unit pressure applied, k_{gas} ($mol\ m^{-2}\ s^{-1}\ MPa^{-1}$), was calculated from the movement of the dye within the microcapillary.

Assuming the constant inward flow rate per unit the interior surface area of the vessel (j_{liq}, $m^3\ m^{-2}\ s^{-1}$) into the refilling vessel, I estimated the pressure in the refilling vessel at the steady state. At the steady state, the water entry into the embolized vessel induces the gas removal from the vessel without increasing the pressure of remained gas in the refilling vessel, that is:

$$j_{liq} = \frac{k_{gas}\,R\,T}{P_{gas}}\,\Delta P \quad (5\text{-}2),$$

where R is gas constant (J K^{-1} mol^{-1}), T is temperature (K), and P_{gas} is the gas pressure in the vessel lumen, which is expressed in absolute pressure not in gauge pressure. The gas pressure in the refilling vessel lumen was expressed as a function of the water inflow rate into the vessel by Eq. 5-2.

According to Zwieniecki *et al.* (2001), an apparent diffusion coefficient D_{gas} (m^2 s^{-1}) for the movement of gas across the stem was also calculated. Here, it was assumed that the gas removal from the vessel was limited by the gas diffusion through the stem segment, not by the gas dissolution into surrounding water. Then, D_{gas} can be calculated based on a cylindrical geometry (Cussler, 1997):

$$D_{gas} = \frac{j_{gas}\, r_o \ln(r_o/r_v)}{\Delta c_{gas}} \quad (5\text{-}3),$$

where j_{gas} is the flow rate of gas per unit interior surface area of the pressurized vessel (mol m^{-2} s^{-1}), r_v is the vessel radius (m), r_o is the radius of the outer boundary of the cylinder (m) which was assumed to be the distance from the pressurized vessel to the nearest edge of the stem segment, and Δc_{gas} is the difference in concentration of dissolved gases in the water at the surface of the vessel and at the edge of the stem (mol m^{-3}). The concentrations of dissolved gases were calculated by Henry's law using Henry constant for air of 7.75×10^{-6} mol m^{-3} Pa^{-1} (Zwieniecki *et al.*, 2001).

RESULTS

Water movement between a vessel and surrounding tissues

The volume flow rates of water movement from the vessels into the surrounding tissues (J) did not change with time when the KCl solution was pushed into the vessels of mulberry stems (Fig. 5-2). The area based hydraulic conductivity between a vessel and surrounding tissues calculated by Eq. 5-1 was $9.12 \pm 6.16 \times 10^{-8}$ m MPa^{-1} s^{-1} (mean ± 1 SD, n = 6) (Fig. 5-3). In laurel, the flow rates did not change with time although the flow rate in one sample gradually decreased with time for all the solutions tested (Fig. 5-4). For the stem sample in which the flow rates were not constant, the hydraulic conductivities were calculated from the initial values of the flow rates. The hydraulic conductivities for laurel were $3.55 \pm 2.15 \times 10^{-7}$ m MPa^{-1} s^{-1} (mean ± 1 SD, n = 5) for the KCl

solution, $1.72 \pm 0.80 \times 10^{-7}$ m MPa^{-1} s^{-1} (mean ± 1 SD, $n = 5$) for the acid fuchsin solution, and $9.82 \pm 3.84 \times 10^{-8}$ m MPa^{-1} s^{-1} (mean ± 1 SD, $n = 3$) for the sucrose solution (Fig. 5-3). The hydraulic conductivity for the 20 mM KCl was larger than those for the others although these differences were not statistically significant. These values obtained in the present study were close to that reported by Zwieniecki *et al.* (2001) for *Fraxinus americana*, 1.62×10^{-7} m MPa^{-1} s^{-1}.

Gas removal from a vessel

The rate at which gas was forced out across the surface of the pressurized vessel remained constant for over 1 h (Fig. 5-5). The rates (k_{gas}) at which gas exited the vessel per unit vessel surface per unit pressure applied, were $1.26 \pm 0.24 \times 10^{-5}$ mol m^{-2} s^{-1} MPa^{-1} (mean ± 1 SD, $n = 12$) for mulberry and $1.55 \pm 0.26 \times 10^{-5}$ mol m^{-2} s^{-1} MPa^{-1} (mean ± 1 SD, $n = 11$) for laurel. Then, the relationship between the inward flow rate per unit the interior surface area of the refilling vessel and the gas pressure in the vessel lumen was estimated using Eq. 5-2 (Fig. 5-6). The pressure in cavitated vessels is considered to be nearly equal to the atmospheric pressure (Tyree and Sperry, 1989). Considering the constant inward flow into the refilling vessel, the pressure in the vessel will gradually increase with time and approach steady state pressure. Thus, the steady state pressure would be the maximum pressure of the refilling vessel for the inflow rate.

I also calculated the diffusion coefficients (D_{gas}) for the movement of gas across the stem. The values were $1.67 \pm 0.50 \times 10^{-8}$ m^2 s^{-1} (mean ± 1 SD, $n = 12$) for mulberry and $5.26 \pm 1.50 \times 10^{-9}$ m^2 s^{-1} (mean ± 1 SD, $n = 11$) for laurel. The calculated diffusion coefficient was found to be larger than the diffusion coefficient of air in water (1.95×10^{-9} m^2 s^{-1}; Yang and Tyree, 1992).

DISCUSSION

In the present study, the area based hydraulic conductivity between a vessel and surrounding parenchyma cells was estimated as the rate at which water moved out from the pressurized vessel. Xylem vessels are surrounded by parenchyma cells, fibers, and sometimes tracheids. Thus, water

might exit from the vessel surfaces facing the tissues other than the parenchyma cells. If this is the case, L_r obtained in the present study will be underestimated for the parenchyma cells. When the safranin dye was pushed into the vessel of the both species tested, however, the dye accumulated strongly at the pits between the vessel and parenchyma cells (Fig. 5-7). This indicates that the water exited mainly from the pressurized vessel across the vessel-parenchyma pits. Thus, it is possible to consider the L_r obtained would actually be the hydraulic conductivity between the vessel and parenchyma cells.

When the KCl solution was pushed into the vessel, there was a significant difference in L_r between mulberry and laurel (Fig. 5-3). The vessels of laurel stems may have greater ratio of the vessel-parenchyma pit area to the total vessel surface and/or the greater the hydraulic conductivity per the vessel-parenchyma pit membrane area than of mulberry stems. Moreover, the hydraulic conductivity of the laurel stem vessel with the KCl solution was larger than those for the acid fuchsin solution and sucrose solutions, although differences were not statistically significant. The hydraulic conductivity across the inter-vessel pit membrane may increase in response to the cation content of the xylem fluid by changing the volume of pectin in nanometer-sized pores in the inter-vessel pit membrane (Zwieniecki *et al.*, 2001; van Ieperen, 2007). The ionic composition of the fluid may also change the hydraulic conductivity across the vessel-parenchyma pit membrane, resulting in the higher conductivity with KCl solution.

When the acid fuchsin and the sucrose solution were introduced into the vessels, the rate at which water moved out from the pressurized vessel decreased with time (Fig. 5-4). Low uptake rates by the surrounding cells for these solute molecules might increase the concentrations of these solutions introduced into the vessel, and osmotically decrease the solution movement from the vessel.

The presence of sucrose causes a reduction of the starch pool in xylem parenchyma cells and induces the expression levels of aquaporins (Secchi and Zwieniecki, 2011). So, I expected that the introduction of the sucrose solution would result in large hydraulic conductivity between the vessel and surrounding tissues due to expression of aquaporins. Contrary to the expectation, the hydraulic

conductivity did not increase when examined with the sucrose solution. Secchi and Zwieniecki (2011) showed the aquaporin genes were significantly up-regulated 2 h after exposure to the sucrose. So, my result may be due to the short exposure time (1 h). Another possibility is that this may be due to the season during the experiments were conducted. The starch content in the laurel stem xylem changed substantially depending on the season (Fig. 5-8). The present experiment with the sucrose solution was conducted in winter, and the starch content in the xylem was much smaller than that in the summer. The aquaporin gene expression level triggered by sucrose may also change depending on the season, and the increase in the hydraulic conductivity with the increase in aquaporin gene expression level may be limited to summer, during which cavitation events should occur frequently.

The rate at which gas could be forced out from the pressurized vessel (k_{gas}) for laurel was significantly larger than for mulberry (*t*-test, P = 0.0104). In contrast, the apparent diffusion coefficient D_{gas} for mulberry was significantly larger than for laurel (*t*-test, P <0.01). Assuming that D_{gas} is constant independent of the test segments, k_{gas} (= $j_{gas}/\Delta P$) would be inversely proportional to $r_o\ln(r_o/r_v)$ because $\Delta c_{gas} \propto \Delta P$ (see Eq. 5-3). However, correlation between k_{gas} and $1/(r_o\ln(r_o/r_v))$ was not positive (Fig. 5-9). I propose that the gas removal from the pressurized vessel would be limited by gas dissolution into surrounding water, not by the gas diffusion through the stem segment to the ambient air. The high diffusion rate of gas molecules through the stem may be caused by the gas-filled fiber cells in xylem (Utsumi *et al.*, 1998). Alternatively, the vessel walls might have the interlinked gas-filled channels that facilitate the movement of gases, resulting in the high diffusion rate (Zwieniecki and Holbrook, 2009). On the other hand, the dissolution rate of gas in the vessel into surrounding water will depend on the cumulative area of vessel-parenchyma pit membrane because the area gives the gas-water interfaces to dissolve the gas into water. The greater cumulative area of vessel-parenchyma pit membranes in laurel may be responsible for the higher gas removal rate.

The pit valve stability depends on the threshold liquid pressure at which it collapse and the liquid pressure in the refilling vessel during the vessel lumen refilling. Assuming that the inward flow rate into the refilling vessel is constant, I estimated the gas pressure in the refilling vessel lumen (Fig.

5-6). Under this assumption, the time necessary to displace the entire volume of the vessel is calculated as $D/(4j_{liq})$ s, where D is the vessel diameter. For a model vessel (60 μm for mulberry and 35 μm for laurel), I estimated the inflow rate into the refilling vessel (j_{liq}) required for the complete refilling of the vessel within the time reported in the previous work or observed in the present study, namely, in 3 h for mulberry (Chapter 2) and in 1 h for laurel (Salleo *et al.*, 2004). Then, the values of j_{liq} were calculated to be 1.39×10^{-6} mm s^{-1} for mulberry and 2.43×10^{-6} mm s^{-1} for laurel. These were within previously reported values, 6×10^{-7} mm s^{-1} for *Vitis vinifera* by Brodersen *et al.* (2010) and of 6.8×10^{-5} mm s^{-1} for *Cucumis sativus* by Scheenen *et al.* (2007). Then, the gas pressures in the refilling vessel lumens will be 4.64 kPa for mulberry and 6.74 kPa for laurel. Even when the refilling in the mulberry stem vessel is assumed to be finished in 1 h, j_{liq} will be 4.17×10^{-6} mm s^{-1} and the gas pressure in the vessel lumen will be only 15.3 kPa. Even when the pressure difference between gas and liquid by the capillary force was considered, the liquid pressures in the refilling vessels are much smaller than the threshold pressures at which the pit valves collapse (Chapter 3). Thus, the pit valves should be retained during the vessel lumen refilling.

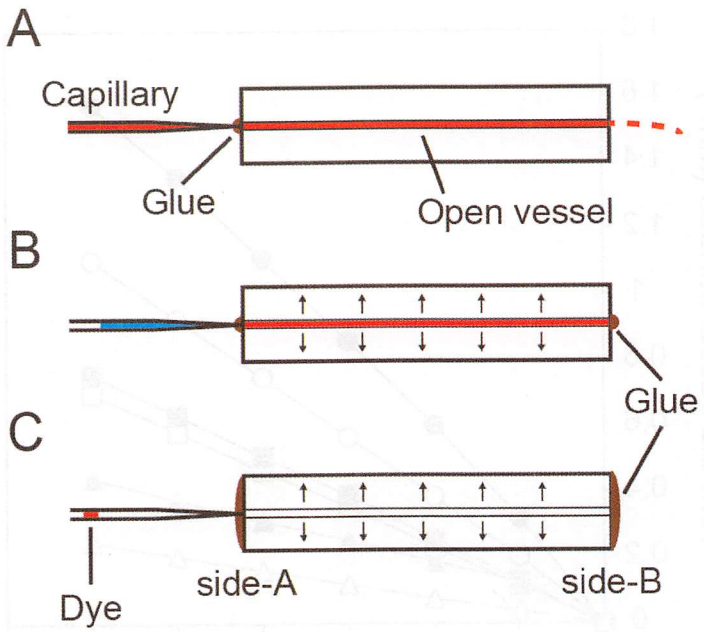

Figure 5-1. The single vessel method. A, An open vessel that did not connect to another vessels was detected by dye perfusion from a microcapillary tube inserted into the vessel lumen. B, Solutions was pushed into the vessel at a positive pressure, and the water movement from the vessel was caculated by observing the movement of the meniscus within the microcapillary. C, The vessel was filled with gas. Then, the gas was pressurized and the rate at which gas exited the vessel was measured by the observing the movement of the dye within the microcapillary.

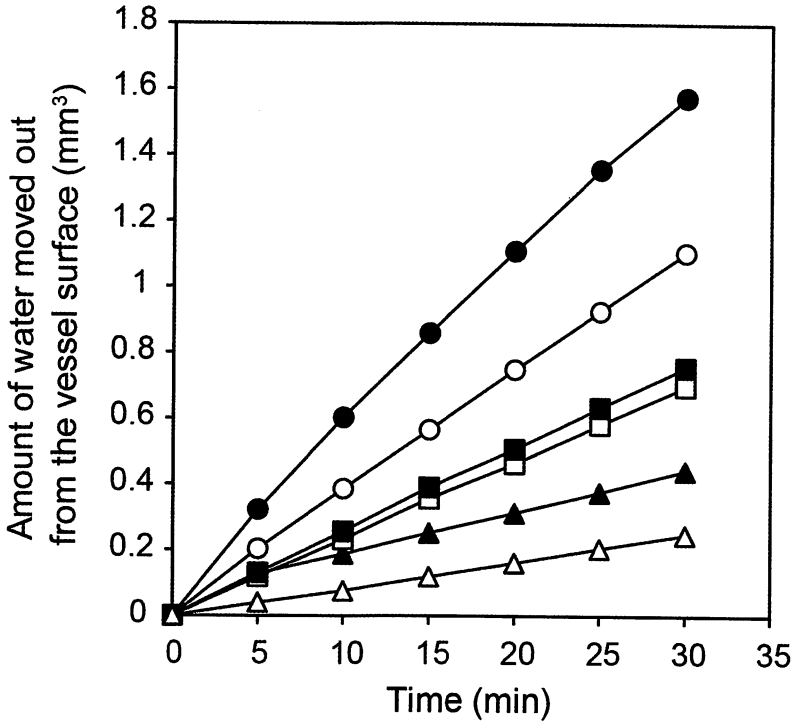

Figure 5-2. Efflux of water (20 mM KCl solution) from single pressurized vessels with time. Different symbols represent different stem samples of mulberry.

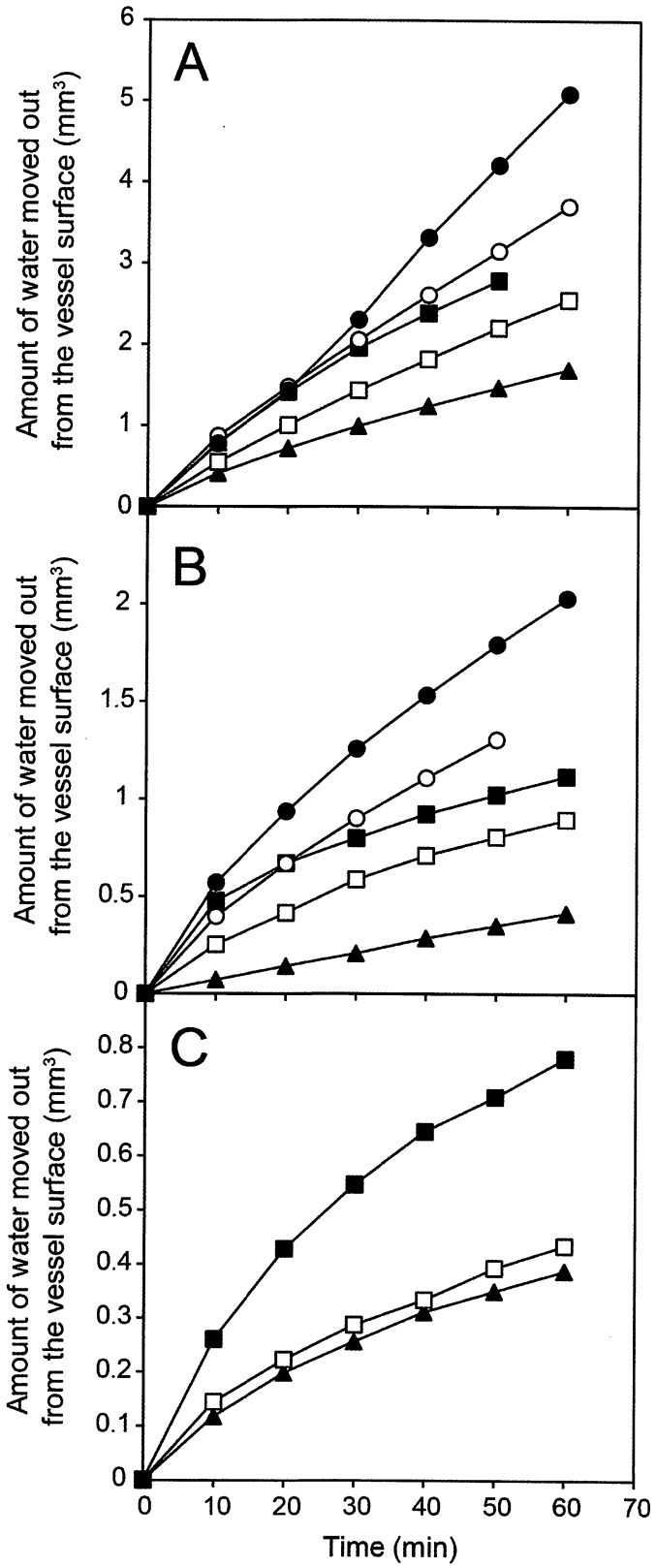

Figure 5-4. Efflux of water (A, 20 mM KCl solution: B, 0.2% acid fuchsin solution; C, 20 mM sucrose solution) from pressurized vessels with time. Different symbols represent different stem samples of laurel.

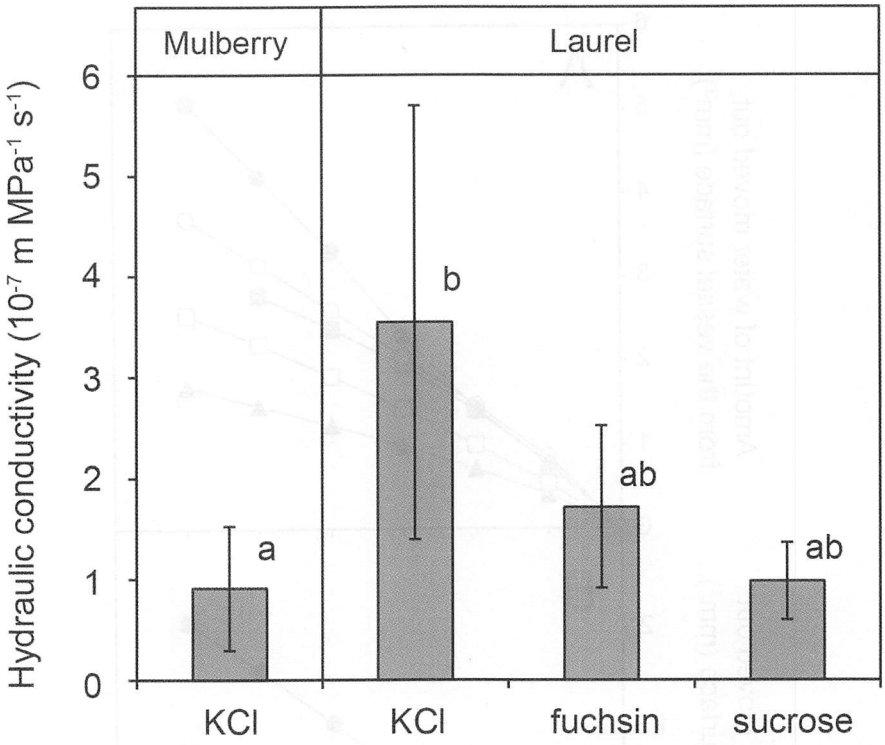

Figure 5-3. Hydraulic conductivity of the single vessel. The solution was pushed into the open vessel, and the rate at which the water exited radially from the individual vessel surface was quantified. Bars represent ± 1 SD. Different letters above the columns indicate statistically significant differences (One-way ANOVA and Tukey's multi-comparison test, < 0.05).

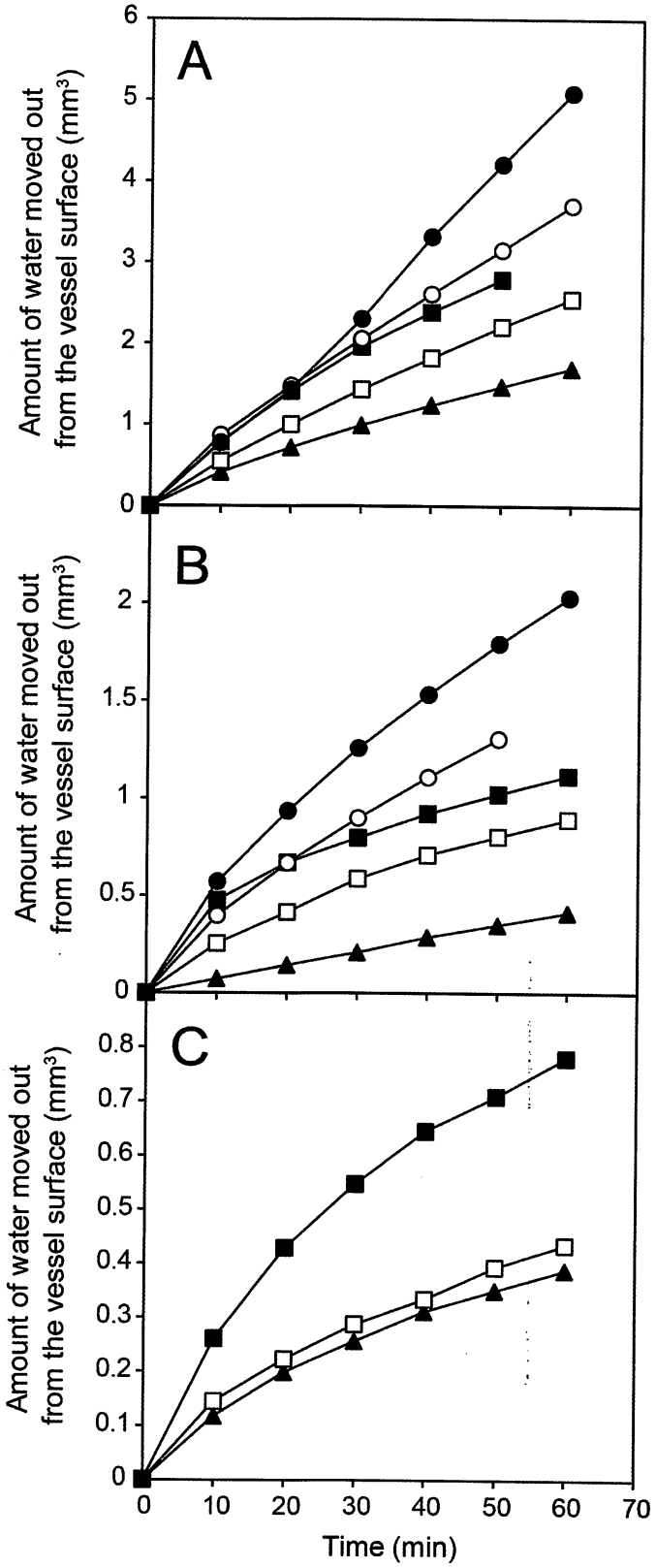

Figure 5-4. Efflux of water (A, 20 mM KCl solution: B, 0.2% acid fuchsin solution; C, 20 mM sucrose solution) from pressurized vessels with time. Different symbols represent different stem samples of laurel.

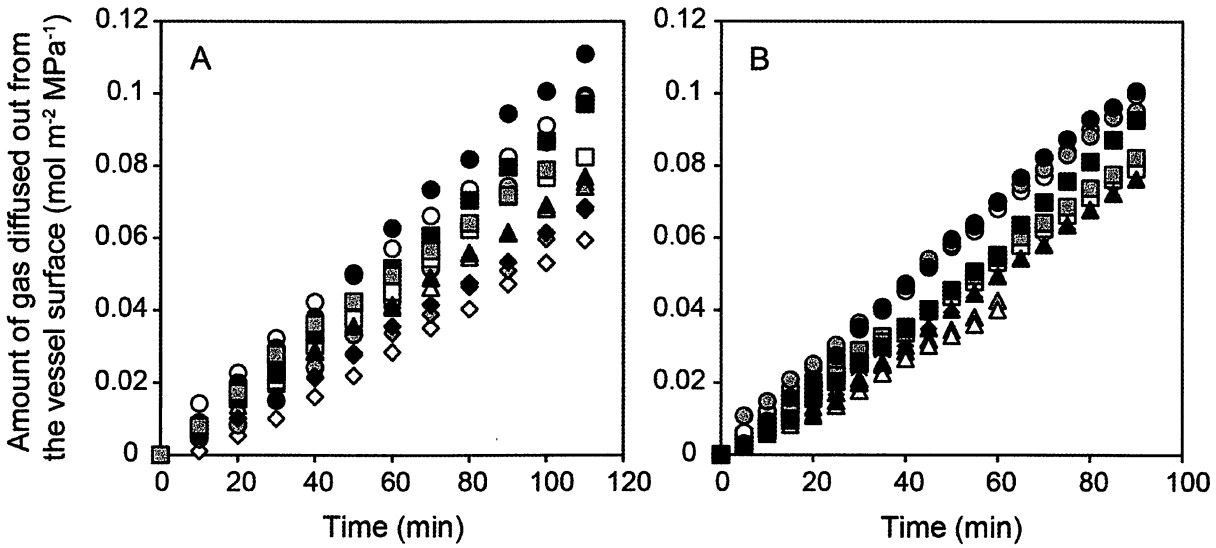

Figure 5-5. Efflux of gas from a pressurized vessel with time for mulberry (A) and for laurel (B). The amounts of gas efflux per vessel surface area per pressure are shown. Different symbols represent different stem samples.

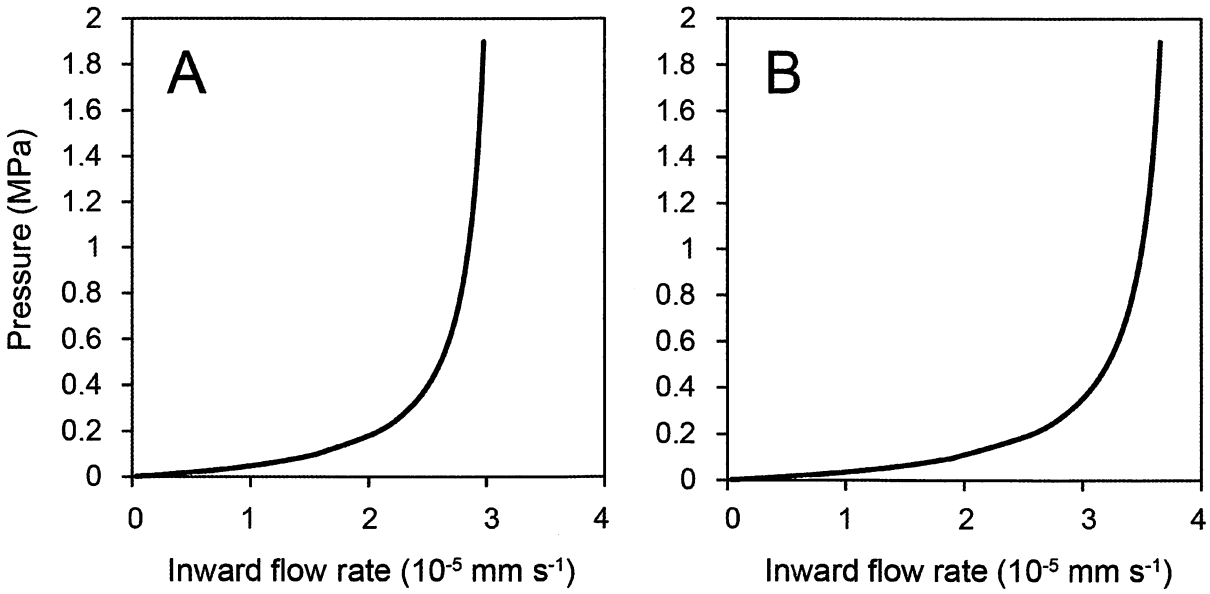

Figure 5-6. The relationship of the gas pressure in the vessel lumen to the inward flow rate per surface area of the refilling vessel. The gas pressure in the refilling vessel lumen was calculated as a function of the inward flow rate by Eq. 5-2. The data is expressed in gauge pressure.

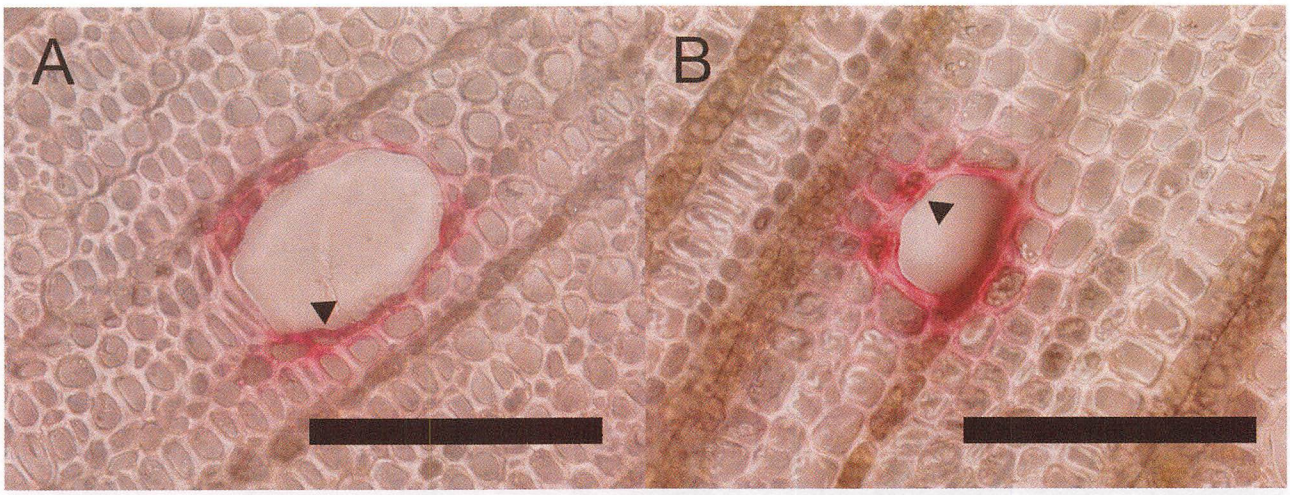

Figure 5-7. Cross-sectional images of the stained vessels in the current-year stem of mulberry (A) and laurel (B). The safranin solution was introduced into the vessels. The dye tended to accumulate preferentially at the pits between the vessel and parenchyma cells (arrow heads). Scale bar is 200 μm.Scale bar is 100 μm.

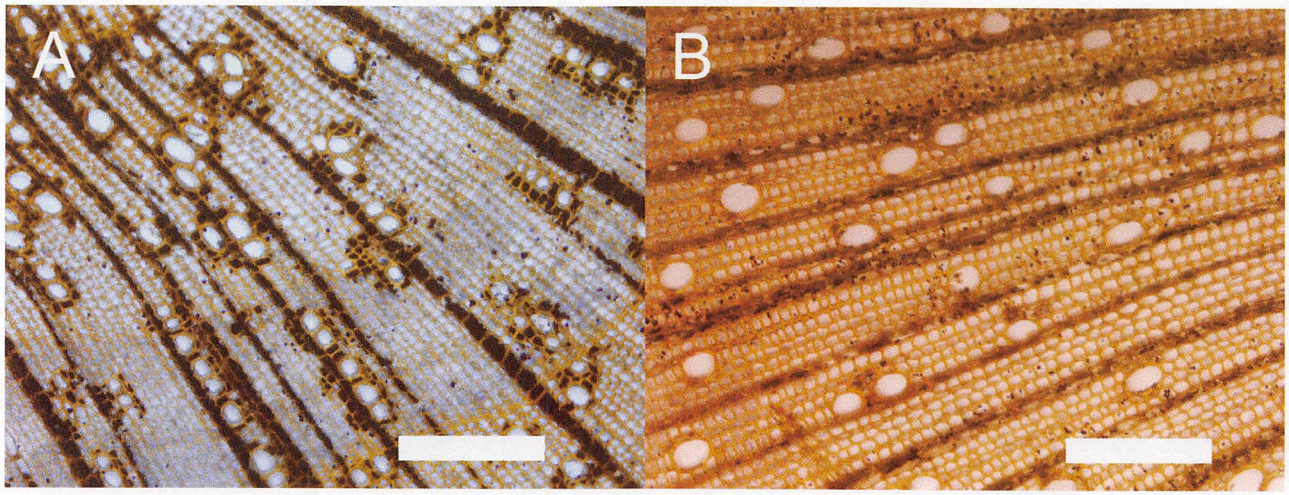

Figure 5-8. Cross-sections of current-year stems of laurel showing wood ray and vasicentric cells. The stems were excised in summer (A) and in winter (B). Starch granules contained in the vascicentric cells were stained in dark blue with Lugol solution. Scale bar is 500 μm.

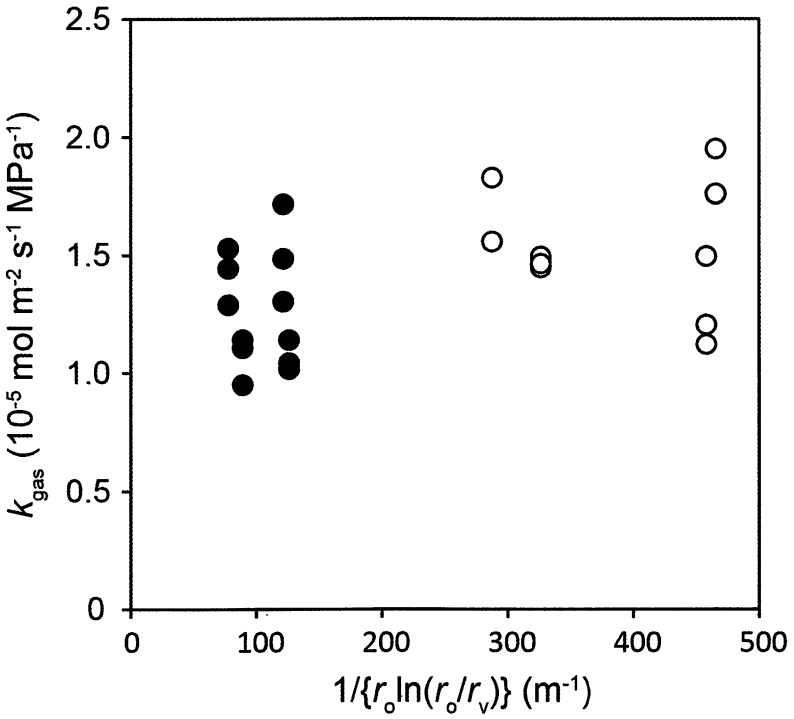

Figure 5-9. The relationship between the rate at which gas was forced out from pressurized vessel (k_{gas}) and $1/\{r_o \ln(r_o/r_v)\}$ in mulberry (solid circles) and laurel (white circles). Assuming that the gas diffusion through the stem limits the gas removal rete, k_{gas} would be proportional to $1/\{r_o \ln(r_o/r_v)\}$ (see Eq. 5-3). However, neither of the correlations was positive (r = 0.0732 for mulberry and r = 0.0397 for laurel).

REFERENCES

Brodersen CR, McElrone AJ, Choat B, Matthews MA, Shackel KA. 2010. The dynamics of embolism repair in xylem: in vivo visualizations using high-resolution computed tomography. *Plant Physiology* **154**, 1088-1095.

Holbrook NM, Zwieniecki MA. 1999. Embolism repair and xylem tension: do we need a miracle? *Plant Physiology* **120**, 7-10.

Salleo S, Lo Gullo MA, Trifilo P, Nardini A. 2004. New evidence for a role of vessel - associated cells and phloem in the rapid xylem refilling of cavitated stems of Laurus nobilis L. *Plant, Cell & Environment*, **27**, 1065-1076.

Scheenen TW, Vergeldt FJ, Heemskerk AM, Van As H. 2007. Intact plant magnetic resonance imaging to study dynamics in long-distance sap flow and flow-conducting surface area. *Plant Physiology* **144**, 1157-1165.

Secchi F, Zwieniecki MA. 2011. Sensing embolism in xylem vessels: the role of sucrose as a trigger for refilling. *Plant, Cell & Environment* **34**, 514-524.

Utsumi Y, Sano Y, Fujikawa S, Funada R, Ohtani J. 1998. Visualization of cavitated vessels in winter and refilled vessels in spring in diffuse-porous trees by cryo-scanning electron microscopy. *Plant Physiology*, **117**, 1463-1471.

van Ieperen W. 2007. Ion-mediated changes of xylem hydraulic resistance in planta: fact or fiction?. *Trends in plant science*, **12**, 137-142.

Yang S, Tyree MT. 1992. A theoretical model of hydraulic conductivity recovery from embolism with comparison to experimental data on Acer saccharum. *Plant, Cell & Environment*, **15**, 633-643.

Zwieniecki MA, Holbrook NM. 2009. Confronting Maxwell's demon: biophysics of xylem embolism repair. *Trends in Plant Science* **14**, 530-534.

Zwieniecki MA, Melcher PJ, Holbrook NM. 2001. Hydraulic properties of individual xylem vessels of *Fraxinus americana*. *Journal of Experimental Botany* **52**, 257-264.

CHAPTER 6

GENERAL DISCUSSION

In chapter 2, I found that the recovery of the hydraulic conductivity occurred in stem xylem of the potted mulberry trees (*Morus australis*) by rehydration for 3 h The xylem pressure after the rehydration was –0.39 ± 0.25 MPa (mean ± 1 SD, n = 4). It was, therefore, confirmed that refilling of the cavitated vessels occurs in mulberry even when the bulk xylem pressure is negative.

To refill the cavitated vessels, the pressure in the gas phase in the vessels must be positive (Tyree and Yang, 1992). Thus, there must exist the mechanism preventing the refilling vessel water from being lost to the adjacent functional vessels under negative pressure. Otherwise, the water in the refilling vessel would be forced to move into the adjacent functional vessels, preventing xylem refilling. Two hypotheses have been proposed to explain the mechanism preventing the refilling vessel water from being lost to the surrounding functional vessels under negative pressure. One is the pit-membrane-osmosis hypothesis, and it proposes that the xylem parenchyma cells release polysaccharides that are impermeable to the inter-vessel pit membranes into the refilling vessel; this osmotically counter-acts the negative pressure, thereby allowing the vessel to refill (Hacke and Sperry, 2003). To examine the pit-membrane-osmosis hypothesis, I estimated the semi-permeability of pit membranes for molecules of various sizes and found that the pit membranes of mulberry stems exhibited very low semi-permeability (Chapter 3). Hence, I considered that the pit-membrane-osmosis hypothesis can not explain the refilling under strong negative xylem pressure.

The other hypothesis is the pit-valve hypothesis (Holbrook and Zwieniecki, 1999). This proposes that gases trapped in the inter-vessel bordered pits isolate the refilling vessel water from the surrounding functional vessels. Assessment of this hypothesis requires clearing several problems. One problem is whether the pit valve can work *in vivo*. Positive pressure is needed to force the gas into surrounding water whereas excessive pressure will cause the collapse of the pit valves before the

completion of the vessel lumen refilling. The pit valve stability depends on the threshold pressure at which it collapse and the pressure in the refilling vessel during the vessel lumen refilling. The threshold liquid pressure to retain the pit valves ranged from 0.025 to 0.10 MPa in mulberry and from 0.050 to 0.150 MPa in laurel (Chapter 3). On the other hand, the gas pressures required for refilling of the vessel lumen in 3 h for mulberry and in 1h for laurel were calculated to be 0.00464 MPa and 0.00674 MPa, respectively. Even when the refilling in the mulberry stem vessel is assumed to be completed in 1 h, the gas pressure in the refilling vessel lumen will be only 0.0153 MPa. Even when the capillary force was considered, the liquid pressure in the refilling vessel will not increase. Therefore, the pit valve will work during the refilling of the cavitated vessel lumen. In this case, the gases in the vessel lumen will be removed at first, and only the gases in the pit chambers will remain.

After refilling of whole vessel lumen, the further inward flow from surrounding parenchyma cells should lead to pressurization of the gases in the pit chambers, resulting in collapse of the gases in the pit chambers. Unless the gases in the pit chambers (pit valves) are simultaneously dissolved, it could be possible that remaining gases expand to re-embolize the vessel because the water in the vessel connected with that of the surrounding functional vessels is under negative pressure (Hacke and Sperry, 2003; Brodersen *et al.*, 2010). The present results, however, indicate that the pit valves can not collapse simultaneously (Chapter 3). To overcome this problem, the inward water flow from parenchyma cells to the refilling vessel will have to be more than the outward flow from the refilling vessel to the surrounding functional vessels under negative pressure to keep pressurizing the remaining gases even when some pit valves are collapsed (Brodersen *et al.*, 2010).

The outward flow rate is proportional to the inter-vessel pit area and the hydraulic conductivity across the pits. Then, the outflow rates of the refilling vessel, almost all pits of which are permeable, will be calculated by the product of the inter-vessel pit area and the area based hydraulic conductivity across the pits. For a model vessel of mulberry (60 μm in diameter and 10 cm in length, see Fig. 2-2 and 4-9), I estimated the outflow conductance to be 5.1 mm^3 MPa^{-1} s^{-1} using the resistance of the inter-vessel pits per pit area in mulberry of 279 MPa s m^{-1} and the inter-vessel pit

area per unit vessel length of 14.2 $mm^2\ m^{-1}$, both measured in chapter 4.

The inward flow rate is proportional to the contact wall area between the vessel and parenchyma cells ($\propto$ non-inter-vessel pit area) and the hydraulic conductivity between them. Assuming the columnar shaped vessel, the non-inter-vessel pit area per unit vessel length can be calculated as the difference between total vessel wall area per unit length (πD, where D is the vessel diameter) and inter-vessel pit area per unit length. Then, for the model vessel, I estimated the inflow conductance to be 1.6×10^{-3} $mm^3\ MPa^{-1}\ s^{-1}$ using the area based hydraulic conductivity of 9.12×10^{-8} $m\ MPa^{-1}\ s^{-1}$, measured in chapter 5, and the non-inter-vessel pit area per unit vessel length of 174 $mm^2\ m^{-1}$.

Assuming that the difference in the water potentials between the refilling vessel sap and surrounding parenchyma cells equals the difference in the pressure potentials between the refilling vessel and the sap in the surrounding functional vessels, the outflow rate will be three orders of magnitude larger than the inflow rate. The drop of outflow flow due to aspiration of the pit membranes may play a role to overcome this desperate situation partially (Chapter 3). Also, the hydraulic conductivity between the vessel and surrounding parenchyma cells may increase by the aquaporin gene expression, resulting in the high inflow rate. In the roots of *Lycopersicon esculentum*, down-regulation of aquaporins led to a reduction in water transport through the cell membrane by more than 70% (Javot and Maurel, 2002). Or, polysaccharides with molecular size such as PEG 500,000 released by surrounding parenchyma cells might clog the inter-vessel pit membrane, and lower the outflow rate from the refilling vessel to the surrounding functional vessels. If that were the case, the maximum hydraulic conductivities in the stems during xylem refilling would be smaller than that of non-stressed shoots. However, there are no such reports. For explanation of refilling of the cavitated vessel under negative pressure, another mechanism must be required.

The estimation of the outflow rate may include the errors by the underestimation of the resistance of the inter-vessel pits per pit area (r_p). The values of r_p have shown a large range between studies using different techniques. Wheeler *et al.* (2005) and Hacke *et al.* (2006) estimated r_p by

subtracting lumen resistance from total resistance such as my present study. Their experiments yielded values of 30~2040 MPa s m^{-1} across 29 angiosperm species, and the values are close to my data, 48.6~279 MPa s m^{-1}. On the other hand, Choat *et al.* (2006) obtained slightly higher values, 2.56~5.32 × 10^3 MPa s m^{-1}, by measurements on individual vessels in two ring-porous species. So, re-examination may be required to obtain exact values of r_p.

The pit valve hypothesis is plausible for explanation of the vessel lumen refilling. However, there is a considerable difficulty when the gases in the pit chambers dissolve. I proposed several mechanisms for overcoming this difficulty, but unknown mechanisms may be required to realize the xylem refilling under negative pressure.

REFERENCES

Brodersen CR, McElrone AJ, Choat B, Matthews MA, Shackel KA. 2010. The dynamics of embolism repair in xylem: *in vivo* visualizations using high-resolution computed tomography. *Plant Physiology* **154**, 1088-1095.

Choat B, Brodie TW, Cobb AR, Zwieniecki MA, Holbrook NM. 2006. Direct measurements of intervessel pit membrane hydraulic resistance in two angiosperm tree species. *American Journal of Botany*, **93**: 993–1000.

Hacke UG, Sperry JS. 2003. Limits to xylem refilling under negative pressure in *Laurus nobilis* and *Acer negundo*. *Plant, Cell & Environment*, **26**, 303-311.

Hacke UG, Sperry JS, Wheeler JK, Castro L. 2006. Scaling of angiosperm xylem structure with safety and efficiency. *Tree Physiology*, **26**: 619–701.

Holbrook NM, Zwieniecki MA. 1999. Embolism repair and xylem tension: do we need a miracle? *Plant Physiology*, **120**, 7-10.

Javot H, Maurel C. 2002. The role of aquaporins in root water uptake. *Annals of Botany*, **90**, 301-313.

Tyree MT, Yang S. 1992. Hydraulic conductivity recovery versus water pressure in xylem of *Acer saccharum*. *Plant Physiology* **100**, 669-676.

Wheeler JK, Sperry JS, Hacke UG, Hoang N. 2005. Inter-vessel pitting and cavitation in woody Rosaceae and other vesselled plants: a basis for a safety versus efficiency trade-off in xylem transport. *Plant, Cell & Environment*, **28**: 800–812.